# Oral and transdermal delivery of branched amphiphilic peptide capsules *in vivo*

by

Kayla E. Nutsch

B.S., Kansas State University, 2018

A THESIS

submitted in partial fulfillment of the requirements for the degree

MASTER OF SCIENCE

Biochemistry and Molecular Biophysics Graduate Group

KANSAS STATE UNIVERSITY
Manhattan, Kansas

2020

Approved by:

Major Professor
John M. Tomich

# Copyright

# Abstract

Nanocarriers have become a popular platform for delivering nucleic acid for therapeutic and pest control methods. The peptide-based nanocarriers, branched amphiphilic peptide capsules (BAPCs), have shown the ability to deliver plasmid DNA *in vitro* and *in vivo*. The mode of administration for nucleic acid, affects the efficiency of delivery and is dependent on the target tissue and environment advantages. Delivering dsRNA orally in insects can provide pest control in the field with minimal to no effect on surrounding species. However, this delivery method has proven to be highly variable. BAPCs facilitate the uptake of dsRNA in *Tribolium castaneum* when administered orally through their diet. The gene transcripts tested, BiP and Armet, are involved in the unfolded protein response (UPR) and successful knockdown results in lethality. Complexes of dsRNA-BAPCs were shown to cross the gut epithelium and enter the hemolymph, and further visualized in the midgut epithelial cells, fat bodies, and Malpighian tubules.

Transdermal delivery of nucleic acids and compounds is challenging due to the layers of protective barriers of the skin. Magnetic nanobeads surrounded by a bilayer of branched amphiphilic peptides (BAP-MNBs) were tested for transdermal delivery in mice tails with various skin contact times (1 min, 5 min, 15 min, and 30 min) and post exposure incubation times (1 h, 8 h, and 24 h). BAP-MNBs were extracted from tissues using magnetic separation to look at biodistribution as a pilot study. BAP-MNBs suggest a preference for entering through the follicular pathway and accumulate in the spleen, indicating potential for transdermal delivery of DNA vaccines.

# Table of Contents

# List of Figures

# List of Tables

# Abbreviations

AFM.....Atomic Force Microscopy
Armet.....Arginine-Rich, Mutated in Early-stage Tumors
AuNP.....Gold Nanoparticle
BAPC.....Branched Amphiphilic Peptide Capsule
BAP-MNB.....Branched Amphiphilic Peptide - Magnetic Nanobead
BEP.....Both Ears Punched
BiP.....Binding Protein
cDNA.....Complementary DNA
C-Dots.....Cornell-Dots
CD.....Cyclodextrin
CNT.....Carbon Nanotubule
CPP.....Cell Penetrating Peptide
DLS.....Dynamic Light Scattering
DMSO.....Dimethyl Sulfoxide
DNA.....Deoxyribonucleic Acid
dsRNA.....Double-Stranded Ribonucleic Acid
EDTA.....Ethylenediaminetetraacetic Acid
ER.....Endoplasmic Reticulum
FDA.....Food and Drug Administration
GRP78.....78-kDa Glucose-Regulated Protein
HPLC.....High Performance Lipid Chromatography
HPV-16.....Human Papillomavirus-16
IACUC.....Institutional Animal Care and Use Committee
IONP.....Iron Oxide Nanoparticle
LEP.....Left Ear Punched
MALDI-TOF.....Matrix-Assisted Laster Desorption Ionization - Time of Flight
MANF.....Mesencephalic Astrocyte-derived Neurotrophic Factor
MNB.....Magnetic Nanobead
MNP.....Magnetic Nanoparticle
MRI.....Magnetic Resonance Imaging
NEP.....No Ears Punched
NIR.....Near Infrared
NP.....Nanoparticle
pDNA.....Plasmid DNA
PEG.....Polyethylene Glycol
PEI.....Polyethylenimine
QD.....Quantum Dot
REP.....Right Ear Punched

RISC.....RNA Induced Silencing Complex
RNA.....Ribonucleic Acid
RNAi.....RNA Interference
SB.....Stratum Basale
SC.....Stratum Corneum
SG.....Stratum Granulosum
siRNA.....Small Interfering RNA
SS.....Stratum Spinosum
T4-PNK.....T4 Polynucleotide Kinase
TDDS.....Transdermal Drug Delivery System
TEM.....Transmission Election Microscopy
TFE.....2,2,2-Trifluoroethanol
UPR.....Unfolded Protein Response
ZP.....Zeta Potential

# Acknowledgements

The results presented in this thesis are not exclusively the work of my effort, but also of various collaborations and partnerships.

I would like to thank my major professor Dr. John Tomich, who believed in my ability before I was even enrolled at K-State. For continually pushing and challenging me throughout my undergraduate and graduate careers and providing many insightful conversations about science and life in general.

I would also like to thank my committee members: Dr. Gerald Reeck who guided my research working with *Tribolium* and dsRNA, and always poses intriguing points to explore; Dr. Yoonseong Park for his help in generating the confocal images, pushing me to explore difficult questions and experimental troubleshooting, and for providing continued advice; and Dr. Michael Kanost for helpful academic guidance and support throughout my time at Kansas State.

The following deserve a special thanks: Dr. L. Adriana Avila, for being my first mentor in the lab who has believed in me since the beginning and who I continue to look up to today. Dr. Chandrasekar Raman for teaching me various techniques in the Reeck lab. Dr. Sherry Fleming and Jennifer Rowe for teaching me how to properly handle mice and for answering my countless questions. Dr. Shelia Barros de Mello, for continued support and encouragement throughout my writing process. Pavithra Natarajan for preparing the BAP-MNBs, performing the Prussian blue staining, and always answering my questions. Susan Whitaker for preparing peptides and for guiding me in the lab.

I also want to extend my gratitude for all past and present Tomich and Reeck lab members who have contributed to the research and development to get to this point and are always there to help.

To my friends Cameron Gillespie, Joseph McIntosh, and Gary Davis for always being down to get a drink over entertaining discussions about experiments, science, and life in general. You were my lifeline throughout my undergraduate and graduate careers. I continue to cherish our friendship and I hope to see you all again soon.

I especially want to thank my parents, Rhonda and Tom Wilkinson, for always being my biggest cheerleaders from day one for the spectrum of different career paths and goals I had, from Barbie princess to photographer to biochemist. You continue to be my role models and I have learned many lessons from you that continue to help me improve my personal and professional life. I thank my sister Ashlee for reminding me of the wonder and curiosity in science that has driven me to where I am today. I thank my in-laws for their continued support and for truly becoming my second family.

Last but far from least I want to thank my husband, Josh Nutsch, who has been my partner and best friend for almost a decade. Your work ethic and patience inspire me, and you push me to be my best self. Your support and encouragement throughout the past 5 years have helped me through frustrating times. Thanks for always having my back and making sure I get stuff done.

# Dedication

To my parents, Rhonda and Tom Wilkinson, and my husband, Josh Nutsch, for their continued support and advice, and for always encouraging me to dream bigger.

# Chapter 1 - Nanocarriers

In the past two decades nanocarriers have shown tremendous advances in nanotechnology and medical applications [1]. Nanocarriers have been explored extensively in research and in clinical settings for drug delivery, gene therapy, vaccinations, regenerative medicine, tissue engineering, cancer therapy, disease diagnosis, and molecular imaging [2, 3, 4, 5, 6, 7, 8, 9, 10, 11, 12, 13].

When designing nanoparticles for the delivery of low molecular weight drugs or nucleic acids the surface properties, biodistribution, and toxicity are important characteristics that need to be addressed [25, 26, 27, 28, 29]. The higher surface area to volume ratio provided by nanocarriers improves the pharmacokinetics and biodistribution, which in turn minimizes toxicity [30, 31, 32, 33]. Nanocarriers with extended blood circulation times, targeted delivery, and endosomal escape, have proven to be especially efficient in delivery and are aspects that are highly sought after [49, 50, 51, 52, 53, 54, 55]. In addition to these attributes, an ideal delivery system would be able to hold a high volume of payload and have affordable and easy producibility [37, 38, 39, 40, 41, 42].

Gene therapy utilizes exogenous nucleic acid to influence gene expression in living organisms to treat or prevent diseases [15, 16]. Nucleic acids (DNA, RNA, and oligonucleotides) have great therapeutic potential, but their large molecular weight and anionic nature prevent them from crossing the negatively charged plasma membrane and reaching their targets in the cytoplasm or nucleus. Viral vectors such as adenoviruses, lentiviruses, and adeno-associated viruses, were the first form of gene delivery to overcome biological barriers and advanced gene-delivery technology [14, 15, 16, 17, 18, 19]. However, they have limited load packing capacities and complicated production processes with high production costs [22, 23, 24]. The cytotoxicity,

insertional mutagenesis, and lethal immune responses of viral-associated gene delivery, which have yet to be resolved, have prompted the interest in less pathogenic/immunogenic options [14]. Non-viral vectors have the potential to address many of these shortcomings.

## Inorganic Nanoparticles

Gold nanoparticles (AuNPs) possess several characteristics which make them useful for drug or gene delivery, diagnostics, and therapeutic applications. They are easy to synthesize, have shown excellent biocompatibility, have a well-defined surface chemistry for easy functionalization, can be used for imaging due to their light scattering properties and tumor ablation based on their photothermal ability to absorb light, and have a unique surface plasmon resonance which can be exploited to facilitate on-demand release [24, 56, 57, 58, 59, 60]. Many of these properties can be tuned and optimized based on size, shape, structure, and composition of AuNPs. Plasmonic nanoparticles, which are based on gold or silver cores, are defined as nanoparticles which display localized surface plasmon resonance bands in the ultra violet-visible-near infrared range, that are highly sensitive to subtle changes in the physiochemical environment [61]. *Listeria monocytogenes* have been detected by aggregation with functionalized AuNPs, based on the surface plasmon resonance-based color shift when aggregated with the bacteria [61]. AuNPs have also been shown to conjugate with nucleic acid through surface functionalization with positively charged molecules such as amino acids, cationic peptides, and tertiary amine-containing molecules, or by directly binding to the AuNPs unfunctionalized surface using gold-thiol chemistry [62, 63]. Both forms of functionalized or non-functionalized AuNP-DNA conjugates were shown to be effective in gene delivery [24]. While no AuNPs have been clinically approved, a handful which utilize light absorbing

properties are being investigated for use against solid tumors and acne. One example is AuroLase®. These silica-gold nanoshells, are coated with polyethylene glycol (PEG) and are designed to thermally ablate solid tumors post near infrared (NIR) activation [64, 65, 66]. This is achieved by inducing photothermal cell death *in vitro* and by increasing solid tumor tissue temperatures high enough to induce irreversible thermal damage *in vivo* [67, 68, 69]. Another AuNP being investigated, Sebashells, use a similar design of silica-gold nanoshells coated with PEG to absorb NIR and disrupt overactive sebaceous glands for acne treatment [70]. While AuNPs have unique advantages and uses, optimizing the surface and physical properties of AuNPs to ensure maximum functionality has been challenging [61, 72]. Key aspects of AuNPs that still need to be systematically investigated include the biological fate, long-term biocompatibility, cellular interactions, biodistribution, and clearance [56, 192, 16, 73].

Magnetic nanoparticles (MNPs), which are often iron oxide nanoparticles (IONPs), have many uses related and unrelated to biomedicine and biotechnology, ranging from audio speakers and magnetic data storage to magnetic resonance imaging (MRI) and bioseparation [24, 74, 75, 76, 77]. MNPs are most often used as contrast agents for non-invasive diagnostic imaging in MRI and cell imaging in transmission electron microscopy (TEM) [78, 79, 80]. Once the surface of MNPs are functionalized and coupled with DNA, proteins, peptides, or antibodies they have additional uses for drug and gene delivery, anemia treatment, tissue engineering, magnetic targeting, and thermal ablation of tumors [56, 71, 24, 81, 82, 83, 132, 85]. IONPs have been tested in clinics more than any other inorganic nanoparticle, yet a majority of the approved IONPs have since been discontinued without specifying any scientific reasons [56]. Many clinically relevant studies currently being conducted are focused on Ferumoxytol to treat iron deficiency in adults with chronic kidney disease intravenously where iron becomes available

upon degradation [86, 87]. Clinical studies of IONPs have shown that large safety concerns still need to be addressed, applications are limited by low doses, and many side effects have been reported [56, 88, 89, 90].

Silica Nanoparticles (Silica NPs) are often used in conjunction with other nanoparticles (NPS) due to their favorable biodegradability and low toxicity [91, 92]. Depending on the biological application of interest, one can precisely tune the size, shape, porosity, and surface modifications of silica NPs, which all independently influence circulation time, targeting, drug loading/release, and cellular internalization [93, 94, 95, 96, 97, 98, 99, 100]. Due to the high porosity, there is a large surface area that can be used to store and release a variety of drugs, hydrophilic or hydrophobic. Hollow silica spheres with ordered pore structures (2.5 or 1.8nm) have been used as a drug delivery and gene transfection system [72]. Sumistha Das et al. reported that amine functionalized silica NPs were ineffective for oral dsRNA delivery to mosquitos without further extensive modifications [104]. Cornell-Dots (C-Dots), which are hybrid silica NPs with a near infrared fluorophore, PEG coating for immune system avoidance, and a $^{124}$I radiolabeled cRGDY targeting peptide for PET imaging and improved targeting and accumulation, are in clinical trials for imaging and diagnostics of tumors (ClinicalTrials.gov identifiers NCT01266096 and NCT02106598) [101]. C-Dots have no reported toxicity or adverse effects, are stable *in vivo*, have consistent pharmacokinetic properties, and are capable of imaging metastatic lesions [101, 102]. Despite these successes, for silica NPs to progress, long term *in vivo* fate and optimal size/shape/porosity still need to be determined.

Quantum Dots (QDs) are inorganic semiconductor nanocrystals 2-8 nm in size, which can be observed with confocal microscopy, total internal reflection microscopy, or basic wide-field epifluorescence microscopy [71, 105]. QDs are brighter than fluorescent dyes, resist to

photobleaching, and have multicolor emission, making them favorable fluorescent probes [103]. Additionally, QDs can be covalently linked to biorecognition molecules making them useful for gene delivery, fluorescent labeling of cellular proteins, cell tracking, pathogen and toxin detection, and *in vivo* animal imaging [71].

Carbon Nanotubules (CNTs) were the first inorganic nanomaterial to show that biocompatibility may be determined by surface functionalization rather than size, shape, or material, and have been widely explored since they were first described in 1991 [24, 106]. CNTs were found to have low toxicity and were easily translocated across the cell membrane but had limited biocompatibility alone [107, 108]. Water-soluble functionalized CNTs however, helped increase biocompatibility and were shown to be rapidly cleared from systemic blood circulation in mice [109]. Due to their hollow cores, CNTs can be used to carry a wide variety of drugs or nucleic acid based on surface modifications to accommodate the load [110, 111]. Gene expression for CNT-DNA conjugates was shown to be 10x higher than DNA alone, likely due to their ability to penetrate the cell like a nano-needle, bypassing the endocytosis pathway for delivery [24, 106, 112]. However, CNTs have a wide size distribution, which can influence systemic biodistribution, target ability, and drug release [72].

While inorganic nanoparticles offer unique diagnostic and therapeutic opportunities, they often cannot be used without organic modifications, and have not been approved for any drug/gene delivery applications [72].

## Organic Nanoparticles

Organic nanoparticles are promising non-viral vectors due to their improved circulation and reduced toxicity making them ideal for loading genes for chemotherapy [113]. They have

higher biocompatibility and biodegradability compared to inorganic nanoparticles and can be based on a large variety of compounds including lipids, polymers, and peptides [45, 46, 47].

### *Lipid-Based Nanoparticles*

Lipids are hydrophobic or amphiphilic in nature. Amphiphilic lipids have a hydrophilic region as well as a hydrophobic region, such as a phospholipid. When these lipids are placed in an aqueous solution, the hydrophobic regions are drawn towards each other and often form micelles, where the core is all hydrophobic tails facing each other, or more likely liposomes, where the hydrophobic tails face each other forming a bilayer with an aqueous core and hydrophilic heads also interacting with the aqueous solution surrounding the liposome. These structures were first described by Alec Bangham and his coworkers in 1964 and have since been researched and used extensively [114, 115]. The lipids used to form liposomes can be natural or synthetic and can determine the physiochemical and colloidal characteristics such as size, composition, loading efficiency, stability, and biological interaction [116, 117]. Cationic lipids are preferred for cellular uptake due to the natural electrostatic attraction to the negative charge on the cellular membrane. Charge neutral lipids, also known as helper lipids such as cholesterol, are integrated with cationic lipids to help form and stabilize the bilayer [15, 20, 21]. Liposomes are one of the most clinically established nanocarrier systems used to deliver drugs, nucleic acid, and imaging agents [1]. They have been used in ocular and pulmonary applications as well as cancer and gene therapy [116, 118, 130, 119].

New generation liposomes have altered characteristics to improve tissue targeting over standard liposomes. These include liposomes with modified lipid composition such as archaeosomes, containing lipids with diether linkages, and ethosomes, which have a high

concentration of alcohol functionalities [116, 120, 121]. Others have surface modifications such as virosomes which have fusogenic viral envelope proteins on their surface and cryptosomes which have a PEG coating [116, 122, 123]. Additional new generation liposomes include niosomes with a non-ionic surface, transferosomes for transdermal delivery, novasomes with 2-7 bilayer shells, emulsomes which have a solid fat core surrounded by bilayer, and genosomes for gene or DNA delivery [116, 124, 125, 126, 127, 128].

While liposomes have been the focus of most lipid-based nanocarriers, other lipid-based carriers show promising delivery capabilities. Cationic lipids interact with the negatively charged siRNA through electrostatic interactions and form lipoplexes [129]. These lipoplexes form multi-layer sheets where the negatively charged siRNA is layered between the positively charged layers of cationic lipids. These lipoplex layers are approximately 3.7 nm thick, with a 2 nm gap between each layer where the siRNA is situated. Stable nucleic acid-lipid particles were studied to combat the Zaire strain of the Ebola virus in guinea pigs, the hepatitis B virus in mice, and dyslipidemia in monkeys [49, 25, 34, 35, 131, 36].

Despite the success of liposomes for delivery, there remains some concerns for therapeutic use. Some cationic lipids have shown toxicity *in vitro* and *in vivo*, which PEGylation can mediate, and some synthetic lipids have the ability to produce off target effects [133, 134]. Additionally, studies have shown low drug loading efficiency and poor stability of liposomes [135]. While these are characteristics that can be optimized with further research, there have also been reports of variation between batches made, which creates a large roadblock for scale-up production in the future [49].

### *Polymer-Based Nanoparticles*

Polymer based nanoparticles are the simplest form of soft-material gene and drug delivery systems with low immunogenicity, absence of mutagenesis, low production costs, and versatility in structure and chemical makeup [136, 137, 138, 139, 14]. They are made up of repeating polymer segments referred to as blocks. Natural and synthetic polymers are very diverse and can be linear or branched. When designing the polymers composition, solubility, crystallinity, molecular weight, backbone stability, hydrophobicity, and polydispersity are carefully weighed depending on the target environment as well as the cargo being carried, based on its molecular weight and net charge [140, 139, 141]. The block copolymer chemistry used to create polymersomes can be tuned to the needs of the target and cargo based on the block used. Amphiphilic block copolymers can self-assemble into micelles (spherical, prolate, or oblate) or vesicles (polymersomes) depending on the ratio of hydrophilic to hydrophobic block volumes [142]. Micelles form from a single layer of amphiphilic copolymers where the hydrophobic blocks are all at the core and the hydrophilic blocks interact with the aqueous solvent, much like a detergent. Polymersomes on the other hand form a bilayer of amphiphilic copolymers with the hydrophobic blocks interacting with each other and forming a shell with the hydrophilic blocks interacting with the aqueous solution and simultaneously creating an aqueous core. Compared to polymersomes, micellular structures can only encapsulate hydrophobic components in the core in aqueous solutions. Polymersomes can encapsulate hydrophilic components in the aqueous core and hydrophobic components in the thick lamellar membranes simultaneously [143].

Some of the first copolymers made were not fully biocompatible and were not biodegradable. Later polymer vesicles showed the ability to escape the endosome within minutes of endocytosis, due to the reductive environment, by the proposed proton-sponge-effect [142].

Compounds that have high pH buffering capacity or large positive charges within the endosome causes a diffusion of chloride ions into the endosome to neutralize the positive charge followed by an influx of water, causing large osmotic pressure and eventually bursting the endosome, releasing the contents [15, 144].

Common polymer blocks include Polyethylene glycol (PEG), polyethyleneimine (PEI), and cyclodextrins (CDs). PEG is commonly used in polymersomes and in conjunction with other nanocarriers to shield the nanocomplex from interaction with the extracellular environment and prolong its circulatory half-life, often referred to as "stealth-ing" [147]. Polyethyleneimine (PEI) is a broadly investigated delivery carrier that can condense DNA into polyplexes and can escape endosomes [25, 145]. Unmodified PEI is cytotoxic and have low transfection rates due to the high positive charge. Combining with disulfide modified hyaluronic acid (DNA-PEI-HA-SS-COOH) lowers the toxicity. Cyclodextrins (CDs) are natural cyclic polymers composed of alpha-1,4-D-glucose or amylose, with low immunogenicity, that can interact with nucleic acids [15, 146]. CDs have been shown to inhibit tumor growth of mouse metastatic Ewing's sarcoma and can safely be administered to non-human primates [25, 148]. One way to make fully-biodegradable vesicles is to use polypeptides. Sun et al. created poly(L-Lysine)-block-poly(L-phenylalanine) (PLL-b-PPA) which spontaneously assemble into giant vesicles in aqueous solutions [149].

### *Peptide-Based Nanoparticles*

Peptides are an attractive material for nanosized delivery because they can be made of naturally occurring amino acids, serve as biologically active compounds or building blocks, and have sequence and function diversity [2, 37]. Each combination of amino acids will present their

own unique 3D structures, electric charges, and hydrophobicity, allowing for endless possibilities for cargo and delivery needs [37]. Additionally, peptide delivery systems have high drug loading capacity, low drug leakage, are biodegradable, and have high permeability to cellular membranes, giving them large advantages over liposomes and other nanoparticles [2, 150, 151]. As of 2015 more than 60 peptide therapeutics have been approved by the Food and Drug Administration, with many more being researched and in clinical trials [43].

Cell Penetrating Peptides (CPPs) are peptides composed of 10 to 40 amino acids, that are naturally capable of penetrating the cellular membrane and translocating into the cytoplasm [44, 45, 48]. The small size and low immunogenicity of peptides compared to proteins and antibodies allows them to penetrate tissues and solid tumors at a higher rate [43, 152]. CPPs are often attached to cargo intended for delivery, such as nucleic acids and small molecules through covalent or non-covalent interactions [44]. CPP conjugates have been shown to be sensitive to serum, creating mixed results *in vivo* [45]. While there has been some success using CPPs as nanocarrier, the cationic peptides can modify the cargo they are carrying potentially biologically inactivating the cargo, aggregation is likely to occur, and consistency of conjugation with nucleic acid has been an issue [44].

Another peptide-based delivery system with strong potential is self-assembling peptide nanomaterials. Most self-assembled molecules are formed based on weak non-covalent interactions between monomers [153]. These weak interactions can include electrostatic, hydrogen bonds, hydrophobic, and Van der Waals forces. Self-assembled structures have numerous weak interactions between many monomers, thereby greatly increasing stability. Peptides can be formulated to have amphiphilic properties to promote self-assembly into various structures such as nanotubules, nanovesicles, and micelles in a given environment [48]. Cyclic

peptides, made from alternating D- and L-amino acids, often self-assemble into nanotubules by stacking on top of each other [154]. Peptides that form these nanotubule or nanofibrous structures could be used to mimic the natural extracellular matrix for tissue engineering, as well as deliver localized drugs. Other self-assembled peptide carriers have shown successful delivery to the central nervous system, cardiovascular system, inside the eyes, into bones, and able to carry anticancer drugs [2, 155, 156, 157, 158, 159].

### *Branched Amphiphilic Peptide Capsules*

A newer class of self-assembling peptide-based nanocapsules, Branched Amphiphilic Peptide Capsules, were first described by Gudlur et al. [160]. These capsules are composed of two peptides which are amphiphilic in nature with a polar oligo-lysine (K=5) head attached to branched hydrophobic segments, composed of nine or five amino acid residues, and are composed entirely of naturally occurring amino acids (Figure 1.1). If the peptides contain nine or five amino acids in the hydrophobic segments, they are referred to as $h_9$ or $h_5$ respectively. The hydrophobic segments were derived from an internal fragment of a naturally occurring human dihydropyridine sensitive L-type calcium channel segment CaIV3 (DPWNVFDFLIVIGSIIDVILSE). The architecture of these peptides is similar to diacyl

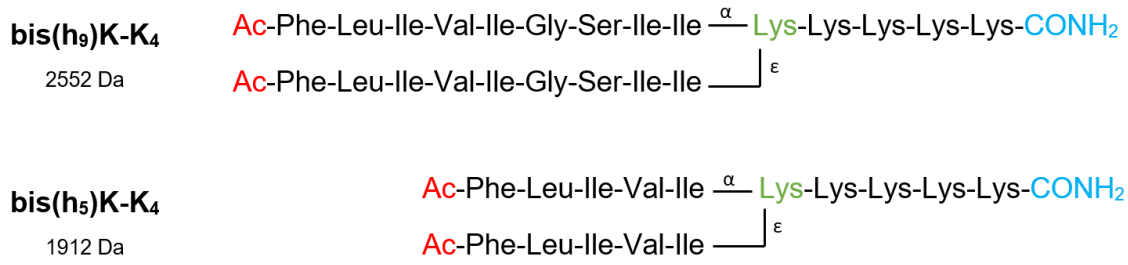


**Figure 1.1 - Sequence of $h_9$ and $h_5$ Peptides**

Sequences of the self-assembling branched peptides $h_9$ (top) and $h_5$ (bottom). The peptides are N-terminal acetylated (Red), the branch point lysine (green) with branches coming off the α-amino group of the N-terminus and the ε-amino group of the side chain.

phospholipids where the branch point lysine (highlighted in green in Figure 1.1) orients the two peptide segments at a ~90° angle off the α- and ε-amino groups. These peptides adopt a helical conformation and remain in a monomeric state in organic solvents such as 2,2,2-Trifluoralethanol (TFE). However, once these peptides are placed in water they adopt very stable beta-like structures, where the hydrophobic segments drive the initial formation of a bilayer, water filled, spherical structures which are referred to as a branched amphiphilic peptide capsules (BAPCs) [160]. This initial formation, driven by hydrophobic effects and Van der Waals forces, is comparable to the forces that stabilize liposomes. However, BAPCs also engage in hydrogen bonding between adjacent beta-structures [160]. This high level of stability helps maintain the structural integrity at low micromolar concentrations where most phospholipid bilayers would disassemble. BAPCs possess many other properties similar to phospholipid vesicles such as fusion, solute encapsulation, and ability to be resized by membrane extrusion through polycarbonate filters with defined pore sizes. Course-grained modeling further supports the hypothesis that these capsules form in a bilayer spherical shape like liposomes [160].

Initial studies demonstrated that BAPCs were able to encapsulate the small water-soluble dye molecules 5(6)-Carboxyfluorescein, tryptophan, and Rhodamine 6G, which provided the platform needed to assess if these peptide assemblies could be used as delivery vehicles *in vitro*. Co-localization of entrapped 5(6)-Carboxyfluorescein and covalently attached Carboxytetramethylrhodamine within the cells shows that intact BAPCs were able to enter the cytoplasm rather than fusing with the cellular membrane and releasing the encapsulated contents [160].

Seeing the potential to use BAPCs as a nanosized drug delivery system, further biophysical and structural studies were conducted [161]. After the $h_9$ and $h_5$ peptides were mixed

in equimolar ratios and dried as monomers, water was added to the solution for BAPC formation and size and morphology were observed for varying timepoints. Within 5 min of adding water, clusters of nanofibrils form. At 10 min post water addition the nanofibril structures break down and you begin to see the first capsules appear (~20nm). After 30 min, an accumulation of uniform ~20-30 nm capsules are present. As the solution continues to sit at room temperature after an hour fusion begins to be observed via "spheres of spheres." By 2 h post water addition, fusion has taken place with sizes ranging from 100 nm to more than 500 nm. After 24 h you can see some fusion capsules with a size close to 1 μm.

The size of nanocapsules is crucial for efficient cell and tissue uptake. To achieve a uniform size of ~20-30 nm, the peptides interacted for 30 min at room temperature (25°C) and then placed at 4°C for 1 h to stop fusion events, then rewarmed to 25°C. BAPCs that are subjected to this thermal cycling, termed "locked" BAPCs, remain in uniform ~20-30 nm size and are unaffected by solvents, salts, chaotropes, or temperature [161].

With the ability to prepared locked BAPCs at a fixed size, and with the success of initial studies, further investigation in cellular uptake and encapsulated solutes was performed. It was hypothesized that after BAPCs entered the cell, cellular degradation processes would eventually break open the BAPCs and release the encapsulated solutes. Observing co-localization of BAPCs and late endosomes, it appears that most BAPCs entered the cells through an endocytic pathway, but quickly escaped the late endosomes. The most likely mechanism for late endosomal escape is the proton-sponge-effect, which is commonly observed for cationic particles. Further, cells incubated at 37°C readily took up BAPCs while those incubated at 4°C accumulated at the cell surface, likely unable to pass through. This indicates the uptake mechanism is energy dependent, but the exact mechanism is not fully understood.

To study BAPC's ability to release encapsulated solutes and small proteins, Cytochrome c and RNase A were encapsulated in the hydrophilic core of the BAPCs and delivered to cells. Both proteins are known to trigger cellular apoptosis, however no significant cellular apoptosis occurred as expected, while the control Pep-1 with the same proteins lead to lethal cytotoxicity. The BAPCs were incubated for 14 days, and still there were no results that indicated the release of these encapsulated proteins. Daughter cells were seen with internalized labeled BAPCs without cytotoxic affects as well. This surprising result indicates that BAPCs are not degraded by cellular machinery as originally hypothesized. This surprising characteristic altered the focus of using BAPCs to deliver drugs, and instead they were used for alpha-particle therapy, which holds potential as a therapeutic treatment for micro metastases. α-Emitting actinium-225 ($^{225}$Ac), which has a half-life of 9.9 days, was encapsulated within BAPCs. Because the capsules are not degraded by cellular mechanisms, $^{225}$Ac and its daughter isotopes are confined within the capsule and do not freely circulate within the body causing off-target cytotoxicity. It was found that the radioactive materials remained encapsulated for days and even through multiple cell divisions [162].

While encapsulation and subsequent release of materials is not likely for BAPCs in higher organisms, creating nanoparticles with nucleic acid bound to the surface emerged as another potential use. Often nucleic acid delivery is used for gene therapy and needs to cross the plasma membrane and reach targeted subcellular organelles to be effective. Macromolecules such as plasmid DNA (pDNA) are anionic and are not able to permeate the negatively charged plasma membrane. To deliver pDNA to a cell, it typically needs to be associated with a molecular carrier. The positive charged lysine heads of the $h_9$ and $h_5$ peptides on BAPCs make this a desirable approach.

Before binding nucleic acids to the BAPC surface the lab attempted to encapsulate DNA within the BAPC core during capsule formation, similar to the small solutes and proteins as previously described. However, when adding an aqueous DNA solution to dried monomeric peptides BAPCs were not able to form in their standard shape. At a high peptide to pDNA ratio long nanofibers were formed. At lower peptide to pDNA ratios the DNA and peptides seemed to compact into nanocondensates.

The ratio of peptide to pDNA was determined and described as a charge ratio (N:P) between the number of $NH_3^+$s (N) in the oligo lysine tails of the peptides and the number of $PO_4^-$ s (P) in the nucleic acid, in this case this was a 4.7 kb pDNA. A N:P ratio of 65.5 here is referring to 50 μM peptides and $3.2x10^{-7}$ μM pDNA for a single transfection reaction of 1 mL. Transfection efficiency in HeLa cells with this N:P ratio was only about 2%. A high N:P ratio was used initially, as this was previously reported to have the highest transfection efficiencies. However, after exploring a range of N:P ratio and including 1 mM $CaCl_2$, which was reported to improve transfection efficiency with cell penetrating peptides/DNA complexes, lower N:P ratio transfection rates increased 10-fold. N:P ratios of 2.6 and 10.4 showed the highest gene

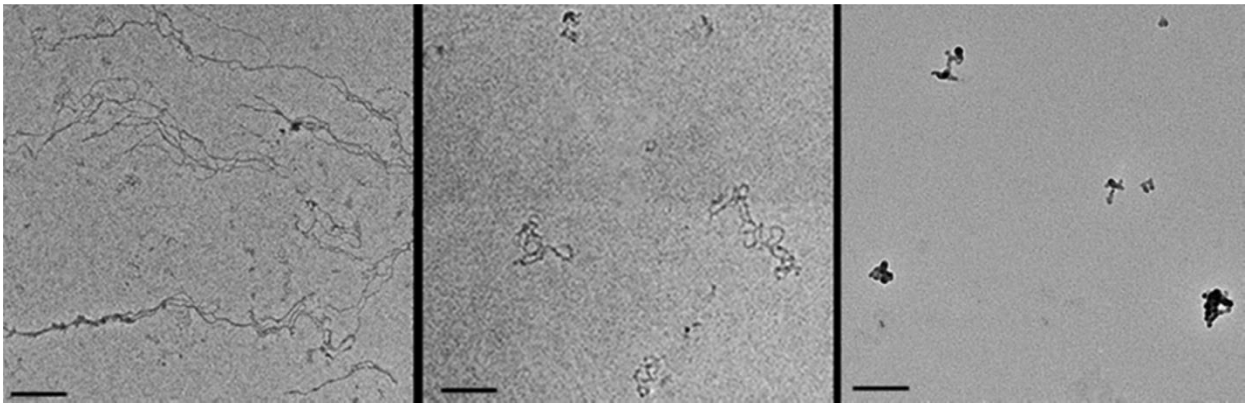

**Figure 1.2 - TEM Images of DNA-BAPC Peptiplexes at Different Ratios**

(A) Nanofiber structures at charge ratio N:P = 65.5. (B) Plasmid DNA in the absence of peptide, shown to compare the different supramolecular structures. (C) Nanocondensate complexes formed at lower charge ratio N:P = 10.4. Scale bar = 200 nm. Reprinted with permission from Avila, L. Adriana et al. 2015. Branched Amphiphilic Cationic Oligopeptides Form Peptiplexes with DNA: A Study of Their Biophysical Properties and Transfection Efficiency. *Molecular Pharmaceutics* 12 (3): 706-715. Copyright 2015 American Chemical Society.

expression with minimal toxicity to the cell. Looking at TEM of the higher N:P ratio of 65.5, lower N:P ratio of 10.4, and plasmid DNA alone in Figure 1.3 shows the varied morphology, and likely explanation for transfection efficiency difference. It is hypothesized that at the higher N:P ratio the peptides coated the pDNA as shown in the left panel, creating the long fibrous structures, while at the lower N:P ratios the pDNA and peptides were more compacted as shown in the right panel. The natural structure of pDNA alone is shown for reference in the middle panel. Additionally, the Zeta potential of the N:P ratio of 10.4 complexes was measured as +5 mV which is suitable to facilitate interactions with the negative cell membranes, but not high enough to cause cell damage [163].

Because the pDNA could not be encapsulated successfully and the highest transfection efficiency with the condensed structures only reached 20%, a different methodical approach was investigated. Locked BAPCs were prepared in water as normal and dried prior to adding pDNA. This methodology allowed for the locked BAPCs to act as nucleation centers for the pDNA to attract to and coat the surface of the BAPCs. Imaging in AFM showed single and clustered pDNA-BAPC nanoparticles, indicating there are several modes of associating with each other and likely compact similarly to histones. These structures showed higher

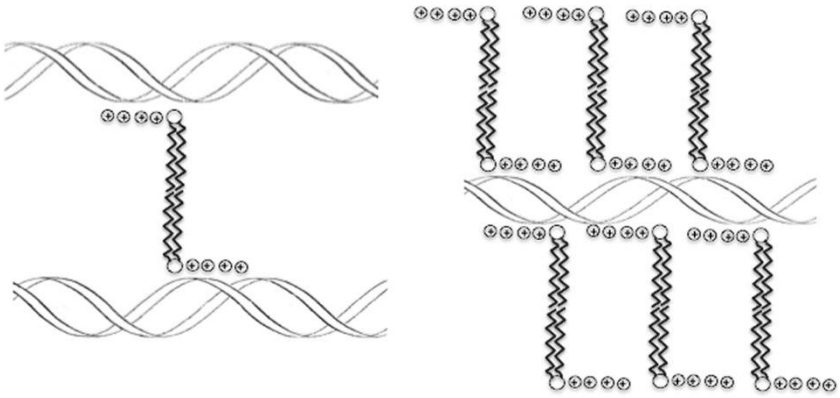

**Figure 1.3 - Scheme Representing DNA-BAPC Interaction at Different Ratios**

Left panel shows scenario in which the branched peptide sequences bridge the DNA at low N:P ratios allowing them to be pulled together. The right panel shows a hypothetical structure where the DNA is encased within a peptide bilayer. Lysines are represented by positive charges in the circles. Reprinted with permission from Avila, L. Adriana et al. 2015. Branched Amphiphilic Cationic Oligopeptides Form Peptiplexes with DNA: A Study of Their Biophysical Properties and Transfection Efficiency. *Molecular Pharmaceutics* 12 (3): 706-715. Copyright 2015 American Chemical Society.

transfection rates and lower cytotoxicity than the commercially available transfection reagent Lipofectin. Additionally, BAPCs were complexed with a larger 19.4 kb plasmid which encodes the entire genome for the North American type I porcine and reproductive system virus (PRRSV): pCMV-SD95-21-GFP. Delivery of this plasmid via BAPCs and expression resulted in shedding of competent RNA virus, making BAPCs a potential vaccine delivery system.

While many transfection reagents and nanoparticles show high gene delivery efficiency *in vitro*, most of them fail to produce the same results *in vivo* [263, 264, 265]. Researchers are continually trying to generate nano-delivery systems that can overcome the extracellular and intracellular obstacles for *in vivo* delivery. BAPCs have previously been shown to be able to deliver the DNA vaccine encoding the oncoprotein of type 16 human papillomavirus intramuscularly in mice, and delayed tumor growth at comparable rates to the HPV-16 DNA alone [164]. If BAPCs can deliver nucleic acid through non-injection methods, this could provide further applications for gene delivery, DNA vaccinations, and RNA interference with minimal invasion and easier administration.

# Chapter 2 - Bioaccumulation of dsRNA delivered orally via BAPCs in *Tribolium castaneum*

## Introduction

Almost three decades ago, Andrew Z. Fire et al. first described the gene silencing ability of RNA in *Caenorhabditis elegans* [165]. It was later determined that the initiator of blocked gene expression was double stranded RNA (dsRNA) and not single-stranded antisense RNA as originally thought [166]. Since then the highly conserved, sequence specific, post-transcriptional process of RNA interference (RNAi) has been a crucial tool in reverse genetics and shows promise for a variety of research fields. In genomics RNAi is used to determine gene function and complete knockdown studies, it can be used for medicinal purposes to control cancer and viral diseases, and its high specificity makes it an intriguing method for biotechnology companies to control pests in agriculture [167, 168, 169, 170, 171, 172, 173, 174].

RNAi can be divided into cell-autonomous and non-cell-autonomous processes. Cell-autonomous RNAi is more commonly discussed and is limited to dsRNA introduced or expressed in a cell [170, 175]. Once the dsRNA is able to reach the cytoplasm, it is cleaved by RNase III, also known as dicer, into small interfering RNAs (siRNAs) that are 21-25 base pairs long at random [266, 268]. An siRNA is then incorporated into the RNA-induced silencing complex (RISC). Argonaute 2 within RISC unwinds the siRNA and cleaves the sense strand, leaving the antisense strand in complex with RISC, activating the complex [267, 268]. Active RISC seeks out, binds to, and cleaves mRNA within the cell complementary to the antisense RNA, thus preventing the translation of the subsequent protein [268, 269].

The non-cell-autonomous RNAi processes, environmental and systemic, refer to the interfering effect that takes place in tissues or cells different from the location of introduced or

produced dsRNA. Environmental RNAi encompasses all processes in which dsRNA is taken up by the cell from the surrounding environment. This can include dsRNA taken up from the gut lumen to gut cells and soaking in a dsRNA solution [176]. When the silencing signal is transported from one cell to another or from one tissue type to another, this is referred to as systemic RNAi. Environmental RNAi can be followed by systemic RNAi and non-cell-autonomous RNAi is always followed by cell-autonomous RNAi [170, 175].

Sensitivity to systemic RNAi has been found to vary considerably among insect species and taxa [175]. Insect species unsusceptible to RNAi show temporary 60% or less knockdown of the target gene, while species sensitive to RNAi, such as coleopterans, show long lasting knockdown rates at 90% or higher with very small doses [177, 170, 175]. This variation indicates the systemic nature may act by different molecular mechanisms across taxa, while the cell-autonomous RNAi pathways remains conserved among different insect species. In insect pests, two different uptake pathways have been described thus far: the transmembrane Sid-1 channel protein-mediated pathway and the endocytic pathway. The Sid-1 channel proteins, which export silencing RNAs to neighboring cells from the intestinal lumen, was first discovered in the nematode *C. elegans*. Since then, Sid-1-like channel proteins have been shown to be involved in the uptake of dsRNA in insect species such as the brown planthopper [182], the Colorado potato beetle [183], and the red flour beetle [184]. Other species like *Drosophila melanogaster* do not have Sid-1 like proteins and utilize pattern recognition receptors to uptake dsRNA through an endocytic pathway. Some species such as the Colorado potato beetle have been shown to utilizes both uptake methods [177].

The most common form of administering dsRNA is through micro-injection into the hemolymph because of its high efficiency [178, 179, 180]. This method is tedious for many

insects, inefficient for large screens, and impractical pest control in the field. To effectively deliver dsRNA to insects in the field, it needed to be taken up autonomously, such as through feeding [170]. Feeding studies have shown variable success between insect species, making it challenging to optimize [181, 185].

The transcripts of BiP (also known as GRP78) and Armet (also known as MANF) were chosen because of their role in the unfolded protein response (UPR) [194, 197]. Proteins intended for secretion or membrane location, fold and mature in the lumen of the ER, with the help of chaperones [192]. Accumulation of misfolded proteins in the endoplasmic reticulum (ER) causes ER stress and activates the unfolded protein response (UPR) [193]. Upon activation of the UPR the ER membrane expands to make room for the extra misfolded proteins and new protein-folding machinery are released to manage the misfolded proteins and reduce ER stress [192]. BiP (Binding Protein), also known as GRP78 (78-kDa glucose-regulated protein), is a major ER chaperone and has many roles, including control of UPR activation [194]. Under standard physiological conditions BiP binds to the intraluminal domains of stress sensors, maintaining their inactive state. As misfolded proteins accumulate in the ER, they compete with the stress sensors to bind with BiP. As BiP releases from the stress sensors to help manage the misfolded proteins as a chaperone, the sensors in turn activate the UPR [193]. It has been shown that low expression levels of BiP can cause severe damage to the ER and cell death [195, 196]. Armet (arginine-rich, mutated in early stage tumors), also known as MANF (mesencephalic astrocyte-derived neurotrophic factor), is suggested to promote neuron proliferation and is shown to be associated with the UPR, though its detailed role is still being studied [197]. HeLa cells treated with siRNA targeting Armet were more susceptible to ER stress-induced death [193].

## Materials and Methods

### *Peptide Synthesis*

The branched amphiphilic peptides bis(Ac-FLIVIGSII)-K-$K_4$-CO-$NH_2$ and bis(Ac-FLIVI)-K-$K_4$-CO-$NH_2$ were synthesized and cleaved as previously described [160]. After cleavage, the peptides are washed with diethyl ether three times, dissolved in water, and lyophilized before storage at room temperature. The peptides were purified by reversed phase HPLC and characterized using matrix-assisted laser desorption/ionization-time of flight (MALDI-TOF/TOF).

### *Locked BAPC Preparation*

A small amount of the peptides bis($h_9$) and bis($h_5$) were individually dissolved in 2,2,2-Triuoroethanol (TFE) where they adopt a helical formation. Their concentrations were determined using molar absorptivity (ε) of phenylalanine (2 per peptide sequence) in water at 257.5 nm, (194 $cm^{-1}M^{-1}$). The absorbances were read using CARY 50 Bio UV/Vis spectrophotometer (Varian Inc., Palo Alto, CA) in a 0.3 cm path length quartz cuvette (Starna Cells Inc., Atascadero, CA). The peptides were then mixed together at an equimolar ratio to achieve a 1mM final concentration. This solution was incubated at room temperature for 10 min, followed by solvent removal under vacuum. Once the solution was completely dried, 1 mL of distilled water was added drop-wise, mixed well with a pipette, and allowed to incubate at room temperature for 30 min to form the water-filled capsules. After this incubation period the solution was placed at 4°C for 1 h to prevent capsule fusion [161], then incubated for 30 min at room temperature again before mixing with dsRNA or drying under vacuum for long term

storage. This procedure of thermal shifting creates locked BAPCs 20-30 nm in diameter which are resistant to fusion and disassembly in the presence of organic solvents [161].

### *RNA extraction and cDNA synthesis*

Seven *Tribolium* larvae, weighing 2 mg each, were homogenized using a polypropylene pestle in 1 mL of TRIZOL reagent according to the protocol supplied by the manufacturer (Invitrogen, CA, USA) to extract the RNA. DNA contamination was minimized in the RNA fraction by using a TURBO DNA-free kit, according to the protocol (Ambion, Austin, TX, USA). RNA (4 μg of DNA free) was reverse-transcribed into complementary DNA (cDNA) using the SuperScript III First Stand Synthesis System for RT-PCR (Invitrogen, CA, USA).

### *dsRNA synthesis*

The nucleotide sequences of target genes (TcBiP: XM_015982882.1; TcArmet: XM_966545.3) were obtained from the NCBI database. Gene-specific primers, including the T7 polymerase promoter sequences at the 5' end, were used to synthesize dsRNA from *T. castaneum* using the AmpliScribe TM T7 Flash Transcription Kit protocol (Cat. No. ASF3507, Epicentre Biotechnologies, USA). PCR products were separated on a 1.4% agarose gel prepared in 40 mM Tris-acetate (pH 8.3) and 1 mM EDTA. Ethidium bromide was added to a final concentration of 0.7 μg/mL before allowing the agarose to solidify. The gels were photographed under UV light and images were captured by gel documentation (UVP-Digital Imaging System, Upland, CA, USA).

### *dsRNA fluorescent dye labeling*

Armet-dsRNA was prepared as previously described. A 5' EndTag Nucleic Acid Labeling Kit (Vector Laboratories, USA) was used to incorporate a thiol functional group to the 5' ends of the unmodified dsRNA, according to the protocol. A thiol-reactive Atto633 maleimide fluorescent dye (Atto-Tec GmbH, Germany) was incorporated on the 5' ends. Upon completion of purification, the concentration was determined using nano-drop (ThermoFisher Scientific, USA), and labeling was confirmed by fluorescent measurements.

### *dsRNA-BAPC Complex Preparation*

Ten μg of dsRNA (enough for 10 insects) was added dropwise to a solution containing 200 μL of 400 μM BAPCs for a N:P ratio of 10. This solution was mixed carefully using a pipette and allowed to incubate at room temperature for 10 min before adding $CaCl_2$ (1 mM final concentration) and bringing the total volume to 400 μL using nuclease free water. This solution incubated at room temperature for 30 min before mixing it with the insect diet.

### *Tribolium castaneum Diet Preparation*

Media to feed 10 insects was prepared by mixing 100 mg Golden Buffalo flour (Heartland Mill, Inc. Marienthal, KS) with 400 μL of BAPC-dsRNA nanoparticle complexes, prepared as previously described. The flour and nanoparticle mixture was held under vacuum for approximately 15 h. When the mixture was completely dried, it was finely ground and distributed to a 96-well plate with 10 mg of flour-nanoparticle mixture in a well, for one larva. Immediately, one larva (2 mg in weight) was placed in each well containing the prepared diet. For the control group containing only dsRNA, 100 mg was mixed with 10 μg of dsRNA and 1

mM $CaCl_2$ final concentration in 400 µL for 10 insects. Other controls included 100 mg of flour mixed with 400 µL of water with and without BAPCs. Insects were kept at 30°C visual monitoring of phenotypes and for mortality.

### *Insects*

*Tribolium castaneum* (GA-1 strain) insects were reared at 30°C on wheat flour containing 5% brewer's yeast under the standard conditions as previously described [199, 200]. Larvae selected for this study were all around 2 mg in weight indicating they were around the same developmental stage.

### *Confocal Laser Scanning Microscopy*

Images shown in Figure 2.5 were captured using a confocal LSM 700 laser-scanning microscope (Carl Zeiss, Gottingen, Germany) using a 639 nm laser. Magenta color was used for ease of visualization and does not reflect true fluorescence color of Atto633 dye.

### *Size and Zeta Potential of Complexes*

Size and zeta potential were measured using a Malvern ZetaSizer (2000) instrument (Malvern Instruments, Malvern, UK). Samples were prepared in water at 25°C with 1 µg of dsRNA and varying concentrations of BAPCs (10-80 µM) or with BAPCs alone (80 µM). Data is representative of five samples and is shown as mean ± standard deviation, unless otherwise noted.

### *Fluorometric Thiol Detection*

A thiol fluorometric detection kit (Kit-0816, Creative BioMart, New York, USA) was used to detect free thiol based on fluorescence resulting from complexion with a non-fluorescent dye according to the protocol. Fifty µL of reaction mixture containing green dye and assay buffer was added to each well in a black 96-well plate, followed by 50 µL of dsRNA that was processed through the thiol addition step of the 5' EndTag Labeling Kit (Vector Laboratories) or glutathione standard at various concentrations. Fluorescence was read at Ex/Em = 490/520 nm with a fluorescence plate reader (Varian Inc., Palo Alto, CA).

### *Statistical Analyses*

Statistics were performed using GraphPad Prism 8 software (GraphPad Software, La Jolla, CA). Statistical significance for DLS and ZP experiments was determined using ANOVA test followed by Bonferroni's post-test. For survival study (Appendix A) the Log-rank (Mentel-Cox) test was used.

## Results and Discussion

As previously described, BAPCs have shown the ability to facilitate uptake of plasmid DNA in several cell lines as well as in mice [163]. The success of these trials indicated the potential of using BAPCs to deliver other types of nucleic acid such as small oligonucleotides or RNA. BAPCs were examined for their ability to facilitate uptake of dsRNA through diet to enhance transcript knockdown in *Tribolium castaneum*, the red flour beetle [186]. *T. castaneum*, a common pest, is also a model organism for biochemical and cell biological processes in humans [187, 188, 189, 190, 191]. In nature they feed on broken grain kernels, typically wheat, but in the lab they are fed a diet of wheat flour with 5% w/w yeast extract. The demonstrated high RNAi efficiency, resistance to all classes of insecticides, and published genome of *T. castaneum* make them ideal for an RNAi-based insecticide [187].

Dynamic light scattering (DLS) and zeta potential (ZP) were evaluated for BAPCs alone and dsRNA-BAPC complexes of varying dsRNA to BAPC ratios. The concentration of dsRNA remained constant at 1 µg while the concentration of BAPCs ranged from 10 µM to 80 µM. DLS of unlocked dsRNA-BAPC complexes showed a range of 260-400 nm as opposed to the BAPCs alone which show 100-200 nm (Figure 2.1 A). It is hypothesized that the dsRNA wraps around several BAPCs, forming these clusters, comparable to histone compacting (Figure 2.1 C). ZP is the potential difference between the surface of a solid particle and the solvent surrounding it. Due to the negative potential of cellular membranes, a positive ZP is favored for cellular uptake. A ZP above +45 mV however, can be toxic. The ZPs for the unlocked dsRNA-BAPC complexes ranged from 30-50 mV (Figure 2.1 B). These complexes of dsRNA with unlocked BAPCs show large sizes that may be harder for the cell to uptake and ZPs higher than ideal for non-toxic cellular uptake. BAPCs which undergo a thermal cycle to prevent fusion and maintain a diameter

of 20-30 nm even in the presence of salts and chaotropes, termed locked BAPCs, were also complexed with dsRNA and evaluated for diameter and zeta potential (Figure 2.2). The concentration of dsRNA remained constant at 1 µg while the concentration of BAPCs ranged from 10 µM to 40 µM. DLS showed a range of sizes 70-300 nm (Figure 2.2 A). The ZPs for the locked dsRNA-BAPCs ranged from 10-28 mV (Figure 2.2 B) indicating that cellular uptake of the complexes is favorable, without posing toxicity risks. The dsRNA-BAPC complexes and BAPCs alone were also observed using atomic force microscopy (AFM) by a previous lab member (Figure A.1). In those images it appears the dsRNA-BAPC complexes form compact clusters varying in size (70-500 nm) and morphology, agreeing with the DLS data and the hypothesized clustering (Figure 2.1 C).

As evaluated by former lab members, feeding *T. castaneum* larvae a combination of BiP- and Armet-dsRNA complexed with BAPCs showed the highest lethality rate at 75% (n=30) with death occurring in the larval or eclosion stages (Figure A.2). Feeding adult beetles, the same mixture showed no death. During the molting phases the peritrophic membrane lining the midgut is reorganized, potentially allowing the complexes to penetrate deeper. Adult beetles no longer go through this phase and explains why oral delivery of BAPC-dsRNA complexes had no effect. To further ensure the dsRNA could cross this midgut barrier a well-studied gene, Vermillion, was also targeted. When the Vermillion gene is accurately targeted by RNAi, adult beetles lack pigmentation in their eyes. To see the expected effect when fed orally, the vermillion dsRNA must migrate from the gut to the hemolymph. Vermillion-dsRNA was complexed with BAPCs and fed to larvae as previously described. 50% (n=20) of the beetles had white eyes upon reaching adult stage. For this effect to be seen, the dsRNA must cross from the

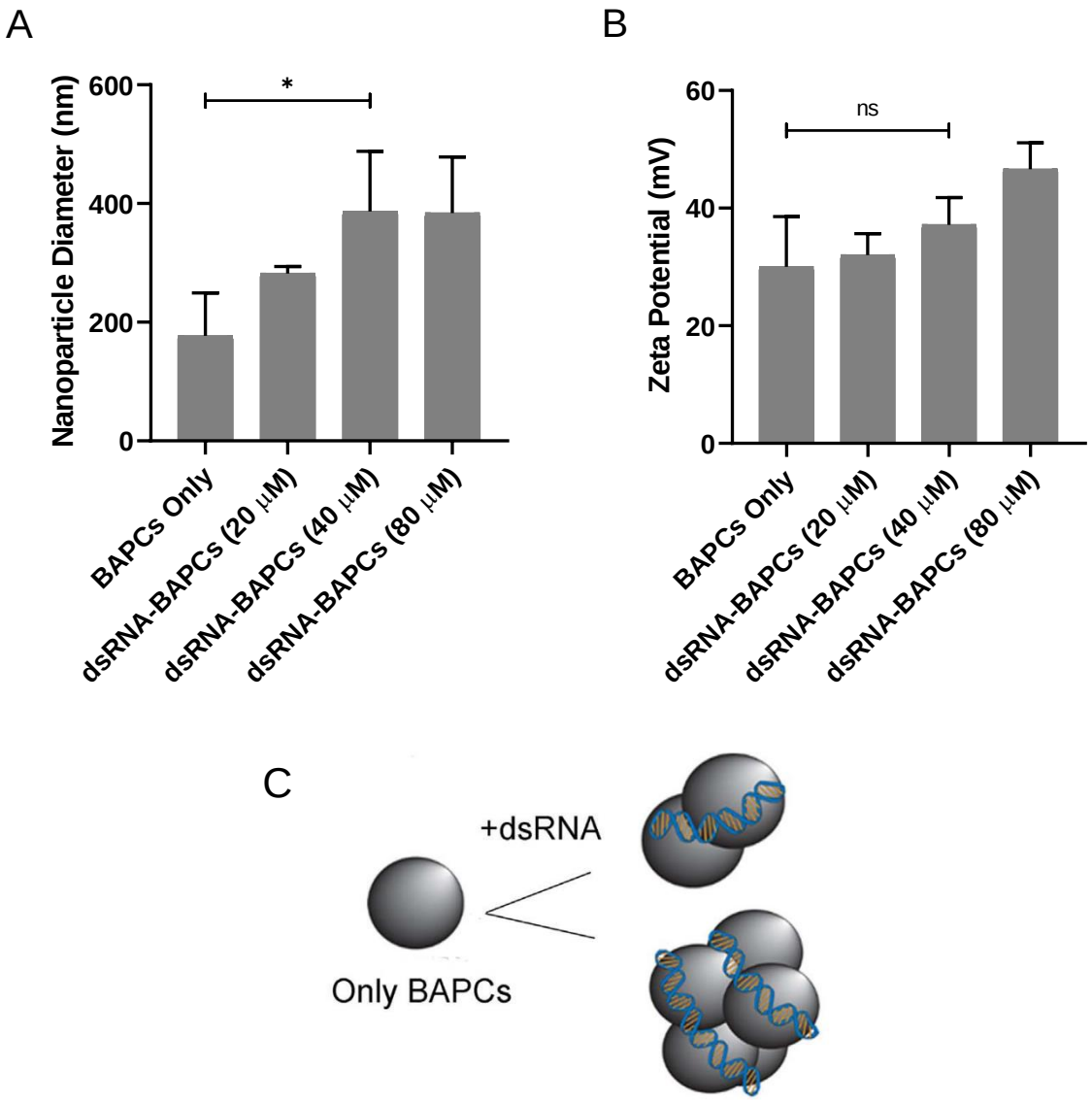


**Figure 2.1 - Dynamic Light Scattering (DLS) and Zeta Potential (ZP) Analyses for BAPCs and dsRNA-BAPC Complexes (Unlocked)**

**(A)** Size (z-average) and **(B)** zeta potential. Data are based on two independent experiments. Different formulations were tested keeping the amount of Armet-dsRNA constant (1 µg) and varying the unlocked BAPCs concentration. Differences between values were compared by one-way ANOVA using Bonferroni as post-test (N = 5). Statistical significance: (*) $p < 0.05$. Non-statistical significance (ns) was considered when $p > 0.05$. (C) Schematic representation of interaction between BAPCs and Armet-dsRNA. Image in panel C reprinted with permission from Avila, L. Adriana et al. 2018. Delivery of lethal dsRNAs in insect diets by branched amphiphilic peptide capsules. *Journal of Controlled Release* 273: 139-146. Copyright 2018 Elsevier B.V.

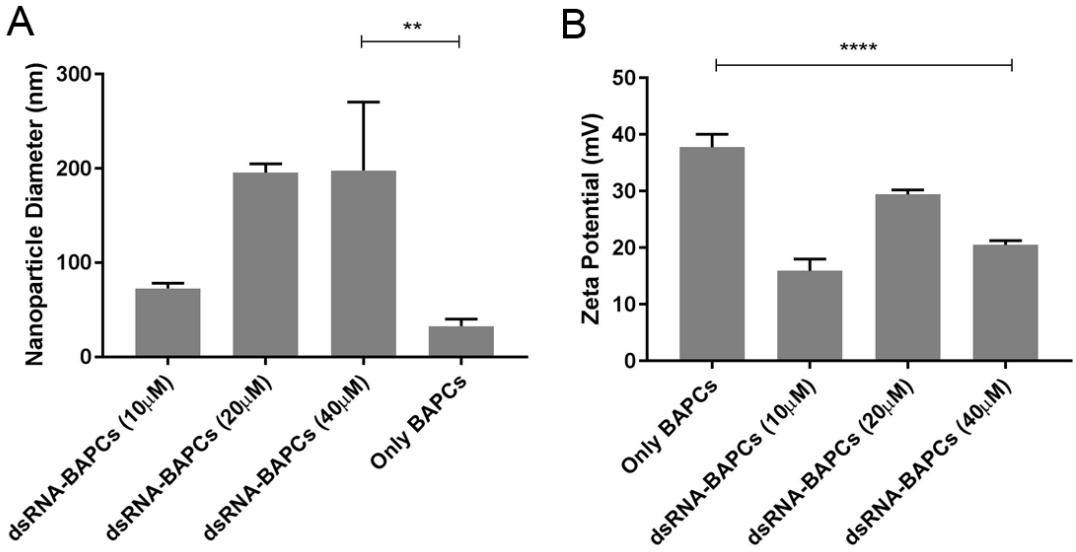


**Figure 2.2 - Dynamic Light Scattering (DLS) and Zeta Potential (ZP) Analyses for BAPCs and dsRNA-BAPC Complexes (Locked)**

Dynamic Light Scattering (DLS) and Zeta Potential (ZP) analyses for different BAPCs-dsRNA formulations. (A) Size (z-average) and (B) zeta potential. Data are based on two independent experiments. Different formulations were tested keeping the amount of Armet-dsRNA constant (1 μg) and varying the unlocked BAPCs concentration. Differences between values were compared by one-way ANOVA using Bonferroni as post-test (N = 5). Statistical significance: (**) $p < 0.01$; (****) $p < 0.0001$. Non-statistical significance (ns) was considered when $p > 0.05$. Reprinted with permission from Avila, L. Adriana et al. 2018. Delivery of lethal dsRNAs in insect diets by branched amphiphilic peptide capsules. *Journal of Controlled Release* 273: 139-146. Copyright 2018 Elsevier B.V.

gut to the circulatory system (Hemolymph). Understanding how the dsRNA can to travel from the gut to the hemolymph is crucial in further understanding systemic RNAi in *T. castaneum*.

To visualize the biodistribution of the dsRNA, a 5' EndTag labeling kit from Vector Labs was used to create Atto633-fluorescently labeled Armet-dsRNA, via thiol-maleimide chemistry. Detection of accurate fluorescent labeling was difficult due to the small maximum amount of dsRNA able to be labeled at a time (0.6 nmols). To ensure the difficulty of detection was not due to malfunction of the kit itself, a thiol fluorometric detection assay was used. This assay can detect as little as 1 picomole of free thiol in 100 μL using a proprietary non-fluorescent dye, that becomes strongly fluorescent upon reacting with thiol. This assay indicated that free thiol was present in 1.8 μM dsRNA after the thiol addition step of the 5' EndTag labeling kit at similar

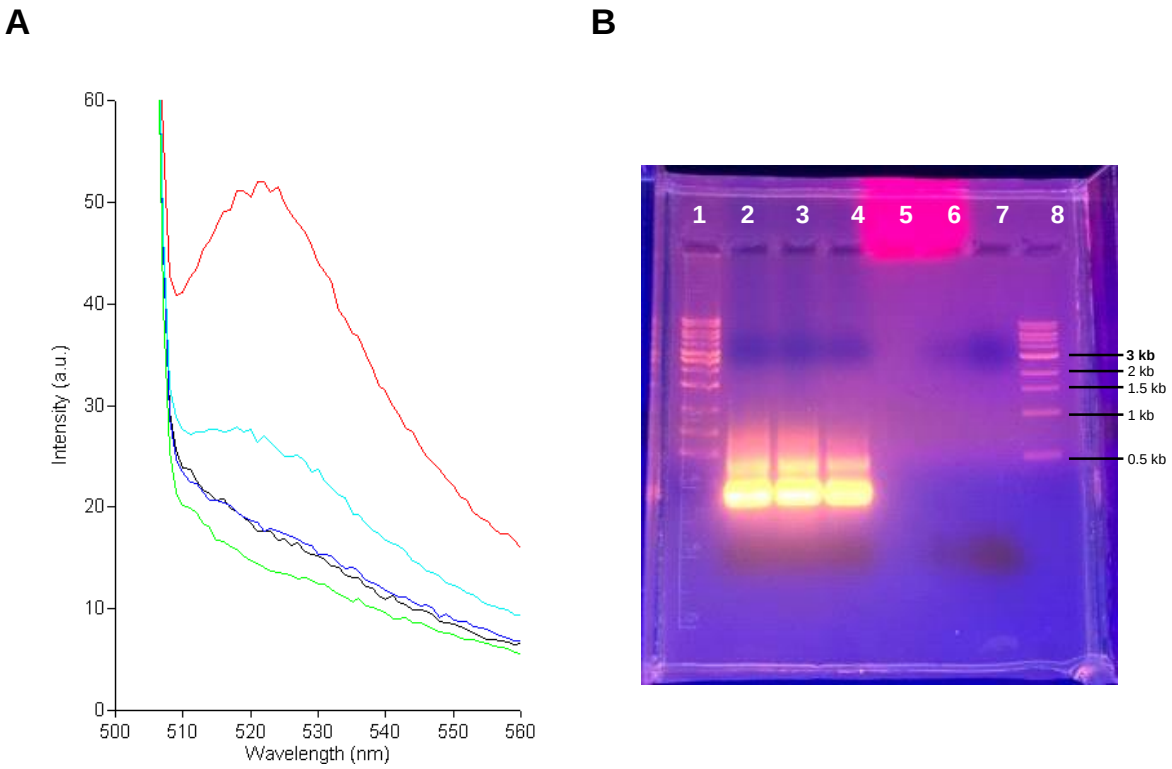


**Figure 2.3 - Thiol Fluorometric Detection Results and Free Dye Detection of Labeled Armet-dsRNA**

**(A)** Fluorescent reading from thiol fluorometric detection assay. Red - 30 µM glutathione standard; Cyan - 10 µM glutathione standard; Blue - 1.8 µM Armet-dsRNA post thiol addition from 5' EndTag Kit ; Black - 3 µM glutathione standard; Green - Blank (assay buffer and green dye alone). Ex: 490 nm. Em: 520 nm **(B)** Agarose gel. Lane 1, 1 kb DNA ladder by Oxygen; Lane 2 & 3, unlabeled Armet-dsRNA (296 bp); Lane 4, Atto633 labeled dsRNA (296 bp); Lane 5, Atto633 maleimide dye alone (1.3 mM); Lane 6, Atto633 maleimide dye (1.3 mM) with loading dye; Lane 7, loading dye alone; Lane 8, 1 kb DNA ladder by Biolabs.

levels of 3 µM glutathione (Figure 2.3 A). This would indicate approximately 2-fold as much thiol present in solution compared to the amount of dsRNA, which would be expected if each 5' end of the dsRNA was labeled. While fluorescent detection of the Atto633-labeled dsRNA did not improve after free thiol confirmation and longer incubation time of the dye at optimal temperature (25°C), the labeled dsRNA was fed to *T. castaneum* larvae complexed with and without BAPCs and visualized with confocal microscopy to determine if any fluorescence was able to be detected within the insect. To ensure excess free dye was properly removed from the labeled dsRNA solution, an agarose gel was run (Figure 2.3 B). While the weight of the dye is

small compared to the weight of the 296 bp Armet-dsRNA and is not able to be visually distinguishable in dsRNA labeled vs. unlabeled, the dye itself highly visible on the gel. These results indicate that any fluorescence detected after feeding, is likely due to dsRNA that has been covalently labeled, and not free dye. *T. castaneum* larvae were fed on a diet containing Atto633-labeled Armet-dsRNA with and without complexion with BAPCs for 24 h, dissected and visualized using confocal microscopy (Figure 2.4). These initial results showed localization of dsRNA within fat body and malpighian tubule of the larvae. Visualization of the dsRNA within Fat Body was a surprising result, as it had not been visualized as a place for dsRNA localization in previous literature, to the best of our knowledge. While imaging these larvae however, it was also noted that an infection had occurred within the colony and was highly concentrated in each insect (noted in red circle in Figure 2.4 D). This could have affected the normal physiology of the insects and could have led to the fat body location, as well as false positives throughout the study.

New colonies of *T. castaneum* were established, maintaining high level of sterility when rearing and selecting for experiments. With the healthy *T. castaneum* colonies, the experiment was repeated as described, and were visualized 8 h post feeding. Fluorescence was detected in the midgut epithelial cells, fat bodies, and Malpighian tubules of *T. castaneum* fed with dsRNA-BAPC complexes, while *T. castaneum* fed with free dsRNA alone showed little to no fluorescence in the same regions (Figure 2.5). Figure 2.5 A and D show the midgut region, with A showing the delivery of dsRNA with BAPCs and D showing the delivery of dsRNA alone. The midgut is the only area of the gut that has exposed epithelial cells and is able to transfer materials from the midgut to the hemolymph. There appears to be accumulation of dsRNA in the epithelial cells of the midgut on the top right edge shown. There is minimal fluorescence

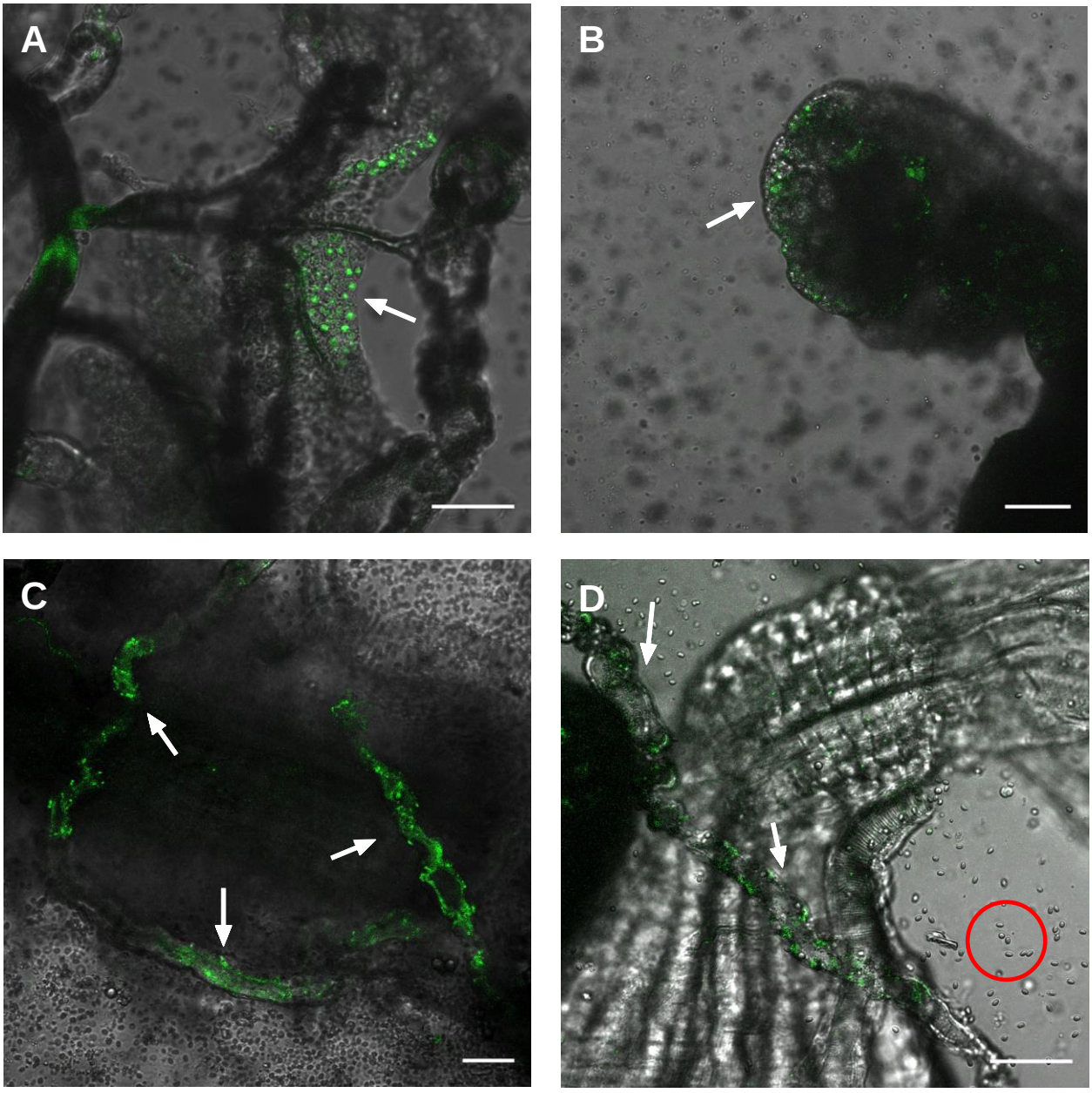


**Figure 2.4 - Localization of Fluorescently Labeled Armet-dsRNA in Infected *T. castaneum* Larvae**

Images taken after feeding. The fluorescence is shown as bright green on the bright-field background. All pictures were captured in the same condition in a LSM700 confocal microscope. (A) and (B) show fluorescently labeled Armet-dsRNA, delivered with and without BAPCs respectively, located in the fat body as emphasized by the arrows. (C) and (D) show fluorescently labeled Armet-dsRNA, delivered with and without BAPCs respectively, located in the malpighian tubule as emphasized by the arrows. While these images were taken, it was noted that the larvae seemed to be infected, highlighted by the red circle in panel D. Scale bar: 50 μm. N = 5.

detected in panel D, but there is slight coloration which would be expected as it passes through the body for excretion. Figure 2.5 B and E show fat bodies, with B showing dsRNA delivered with BAPCs and E showing dsRNA alone. The fat body in insects is involved in many metabolic functions, including the storage and release of energy [201]. It is a large organ distributed throughout the insect body preferentially surrounding the gut among other regions and provides maximal exposure to the hemolymph. Finally, Figure 2.5 C and F show the Malpighian tubule, with C showing the delivery with BAPCs and F showing the delivery sans BAPCs. Malpighian tubules act as the excretory and osmo-regulatory system, are surrounded by the hemolymph, and

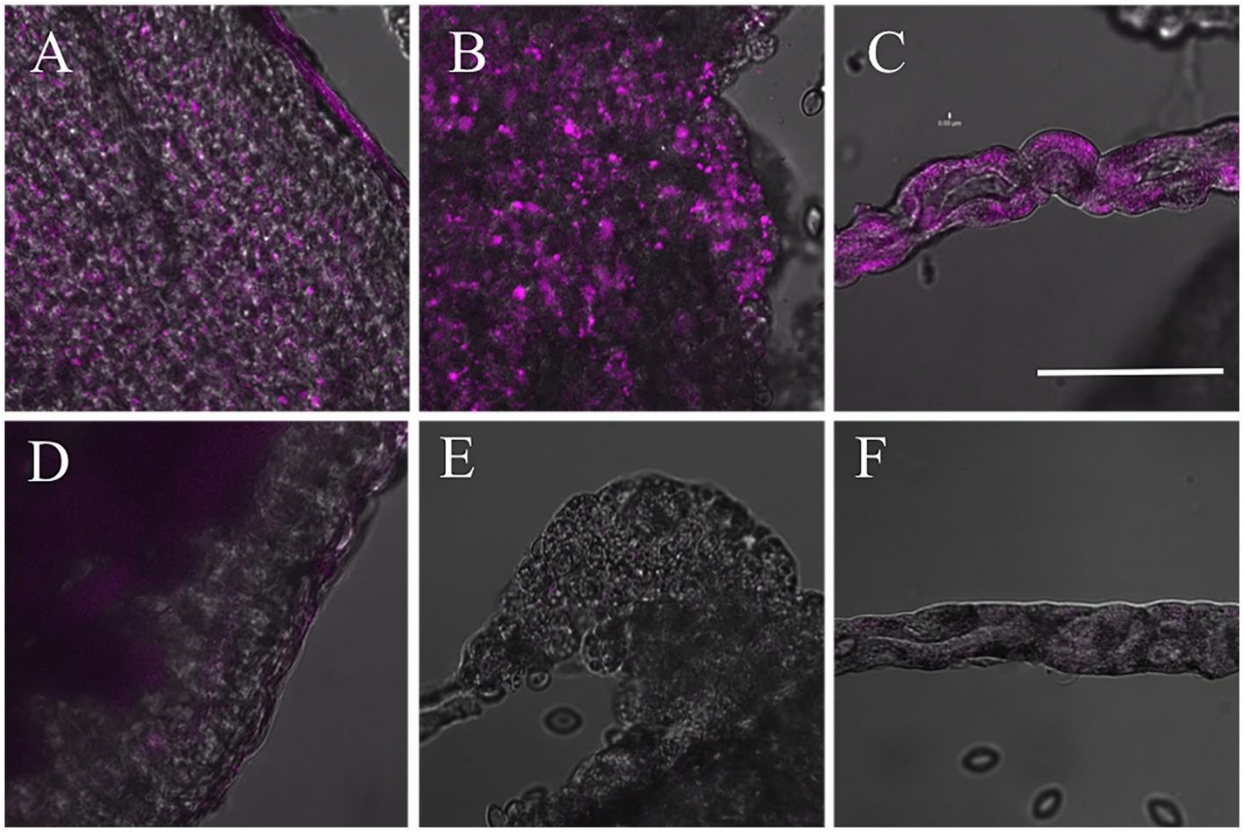


**Figure 2.5 - Localization of Fluorescently Labeled Armet-dsRNA in *T. castaneum* Larvae**

Images taken 8 h after feeding. The fluorescence is shown as magenta on the bright-field background. All pictures were captured in the same condition in a LSM700 confocal microscope. (A) midgut; (B) Fat Body; (C) Malpighian tubule; (D) to (F) are the same tissues in the *Tribolium* fed with Atto633 fluorescently labeled Armet-dsRNA alone. Scale bar: 20 μm. N = 5. Reprinted with permission from Avila, L. Adriana et al. 2018. Delivery of lethal dsRNAs in insect diets by branched amphiphilic peptide capsules. *Journal of Controlled Release* 273: 139-146. Copyright 2018 Elsevier B.V.

are in close proximity to the fat body tissue [202]. Through these results it appears the oral RNAi effects in distal tissues is mediated by the exit of dsRNA from the midgut epithelial cells to the hemolymph and then accumulate in the Malpighian tubules and fat body. These results represent the first bio-accumulation study of orally administered dsRNA associated with nanoparticles in insets and first reported accumulation in fat body ingested from diet.

## Conclusions and Future Outlook

In addition to the bioaccumulation of dsRNA, it would be beneficial to understand the bioaccumulation of BAPCs that help orally administer the dsRNA. Knowing where the BAPCs are able to locate within the insect, as well as when and where BAPCs and dsRNA disassociate from each other, would provide further insight to the systemic exposure of dsRNA in insects. While this experiment was attempted a few times, the level of detection for dye within BAPCs with the amount administered was difficult to distinguish. Further optimization of the amount of dye used, compatibility of dyes, concentration of BAPCs, and concentration of dsRNA while maintaining the N:P ratio, would be worth pursuing.

It has previously been reported that when multiple dsRNAs are injected in *T. castaneum* they compete and result in a less effective RNAi response [203]. That was not the case for this study. This may be because both genes/proteins targeted in this study were a part of the same pathway. Looking at further oral delivery studies with dual dsRNA administered as well as completing further studies in this manner can help clear up the understanding of how or why some dsRNA may compete for RNAi.

The success of *T. castaneum* lethality via oral BAPC delivery presents the opportunity for use in the field as an alternative or complementary insecticide to its chemical counterpart. This form of insecticide can be delivered by transformative RNAi or non-transformative RNAi. Transformative RNAi refers to transgenic plants, new genes inserted in nuclear DNA, and transplastomic plants, new genes inserted in chloroplasts. While these provide efficient long-term control, low consumer acceptance, extensive regulatory process, and high production cost outweigh the benefits. Non-transformative RNAi methods, which are more accepted by consumers, include trunk injection, root absorption, bacterial dsRNA, symbionts, and sprayable

dsRNA. While these methods need a continuous supply of dsRNA, they also have a low cost per tree or acre, are feasible, and non-transgenic [177]. dsRNA-BAPC complexes hold the potential to be used for non-transformative RNAi, and researching these possible methods is a crucial next step. Additionally, understanding the short- and long-term effects of dsRNA-BAPC complexes in the environment is required prior to field application, and studies have been underway. For the future research of RNAi based insecticides resistance, biosafety, and ecological safety remain high concerns that have not been fully established [185].

# Chapter 3 - Transdermal Uptake of BAP-MNB Complexes in Mice

## Introduction

The administration route for a medication should be decided upon based on the purpose as well as advantages and disadvantages for each route to achieve the highest effectiveness. [214, 204]. There are numerous drug administration routes including oral, injection (subcutaneous, intramuscular, intravenous, and intradermal), mucosal, ocular, cutaneous, and transdermal. While oral delivery is the most convenient and is usually the safest and most cost efficient, some drugs are absorbed poorly in the digestive tract or destroyed by acid and digestive enzymes in the stomach [214, 222]. Subcutaneous injection is a popular alternative for many protein-based drugs and nucleic acids which are destroyed by the digestive tract [214]. This injection method delivers medication to the fatty tissue between the skin and muscle [217, 222]. Due to the limited availability of blood vessels in this tissue, there is a slow sustained rate of absorption; slower than intravenous or intramuscular injections but faster than intradermal injections [218, 222]. Medications typically delivered subcutaneously include insulin, hormones, morphine, some vaccines, and sometimes epinephrine [217]. Intramuscular injection delivers medication deep into the muscles and is used for most vaccines [219]. Intramuscular injections are used over subcutaneous or intravenous injections when a larger volume needs to be delivered, the drugs are irritating to veins, or a suitable vein is not able to be located [214, 219]. Medications delivered intramuscularly are absorbed faster than those delivered subcutaneously due to greater blood supply but can be ineffective if not delivered to the right muscular site [219, 222]. Delivering medications directly into the vein (Intravenous) provides rapid absorption and can also be controlled to provide slow constant administration [220, 222]. While intravenous medications are more consistently and completely absorbed with minimal discomfort compared to other injection

routes, not all medications can be delivered in this way and adverse effects can happen rapidly [222]. Intradermal injections are a shallow injection into the dermis using the Mantoux Procedure which injects the needle at a 5-15° angle to the skin and must be performed by skilled medical personnel [221, 222]. This method has the longest absorption time of all parenteral routes and is often used for tuberculosis, allergy, and local anesthesia tests [222].

The skin has two main layers, the epidermis and the dermis. The epidermis is the outermost layer, acting as the physical barrier, and is composed of the stratum corneum (SC), stratum granulosum (SG), stratum spinosum (SS), and stratum basale (SB). The SC and SG together create a highly hydrophobic layer which prevents penetration of molecules larger than 500 kDa [205]. The SC of this region is the rate limiting barrier for transdermal drug diffusion due to its thickness (15-20 μm). The next layer of the skin is the dermis, which is 1-2 mm thick, and is composed of the papillary dermis, reticular dermis, and hypodermis. Hair follicles, sweat glands, blood vessels, nerve fibers, and lymphatic vessels are all embedded in the dermis and can assist in transdermal drug delivery system (TDDS) penetration by trapping nanoparticles and creating a reservoir for long-term controlled release [205]. These dermal structures also provide easy access to systemic circulation, though once they enter blood vessels for systemic circulation, crossing the endothelium of blood vessels to exit near target tissues, is a limiting factor [205].

Vaccination consists of activating the immune system with an infectious agent, or the components of the infectious agent, in a way that the host is not harmed, to build an effective immune response for potential future infections of that agent. Historically, vaccination has been accomplished by delivering specific antigens for the immune system to react with or by introducing a live mitigated infectious agent for replication within the host without causing the

disease, which presents the specific antigens to prepare the immune system [225]. More recently, the approach of delivering plasmid DNA encoding for the antigen of the infectious agent for *in situ* production and subsequent immune response has been developed and studied [225, 226, 227, 228].

The recent recognition the role skin plays in the immune system, beyond a physical barrier, has provided interest and motivation to develop vaccines that can be delivered in the skin and potentially eliminate the need for needles [216]. While vaccines are typically administered subcutaneously and intramuscularly, these tissues contain relatively few dendritic cells. The epidermis and dermis however are densely populated with antigen-presenting cells such as Langerhans cells (LCs), particularly in the epidermis [215, 249, 250, 251]. As the nucleic acid is able to enter the cytoplasm and nuclease of LCs, their activation prompts them to relocate from the epidermis to the T-cell area of the skin draining lymph nodes [249, 252]. Here they process the DNA to produce the antigen gene products and present them to T-cells to stimulate an immune response [249, 253]. This process provides potential for applications in immunotherapy and vaccine development though the skin [249, 254]. Instead of bypassing these skin immune cells via hypodermic injection, dermis injection can evoke a high immune response, and thus will require a lower vaccine dose [215]. However, the complex Mantoux Procedure, needle-phobias, and needle-associated infectious diseases push the development of needle-free skin vaccinations [216].

Transdermal administration provides a non-invasive alternative to oral and hypodermic injection for body-wide delivery through a patch on the skin [213]. This method can slowly release drugs over several hours or days but is limited by how quickly a drug can penetrate the skin [214]. Transdermal drug delivery systems (TDDS) are controlled-release devices that

contain the drug for localized treatment of tissues underlying skin, or for systemic therapy after topical application to the skin surface [205]. Nanoparticles have been in the spotlight for transdermal delivery systems in the past few decades [234, 249, 255, 256, 257, 258]. Compared to other TDDS, nanoparticles show superior drug release, deeper penetration, and allow encapsulation of both hydrophilic and hydrophobic compounds [205, 259]. Transdermal drug exposure has several advantages over other routes. When delivered transdermally, the first-pass effect in the liver caused by oral exposure is avoided. This delivery method also decreases demand for multiple doses due to the long-term controlled release and increased compliance in patients has be observed [205].

Nanoparticles can penetrate the skin through three pathways: intercellular lipid route, transcellular route, and follicular route (Figure 3.1). The intercellular route (Figure 3.1A) travels between corneocytes in the SC. Enhancers such as dimethyl-sulfoxide (DMSO) are used to accelerate drug penetration through reducing diffusional resistance to the lipid bilayer making the SC more permeable to externally applied solutes, which is a reversible effect [211, 212]. The

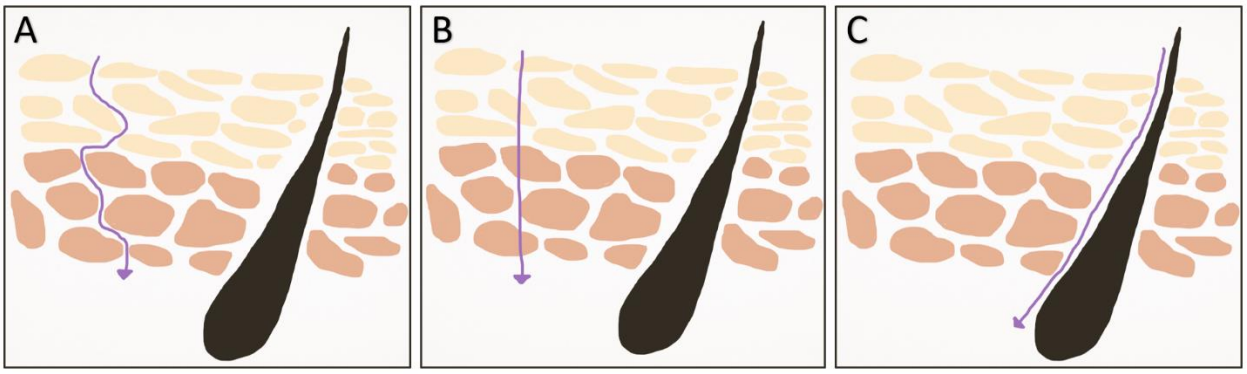


**Figure 3.1 - Simplified Representation of Nanoparticle Penetration Routes**

(A) Intercellular lipid route through the lipid bilayers. (B) Transcellular route through keratin-rich corneocytes. (C) Follicular route, also known as the shunt pathway, through hair follicles and sweat ducts. The light tan objects in the images represent Corneocytes as part of the Stratum Corneum, which is 10-20 µm thick. The darker tan objects represent Keratinocytes in the Epidermis, which is 50-100 µm thick. The large black structure represents a hair follicle and the purple arrows represent the respective transport routes.

transcellular route (Figure 3.1B) travels intracellularly through corneocytes, rather than around them. To accomplish this route the compound must pass through alternating hydrophilic (interior of cells) and hydrophobic (extracellular matrix) regions, which is unfavorable for most drugs [205]. The follicular route (Figure 3.1C) travels though dermal structures via follicular penetration. These dermal structures, which include hair follicles and sweat glands, make up less than 0.1% of the cutaneous surface, making them historically disregarded as a potential transdermal drug delivery route [205]. Recent studies on the follicular pathway have provided evidence that this pathway can provide accelerated transport due to the proximity to capillary vessels [223]. Additionally, these transdermal structures can function as a reservoir for nanoparticles (up to 2 mm into the skin) and can be manipulated for controlled release to provide a pathway for systemic delivery [205, 260]. Variations in efficiency and proposed advantages have been observed for this route, likely due to the range in density of follicles [205].

The size, size distribution, zeta potential, and surface properties influence efficiency for nano-based delivery [205]. The sulfated proteoglycans on the surface of the skin cells create a large negative charge, making positively charged nanocarriers prime candidates for penetration through electrostatic interactions over negatively charged or neutral nanocarriers [204, 205]. Size dependence for transdermal delivery is debated among researchers. Small nanoparticles (10 nm) have been shown to passively penetrate the skin, while a much larger size range of 122-1000 nm were tested on porcine ear skin *in vitro*, with a 643 nm size showing the deepest follicle penetration [224]. Once nanocarriers cross the skin barriers, the immune system recognizes them and tries to clear them as fast as possible. Surface modification such as PEGylation of nanoparticles, in which the surface is coated in polyethylene glycol, have shown to generate a "stealth" effect to avoid the immune system and increase the circulatory half-life [25].

Nanocarriers that can facilitate systemic transdermal delivery, while carrying nucleic acid could provide a potential non-invasive route for DNA vaccinations and gene delivery for wound healing, skin cancers, and skin diseases [206, 229, 230, 231]. Gene therapy via skin delivery can address lack of targeted delivery of genes to diseased sites and cells, degradation of genes during delivery, and fast clearance in circulation, which are common challenges. The skin is also highly immunogenic, making it an ideal target for highly efficient vaccinations [206, 215]. In addition to this, transdermal delivery can be pain free with high efficiency and low side effects [206]. Transdermal delivery of nucleic acids can be categorized into physical, including microneedles and microporation; active, including electroporation, iontophoresis, and sonophoresis; and passive, including polymeric nanoparticles, liposomes, peptides, and dendrimers [231]. Several passive approaches such as viral vectors, cell penetrating peptides, liposomes, dendrimers, gold nanoparticles, and carbon nanotubules have been show to effectively delivery nucleic acid through skin delivery [206, 232, 233, 234, 235, 236].

BAPCs were previously shown to deliver a DNA vaccine that encodes the HPV-16 E7 oncoprotein effectively through intramuscular inoculation in mice [164]. If BAPCs can passively cross the skin barrier, they could provide an alternative DNA vaccination or gene therapy delivery route. For this pilot study, magnetic nanobeads (MNBs) were coated with a bilayer of h9 peptides to mimic standard BAPC formation and allowed to interact with the skin surface of a mouse to determine if they were able to penetrate the skin barrier and systemically circulate. The MNB core allowed for ease of recovery from the tissue samples.

## Materials and Methods

### *Peptide Synthesis*

The branched amphiphilic peptides bis(Ac-FLIVIGSII)-K-$K_4$-C-$CONH_2$, bis(Ac-FLIVIGSII)-K-$K_4$-$CONH_2$, and bis(Ac-FLIVI)-K-$K_4$-$CONH_2$ and were synthesized and cleaved as previously described [160]. After cleavage the peptides were washed with diethyl ether three times, dissolved in water, and lyophilized before storage at room temperature. The peptides were purified by reversed phase HPLC and characterized using matrix-assisted laser desorption/ionization-time of flight (MALDI-TOF/TOF).

### *BAPC Formation with Atto633 Fluorescent Dye*

A small amount of the peptides bis($h_9$) and bis($h_5$) were individually dissolved in 2,2,2-Triuoroethanol (TFE), where they adopt a helical formation. The concentration was determined using molar absorptivity of phenylalanine in water at 257.5 nm, ($\varepsilon$ = 194 $cm^{-1}M^{-1}$), noting that there are 2 phenylalanines present in each peptide. The absorbances were read in a 0.3 cm path

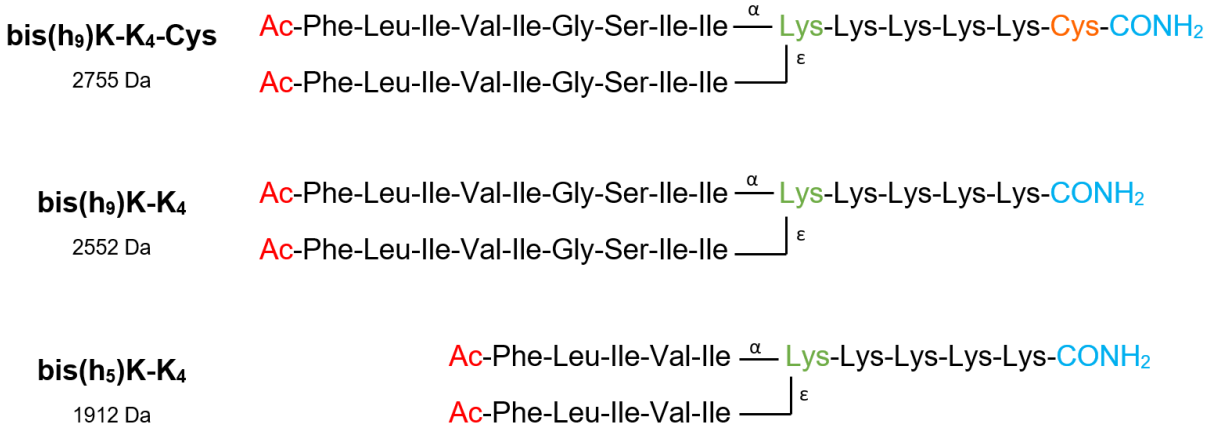


**Figure 3.2 - Sequence of $h_9$-Cys, $h_9$, and $h_5$ peptides**

Sequences of the self-assembling branched peptides $h_9$-Cys, $h_9$, and $h_5$. The peptides are N-terminal acetylated (Red), with the branch point lysine (green) with branches coming off the α-amino group of the N-terminus and the ε-amino group of the side chain.

length quartz cuvette (Cary UV/Vis Spectrophotometer, Varian, Inc. Palo Alto, CA, USA). The peptides were then mixed together at an equimolar ratio to achieve a final concentration of 1 mM in 1 mL. This solution was incubated at room temperature for 10 min, followed by solvent removal under vacuum. Once the peptides were completely dried, 1 mL of 1.5 mM Atto633 fluorescent dye (Atto-Tec GmbH, Germany) in water was added drop-wise, mixed well with a pipette, and incubated at room temperature for 30 min to allow the peptides to form dye-filled capsules. After this incubation period the solution was incubated at 4°C for 1 h to prevent capsule fusion, then incubated at room temperature again for 30 min prior to use [161].

Upon completion of all incubation times, the solution was passed through a 0.22 μm polytetrafluoroethylene syringe-driven filter (EMD Millipore, Billercia, MA) and placed in an Amicon ultra-0.5 mL centrifugal cellulose filter with 30 kDa molecular weight cut-off (eMD Millipore, Billerica, MA) and centrifuged at 13,500 x g for 5 min in an Eppendorf D benchtop centrifuge.

### *BAP-MNB preparation*

BAP-MNBs were prepared by Pavithra Natarajan. The 200 nm Super Mag Maleimide Activated NanoBeads lyophilized powder (Ocean Nanotech, San Diego, CA) contains 1 mg of Magnetic NanoBeads (MNBs) per 20 mg of lyophilized powder, i.e. 5% w/w of the beads. 1 mg MNBs contains $3x10^{10}$ beads. 5 mg of MNBs were suspended in 10 mL of 0.1 M HEPES buffer (pH 7.5). The mixture was vortexed well until the beads were completely suspended in solution, with 75% ethanol. 6 μmoles of $h_9$-Cys peptide were added to the solution in small increments, vortexing between each addition to ensure proper dispersion and maximum available surface binding sites and placed on a shaker overnight at room temperature. After the overnight

incubation at room temperature, the solution was placed in a magnetic separation rack (1 Tesla, Permagen Labware, Peabody, MA, USA) for 2 h, followed by two washed to remove excess peptides and resuspended in TFE. Twelve μmoles of $h_9$ peptide were added to the solution, vortexed, and placed in a sonicator for 5 min, followed by magnetic separation and resuspension in water. The solutions were placed in the magnetic separation rack (source) for another 10 mins, collected, and incubated at 4°C overnight. Following overnight incubation, the BAP-MNBs solution was sonicated and filtered through a sterile 0.22 μm syringe filter (EMD Millipore, Billercia, MA). The concentration of BAP-MNBs was then calculated using the Ferene-s assay Reference.

### *BAP-MNB DMSO Working Solution Preparation*

A 1 L 0.85% normal saline solution was prepared in deionized water. This solution was passed through a sterilization filter (EMD Millipore, Billercia, MA) and kept at 4°C maintaining sterile techniques. BAP-MNBs ($5x10^9$ particles) suspended in saline, prepared as previously described, was brought to a final volume of 1 mL containing 0.1% DMSO. This solution was incubated at room temperature for 30 min and remixed by inversion immediately prior to use, to ensure adequate dispersion.

### *Mice*

Male mice (C57BL/6, 8-10 weeks old) were obtained from Jackson Laboratories and maintained in the Division of Biology at Kansas State University. All mice were kept in a 12 h, light to dark, temperature-controlled room and allowed food and water ad libitum. All mice were housed in a specific pathogen free facility. All research was approved by the Institutional Animal

Care and Use Committee (IACUC) and conducted in cooperation with the Animal Welfare Act and other federal statues and polices that concern the animals.

### *Exposure and Conditions*

Individually, a mouse was placed in a modified 50 mL tube, where the tip was removed to allow the mouse to breath and a hole was created in the lid to allow the tail to be exposed outside of the tube, to restrain the mouse while the tail was exposed to 1 mL of the BAP-MNBs solution, prepared as previously described, for the given exposure time (Figure 3.3). After exposure the mouse was returned to its cage for an incubation period of 1 h, 8 h, or 24 h, to allow the BAP-MNBs to circulate. After this incubation period the mice were euthanized by $CO_2$ exposure followed by cervical dislocation. The kidney, spleen, large left liver lobe, and right lung were removed, and feces were extracted from the rectum. Samples were immediately placed in at -80°C and stored for up to two weeks prior to analysis.


**Figure 3.3 - Apparatus Used for Administering BAP-MNB Solutions**

A hole was created at the tip of the tube, to allow airflow and for the mouse to breath, and in the lid to allow for the tail to protrude from the tube. The tail was able to be placed in 1 mL of the BAP-MNBs solution for the given exposure time while the mouse was restrained. The binder clips seen in the image prevented the tube from rolling with the mouse movements.

There were four exposure times in which the tail was dipping in the BAP-MNB solution (1 min, 5 min, 15 min, and 30 min), with an additional exposure time of 30 minutes for a solution without DMSO, and three incubation periods (1 h, 8 h, and 24 h) prior to tissue collection, which were all performed

in triplicate, except for one group which was only able to be performed in duplicate due to a premature death (Table 3.1)

| Method | Exposure Time | Incubation time within body before recovery | Mice per treatment |
|---|---|---|---|
| 0.1% DMSO | 1 min | 1 h | 2 |
| | | 8 h | 3 |
| | | 24 h | 3 |
| | 5 min | 1 h | 3 |
| | | 8 h | 3 |
| | | 24 h | 3 |
| | 15 min | 1 h | 3 |
| | | 8 h | 3 |
| | | 24 h | 3 |
| | 30 min | 1 h | 3 |
| | | 8 h | 3 |
| | | 24 h | 3 |
| No DMSO | 30 min | 1 h | 3 |
| | | 8 h | 3 |
| | | 24 h | 3 |

**Table 3.1 - Summary of Experimental Groups**

There are four exposure times (1 min - 30 min) for dipping the mouse tail in a solution containing BAP-MNBs in 0.1% DMSO as well as a control group with an exposure time of 30 min in a solution containing BAP-MNBs without DMSO. Each exposure time was followed by circulatory times of 1 h, 8 h, or 24 h and 3 trials were performed for each set of conditions.

### *MNB Acquisition and Quantification*

Organ and fecal samples were removed from -80°C and allowed to thaw at room temperature for 30 min. Individually, the samples were homogenized using a glass homogenizer in 1mL of a solution containing 4% SoluLyse-M (Genlantis, San Diego, CA, USA) in Normal Saline. The samples were then placed on a ~1 Tesla magnetic separator (Permagen Labware, Peabody, MA, USA), washed 3 times with normal saline and stored at -20°C for up to 1 week.

### *MNB Quantification/ Ferene-S Assay*

The iron present in the samples after magnetic separation, was quantified according to the protocol by Hedayati et al. [207]. Samples were placed in a white 96-well plate and the absorbances were read using Bio-rad model 680 microplate reader (Bio-rad, USA) at 600 nm. The standards were graphed and used to calculate the μg/mL of iron in each sample. Using the information that each magnetic nanobead contains $1.04x10^{-8}$ μg of iron, the μg/mL of iron data was converted into the number of magnetic nanobeads (Table A.3). These were then normalized based on the weight of the sample the beads were extracted from (Table A.4).

### *Tail Sectioning*

One mouse from each condition of 15 min exposure - 1 h incubation, 15 min exposure - 8 h incubation, and 15 min exposure - 24 h incubation, were administered a solution that contained BAP-MNBs as well as Atto633 encapsulated BAPCs. The tails from these mice were removed at the same time as the other tissue samples and immediately placed in 4% formalin with an overnight incubation at 4°C. After overnight incubation, the tails were transferred to 70% ethanol and stored at 4°C. These samples were submitted to the Histopathology lab as part of the Kansas State Veterinary Diagnostic Laboratory where they were subjected to decalcification of the tailbone using 10% HCL, paraffin embedded, cross-sectioned, and placed on a slide for confocal visualize or Prussian blue staining.

### *Prussian Blue Staining of Cells for Visualization of MNBs within Cells*

Potassium Ferrocyanide is used to stain the magnetic iron nanobeads, to visualize them within cells. Fresh stain is prepared by mixing equal volumes of 10% Potassium Ferrocyanide

solution (5 g in 50 mL deionized water) and 20% HCl (10 mL HCl to 50 mL deionized water). One mL of fresh acidified potassium ferrocyanide solution is added to the slide, allowed to incubate at 37°C for 30 min. The stain is then aspirated out and the tail section was washed with deionized water to remove excess stain. The tail sections were then imaged using a light microscope at 45x magnification and a Nikon lens attached to the eyepiece for capturing images. The MNBs are visualized as Prussian blue aggregates within cells (Figure B.2).

### *Confocal Laser Scanning Microscopy*

Images shown in Figure 3.3 and Figure 3.6 were captured using a confocal LSM 700 laser-scanning microscope (Carl Zeiss, Gottingen, Germany) using a 639 nm laser. Green color was used for ease of visualization and does not reflect true fluorescence color of Atto633 dye.

### *Statistical Analyses*

Statistics were performed using IBM SPSS Statistics software (Version 25, IBM Corporation, Armonk, NY). Statistical significances for 1 h, 8 h, and 24 h incubation period data were determined using a two-way ANOVA test followed by Bonferroni's post-test. Data are mean ± standard error, unless otherwise stated.

A two-way ANOVA was conducted to examine the effects of exposure time and tissue location on number of MNBs for a 1 h incubation period. Each exposure time was completed in triplicate, except for the exposure time of 1 min which was only able to be completed in duplicate. Residual analysis was performed to test for the assumptions of the two-way ANOVA. There were no outliers are assessed by inspection of a boxplot. The assumption of normality, as assessed by Sharpio-Wilk's test, was satisfied for group combinations of exposure time and

tissue location ($p > 0.05$) except for the following combinations which violated the assumption of normality ($p < 0.05$): 15 min exposure in feces, 30 min exposure in liver, 30 min exposure in lungs, 30 min exposure in feces, 30 min exposure without dmso in lungs and 30 min exposure without dmso in feces. Transformation did not address this problem. The assumption of homogeneity of variances was violated, as assessed by Levene's test for equality of variances, $p < 0.0005$). Transformation did not address this problem and the two-way ANOVA was carried out regardless due to the equal group sample sizes. The interactions effect between exposure time and tissue location on number of MNBs was not statistically significant, $F(2,52) = 0.500$, $p = 0.934$, partial $\eta 2 = 0.151$. Therefore, an analysis of the main effect for exposure time was performed, which showed statistically significant main effect of exposure on MNBs, $F(1,52) = 1.414$, $p = 0.245$, partial $\eta 2 = 0.112$. An analysis of tissue location also showed no statistically significant main effect of tissue on MNBs, $F(1,52) = 1.160$, $p = 0.341$, partial $\eta 2 = 0.093$.

A two-way ANOVA was conducted to examine the effects of exposure time and tissue location on number of MNBs for an 8 h incubation period. Each exposure time was completed in triplicate. Residual analysis was performed to test for the assumptions of the two-way ANOVA. There were no outliers are assessed by inspection of a boxplot. The assumption of normality, as assessed by Sharpio-Wilk's test, was satisfied for group combinations of exposure time and tissue location ($p > 0.05$) except for the following combinations which violated the assumption of normality ($p < 0.05$): 1 min exposure in lungs, 5 min exposure in kidney, 30 min exposure in spleen, 30 min exposure in liver, 30 min exposure in lungs, 30 min exposure without DMSO in kidney. Transformation did not address this problem. The assumption of homogeneity of variances was violated, as assessed by Levene's test for equality of variances, $p < 0.0005$). Transformation did not address this problem and the two-way ANOVA was carried out

regardless due to the equal group sample sizes. This should be considered when interpreting the results. There was a statistically significant interaction between exposure time and tissue location on number of MNBs, $F(2.52) = 2.781$, $p = 0.003$, partial $\eta 2 = 0.471$. Therefore, an analysis of simple main effects for exposure time was performed with statistically significance receiving a Bonferroni adjustment and being accepted at the $p < 0.025$ level. There was a statistically significant difference in mean number of MNBs for location in spleen with 1 min, 5 min, 15 min, 30 min, and 30 min without DMSO exposure times, $F(2,52) = 14.387$, $p < 0.0005$, partial = 0.535. All pairwise comparisons were run for each simple main effect with reported 95% confidence intervals and p-values Bonferroni-adjusted within each simple main effect. Mean number of MNBs for spleen location after 1 min, 5 min, 15 min, 30 min, and 30 min without DMSO exposure times were 4.35E9 ± 4.32E9, 2.34E9 ± 1.37E9, 1.31E10 ± 1.02E10, 3.40E8 ± 5.89E8, and 6.58E8 ± 1.01E9, respectively. 15 min exposure time had a statistically significantly higher mean number of MNBs than 1 min exposure, 8.72E9 (95% CI, 2.99E9 to 1.45E10), $p < 0.0005$, 5 min exposure, 1.07E10 (95% CI, 5.00E9 to 1.65E10), $p < 0.0005$, 30 min exposure, 1.27E10 (95% CI, 7.00E9 to 1.85E10), $p < 0.0005$, and 30 min exposure without DMSO 1.24E10 (95% CI, 6.68E9 to 1.82E10), $p < 0.0005$. Mean number of MNBs after 15 min exposure in the kidney, spleen, liver, lung, and feces tissues were 1.02E9 ± 1.49E9, 1.31E10 ± 1.02E10, 3.20E8 ± 1.95E8, 1.68E9 ± 1.13E9, and 1.03E9 ± 1.11E9 respectively. Spleen tissue had a statistically significantly higher mean number of MNBs than kidney tissue, 1.21E10 (95% CI, 6.32E9 to 1.78E10), $p < 0.0005$, liver tissue 1.28E10 (95% CI, 7.02E9 to 1.85E10), $p < 0.0005$, lung tissue, 1.14E10 (95% CI, 5.66E9 to 1.71E10), $p < 0.0005$, and feces, 1.20E10 (95% CI, 6.31E9 to 1.78E10), $p < 0.0005$.

A two-way ANOVA was conducted to examine the effects of exposure time and tissue location on number of MNBs for a 24 h incubation period. Each exposure time was completed in triplicate. Residual analysis was performed to test for the assumptions of the two-way ANOVA. There were no outliers are assessed by inspection of a boxplot. The assumption of normality, as assessed by Sharpio-Wilk's test, was satisfied for group combinations of exposure time and tissue location ($p > 0.05$) except for the following combinations which violated the assumption of normality ($p < 0.05$): 5 min exposure in spleen, 5 min exposure in liver, 15 min exposure in spleen, 30 min exposure in spleen, 30 min exposure in lungs, 30 min exposure without DMSO in spleen, 30 min exposure without DMSO in feces. Transformation did not address this problem. The assumption of homogeneity of variances was violated, as assessed by Levene's test for equality of variances, $p < 0.0005$). Transformation did not address this problem and the two-way ANOVA was carried out regardless due to the equal group sample sizes. The interactions effect between exposure time and tissue location on number of MNBs was not statistically significant, $F(2,52) = 0.720$, $p = 0.761$, partial $\eta 2 = 0.187$. Therefore, an analysis of the main effect for exposure time was performed, which showed statistically significant main effect of exposure on MNBs, $F(1,52) = 1.348$, $p = 0.265$, partial $\eta 2 = 0.097$. An analysis of tissue location also showed no statistically significant main effect of tissue on MNBs, $F(1,52) = 1.416$, $p = 0.242$, partial $\eta 2 = 0.102$.

## Results and Discussion

Initial work performed by a former lab member looked at the potential transdermal uptake of BAPCs in mouse tails that had been obtained from deceased mice. The tails were subjected to dipping in a solution containing 0.1% DMSO with 100 μM of BAPCs encapsulating Atto633 fluorescent dye. These tails were dipped in the solution for four short durations of time: 1 s, 5 s, 10 s, and 20 s in triplicate. These samples were then paraffin embedded and cross sections were prepared for visualization via confocal microscopy. Fluorescence was seen at the epidermis and in hair folicles for these initial exposures, indicating the potential for BAPCs to penetrate transdermally when delivered to a mouse with an active metabolism and circulatory system. Autofluorescence is often seen in hair follicles as well, so to determine if there was a true transdermal interaction further studies in live mice were performed.

The nanoparticles for this study are modified versions of the previously discussed traditional hollow BAPCs. Instead, these nanoparticles contain a 200 nm mangnetic nanobead (MNB) core, surrounded by a dual layer of the branched amphiphilic peptide $h_9$, mimiking the

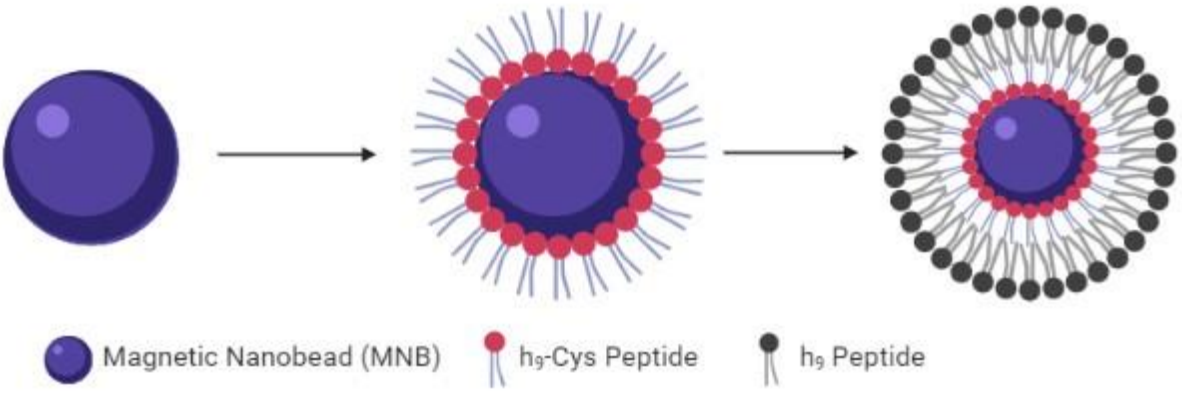


**Figure 3.4 - Schematic of BAP-MNBs Formation**

Simplified schematic of BAP-MNBs formation. A 200 nm MNB is first coated in a layer of $h_9$-Cys peptides, where the red dot indicates the cysteine residue on the C-terminus of the branched amphiphilic peptide. Next $h_9$ peptides are added to form the bilayer of amphiphilic peptides around the MNB. Peptides are not to scale. Created with biorender.com.

peptide bilayer of hollow BAPCs (Figure 3.4). The first layer consists of the $h_9$-Cys peptides, where an additional cysteine thiol is at the C-terminus of the sequence (Figure 3.2), which are directly bound to the MNB using thiol-maleimide interaction chemistry. The thiol group of the cysteine reacts with the maleimide adduct on the surface of the MNB and forms a covalent bond, covering the surface of the MNBs in a layer of $h_9$-Cys peptides where the brached N-terminuses are exposed. Additional $h_9$ peptides are added to form the bilayer of peptides as previously described (Figure 3.4). These nanoparticles will be referred to as branched amphiphilic peptide-magnetic nanobeads (BAP-MNBs). BAP-MNBs are useful for this study as they circulate through the body similarly to a BAPC due to the boundary peptide bilayer, but are easily separated one released from the tissues using a strong neodymium magnet. These nanoparticles were designed in the same fashion as BAP-AuNPs as described in Natarajan et al. [248].

For further studies in passive transdermal uptake, a range of exposure and circulatory times were studied. There were four exposure times (1 min - 30 min) for dipping the mouse tail in a solution containing BAP-MNBs in 0.1% DMSO as well as a group with an exposure time of 30 min in a solution containing BAP-MNBs without DMSO. Each exposure time was followed by three different incubation times (1 h, 8 h, and 24 h) prior to tissue collection, to allow the MNBs to enter the bloodstream and accumulate in different tissues. DMSO was used as an enhancer for uptake as previously described, at a concentration of 0.1% in saline, due to the potential toxicity at higher concentrations for transdermal use [237, 238, 239]. The average number of MNBs per gram of tissue, was calculated based on the iron content that was captured by the magnetic separator (Table B.3) and grouped by incubation time and tissue in Figures 3.5 - 3.7. On average 1 mL of blood will contain 0.5 mg of iron, which equates to approximately 8-12 ng of iron per red blood cell [261, 262]. Some tissues such as the spleen and liver also have a

high iron concentration, and thus it is important to separate endogenous iron from the BAP-MNBs using the magnetic separation rack [270]. If there was excess iron captured by the magnetic separator, the samples with a higher red blood cell content could result in higher levels of iron detected, however no studies have shown magnetic separation racks to be able to capture endogenous iron. If BAP-MNBs are able to enter the bloodstream, and potentially become entrapped, tissue samples with higher blood content would reflect higher levels of MNBs detected. Further studies to clarify the baseline level of iron present, the background detected by the ferene-s assay, as well as the ability of BAP-MNBs to enter and/or exit the circulatory system would provide further insight.

The size of nanoparticles is a key factor in the biodistribution and clearance route taken. Small nanoparticles (less than 30 nm in diameter) have been shown to be rapidly cleared by renal excretion [240, 241, 242] . This is due to the small pore sizes in the renal corpuscles which help filter the blood to produce urine. Adversely, larger nanoparticles (150-300 nm in diameter) are rapidly taken up by the mononunclear phagocytic system cells and accumulate in the liver and spleen. [208, 243, 240, 244]. Some studies have shown that medium sized nanoparticles (30-150 nm) are also taken up by the mononuclear phagocytic system cells in bone marrow, heart, kidney, and stomach [240, 245, 246]. If these size-dependent clearance routes are true for all nanoparticles, 200 nm BAP-MNBs that were able to enter the circulatory system would be expected to accumulate the most in the liver and spleen.

The average number of MNBs per gram of tissue for 1 hour incubation, post exposure are summarized in Figure 3.5 with three animals per treatment, with exception of 1 min exposure which consisted of two animals, due to a premature death before the study. The number of detectable MNBs recovered fell within the range of $10^6$-$10^{11}$ MNBs per gram of sample tissue

for each exposure time (1-30 min), with or without DMSO, and for each tissue type, while some samples showed no detectable levels of MNBs. From these trends, for a 1 h incubation time, the exposure time does not seem to strongly influence the number of MNBs that are able to penetrate or the locatoin of MNBs among the tissues assessed. It is important to note that the group which was treated with a BAP-MNBs solution without DMSO, shows comparable levels of MNBs present in all tissue types, and thus DMSO does not appear to be significant for the transdermal penetration of BAP-MNBs. The higher levels of MNBs within the feces samples, could indicate that a large portion of MNBs are already being excreted after only 1 h of circulation.

The interaction effect between the tissue location of the MNBs and the exposure time on the number of MNBs detected with a 1-hour incubation period was determined to not be statistically significant as assessed by a two-way ANOVA. Further analysis of the main effects for tissue location and exposure time both showed no statistically significant effect on the number of MNBs detected. The main effect is the overall measure of effect of one factor on the dependent variable, ignoring the other factor: the effect of tissue location on the number of MNBs, ignoring the exposure time and the effect of exposure time on the number of MNBs, ignoring tissue location. This analysis was carried out due to no statistically significant interaction effect on the number of MNBs between the two variables.

The average number of MNBs per gram of tissue for 8 h incubation post exposure are summarized in Figure 3.6. The number of detectable MNBs fell within the range of $10^{7}$-$10^{11}$ MNBs per gram of sample tissue for each exposure time (1-30 min), with or without DMSO, and for each tissue type. Some samples did not contain detectable levels of MNBs. This range of MNBs is much more diverse than that of the 1 h incubation time. There is an increase in the number of MNBs located in the spleen for lower exposure times (1-15 min), while there seems to

be a decrease in the number of MNBs located in the liver for a 1 min exposure time, as compared to 1 h incubation time. The increased accumulation in the spleen indicates that MNBs could be localized to the spleen as early as 1 h post exposure and continue to accumulate 8 h post exposure. The lower level of MNBs present in the liver and lungs for 1 min exposure, could indicate that these MNBs are excreted from these areas by 8 h, but this trend is not consistant for the other exposure times, and further studies will need to be conducted to further understand the biological accumulation and excretion.

The interaction effect between the tissue location of the MNBs and the exposure time on the number of MNBs detected with an 8-hour incubation period was determined to statistically significant based on the F-value of 2.781, which had p-value of 0.003 and partial eta squared value of 0.471. If the null hypothesis, that there is no significant difference between groups, is true the F-value would be close to 1.0. A larger F-value indicates the variation among group means are more than you would expect to see by change. The p-value is the probability of observing the given F-value given the null hypothesis is true. The partial eta squared ($\eta 2$) is a measure of effect size and reflects the percentage of variance in the number of MNBs detected explained by the factors in the sample. This means that 47.1% of the variance in number of MNBs detected is due to the tissue location and exposure time, while all other variance in the number of MNBs detected is due to experimental variance and chance. This statistically significant interaction indicates that the effect that exposure time has on the number of MNBs detected, depends on the tissue location. Due to this interaction effect, analysis of simple main effects for each factor (tissue location and exposure time) were conducted. Simple main effects determine the effect of one factor within one level of the other factor. The simple main effects for exposure time are the effects of exposure time in each tissue type. There were no statistically

significant effects of exposure time in the mean number of MNBs detected in the kidney, liver, lungs, or feces, but there was a statistically significant difference in the mean number of MNBs detected within the spleen between each exposure time based on the F-value of 14.387, which had a p-value of <0.0005 and partial eta squared value of 0.535. The 15 min exposure time had a statistically significant higher mean number of MNBs within the spleen than the 1 min, 5min, 30 min, and 30 min without DMSO exposure times ($p < 0.0005$) and the spleen had a statistically significant higher mean number of MNBs detected with 15-minute exposure than the kidney, liver, lungs, or feces ($p < 0.0005$). It is important to note here that the homogeneity of variances for this data set was violated and could not be fixed by a simple transformation, which could impact the significance interpretation of the two-way ANOVA.

The average MNBs per gram of tissue for 24 h incubation time are summarized in Figure 3.7. The number of dectectable MNBs fell within the range of $10^6$-$10^{11}$ MNBs per gram of sample tissue for each exposure time (1-30 min), with or without DMSO, and for each tissue type. Some samples did not have detectable levels of MNBs. Two of the three trials for 5 minute exposure had no detectable levels of MNBs within the liver. This anomaly should be re-evaluated with repeated studies. As compared to 8 h incubation, similar levels of MNBs after 24 h incubation are present within the spleen, further suggesting this as a main site of accumulation. Elevated levels within the feces, also indicates that BAP-MNBs are continually being excreted, even 24 h post exposure.

The interaction effect between the tissue location of the MNBs and the exposure time on the number of MNBs detected with a 24-hour incubation period was determined to not be statistically significant as assessed by a two-way ANOVA. Further analysis of the main effects for tissue location and exposure time both showed no statistically significant effect on the

number of MNBs detected. The main effect is the overall measure of effect of one factor on the dependent variable, ignoring the other factor: the effect of tissue location on the number of MNBs, ignoring the exposure time and the effect of exposure time on the number of MNBs, ignoring tissue location. This analysis was carried out due to no statistically significant interaction effect on the number of MNBs between the two variables.

The level of MNBs present for the groups administered without DMSO are at similar levels to the other exposure times with DMSO on average. When looking at the data for all three trials however, (Table B.2) there are some tissues and circulation times that did not have detectable levels of MNBs; this variability should be studied in more detail. These results could indicate that DMSO is not necesarry for pentration of BAP-MNBs.

In an attempt to visualize the mode of entry through the skin, one mouse from each of the following conditions was administered a solution that also contained 100 μM of Atto633-encapsulated BAPCs: 15 min exposure - 1 h incubation; 15 min exposure - 8 h; and 15 min exposure - 24 h incubation. For these three mice, the tail was also collected for cross-section analysis, just as the preliminary study by a former lab member was performed. While autofluorescence is likely present from hair follicles, if many BAPCs accumulate within dermal structures or penetrate further through the skin as compared to the pre-liminary trails where no active metabolism or circulation was present, they would be able to be visualized. Confocal imaging of these tail samples showed a minimal level of fluorescence and was likely the basal level from autofluorescence (Figure B.1) [247]. Nanoparticles and molecules that use the follicular route, are captured to provide a reservoir and have been shown to have storage time in the hair follicles for up to 10 days [205]. Thus, the presence of potential Atto633-encapsulated BAPCs in the epidermis and dermal structures at 24 h post exposure would be expected for this

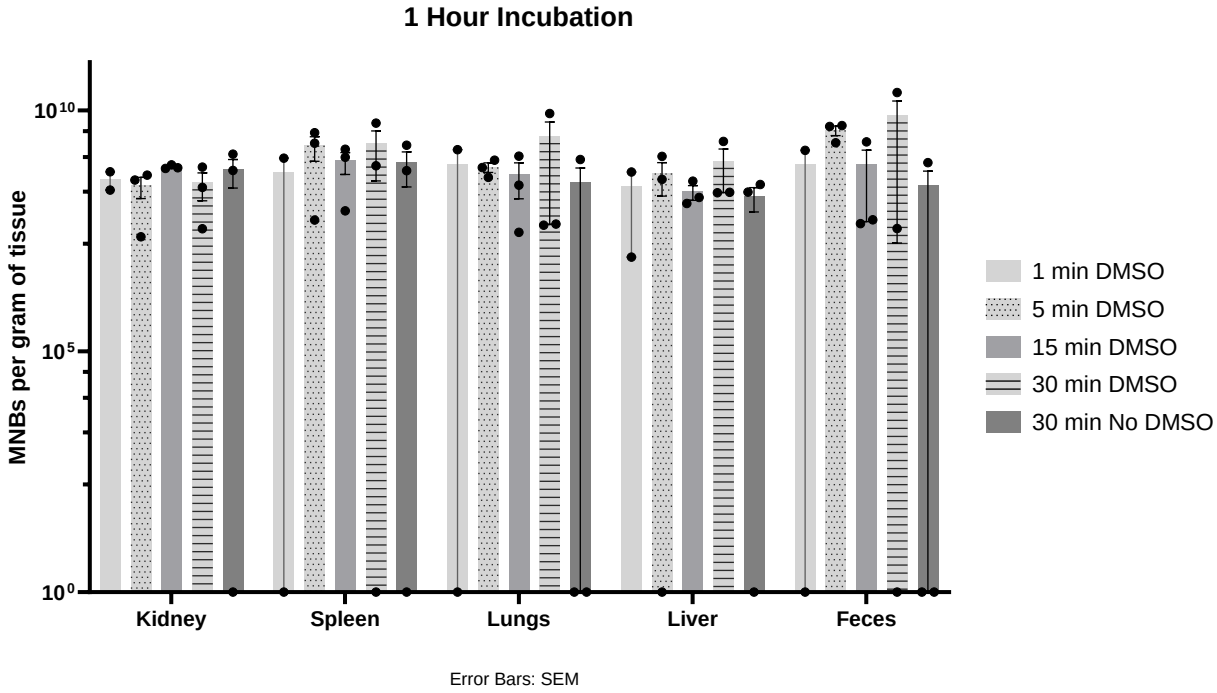


## Figure 3.5 - Mean MNBs/g for 1 Hour Incubation Time

Data are shown as mean ± standard error, unless otherwise stated. N = 3 for each exposure time, except for 1 min N = 2. The bars represent the mean number of MNBs per gram of tissue in sample. A two-way ANOVA to examine the effects of exposure time and tissue location of MNBs on the number of MNBs was conducted and found that the interaction effect between exposure time and tissue location was not statistically significant. Analysis of main effects for exposure time and tissue location were performed and showed no statistical significance.

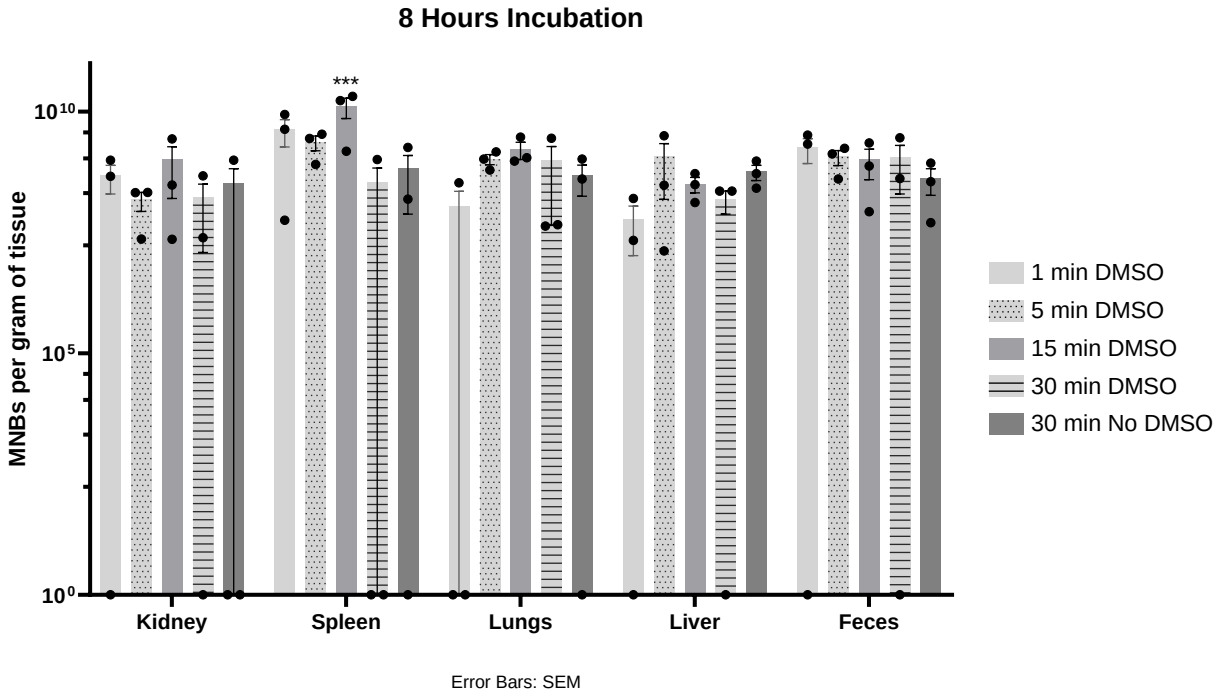


**Figure 3.6 - Mean MNBs/g for 8 Hours Incubation Time**

Data are shown as mean ± standard error, unless otherwise stated. N = 3 for each exposure time. The bars represent the mean number of MNBs per gram of tissue in sample. A two-way ANOVA to examine the effects of exposure time and tissue location of MNBs on the number of MNBs was conducted and found that the interaction effect between exposure time and tissue location was statistically significant ($p = 0.003$). Analysis of simple main effects for tissue location and exposure time was performed and showed a statistically significant difference in mean number of MNBs for location in spleen with a 15 min exposure time: (***) $p < 0.0005$.

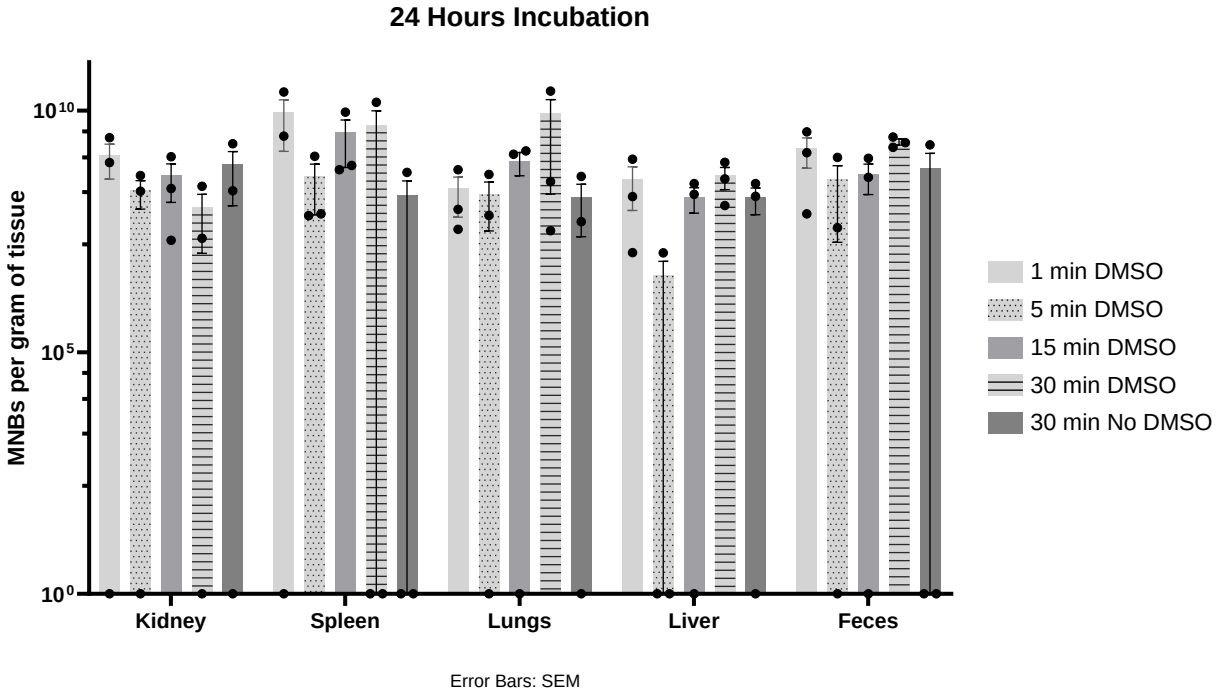


**Figure 3.7 - Mean MNBs/g for 24 Hours Incubation Time**

Data are shown as mean ± standard error, unless otherwise stated. N = 3 for each exposure time. The bars represent the mean number of MNBs per gram of tissue in sample. A two-way ANOVA to examine the effects of exposure time and tissue location of MNBs on the number of MNBs was conducted and found that the interaction effect between exposure time and tissue location was not statistically significant. Analysis of main effects for exposure time and tissue location were performed and showed no statistical significance

route. An untreated control mouse tail should be processed and visualized under the same conditions to verify the level of autofluorescence. Since MNBs were also used in these studies, cross-sections from the same tails were used to visualize MNBs with Prussian blue staining. Prussian blue is an insoluble bright blue pigment that formulates when potassium ferrocyanide encounters ferric ions, resulting in ferric ferrocyanide, also known as Prussian blue. A few MNBs or MNB aggregates were visualized, but not in a large quantity (Figure B.2). These tail sections were not taken in triplicate and thus are not a valid representation of the population. As such, visualizing these MNBs and/or BAPCs cannot provide conclusive insight at this time. Overall this pilot study showed some interesting and useful insight for the potential use of BAP-MNBs and/or BAPCs via transdermal uptake and warrants additional investigation.

## Conclusions and Future Outlook

The results shown were part of a pilot study to determine the potential of BAP-MNBs and/or BAPCs for transdermal delivery. While these initial results provide some insight, there are still a lot of remaining questions and conditions to be addressed. Looking at the full biodistribution and pharmacokinetics of BAP-MNBs and/or BAPCs via transdermal delivery, intravenous delivery, or oral delivery are needed to understand how the nanocarriers behave *in vivo*. In addition to looking at more tissues and fluids such as blood, brain, and urine among others, important parameters of pharmacokinetics to measure include maximum concentration, circulatory half-life, clearance, area under the curve, and mean resident time which is the average time a molecule stays in the body [209].

Previous studies on biodistribution of nanoparticles that vary in size, show that larger nanoparticles tend to accumulate less than the smaller nanoparticles, and in different areas [210, 240]. These larger nanoparticles also tend to have much shorter half-lives, which could contribute to the lower accumulation [208]. These measurements and observations for 200 nm BAP-MNBs, 50 nm BAP-MNBs, 20 nm locked BAPCs, all with or without nucleic acid such as pDNA or dsRNA, would provide invaluable data for the future of BAPCs *in vivo* and the field of nanodelivery systems. Additionally, if passive penetration is not as robust as initially thought, delivering BAPCs and nucleic acid-BAPC complexes via active or mechanical transdermal penetration methods could prove to be more efficient.

# References


[1] Wafa' T. Al-Jamal, Kostas Kostarelos. 2011. “Liposomes: From a Clinically Established Drug Delivery System to a Nanoparticle Platform for Theranostic Nanomedicine.” *Accounts of Chemical Research* 44 (10): 1094-1104. doi:10.1021/ar200105p.

[2] Honggang Cui, Xiaoyuan Chen. 2017. “Peptides and Peptide Conjugates in Medicine.” *Advanced Drug Delivery Reviews* 110-111: 1-2. doi:10.1016/j.addr.2017.04.004.

[3] Kazuki N. Sugahara, Tambet Teesalu, Priya Prakash Karmali, Venkata Ramana Kotamraju, Lilach Agemy, Olivier M. Girard, Douglas Hanahan, Robert F. Mattrey, Erkki Ruoslahti. 2009. "Tissue-Penetrating Delivery of Compounds and Nanoparticles into Tumors." *Cancer Cell* 16 (6): 510-520. doi:10.1016/j.ccr.2009.10.013.

[4] Pirjo Laakkonen, Maria E. Akerman, Hector Biliran, Meng Yang, Fernando Ferrer, Terhi Karpanen, Robert M. Hoffman, Erkki Ruoslahti. 2004. "Antitumor activity of a homing peptide that targets tumor lymphatics and tumor cells." *PNAS* 101 (25): 9381-9386. doi:10.1073/pnas.0403317101.

[5] Valentina Fogal, Lianglin Zhang, Stan Krajewski, Erkki Ruoslahti. 2008. "Mitochondrial/Cell-Surface Protein p32/gC1qR as a Molecular Target in Tumor Cells and Tumor Stroma." *Cancer Research* 66 (17): 7210-7218. doi:10.1158/0008-5472.CAN-07-6752.

[6] Ruoslahti, Erkki. 2012. "Peptides as Targeting Elements and Tissue Penetration Devices for Nanoparticles." *Advanced Materials* 24 (28): 3747-3756. doi:10.1002/adma.201200454.

[7] Juan Li, Yuchen Tian, Aiguo Wu. 2015. "Neuropeptide Y receptors: a promising target for cancer imaging and therapy." *Regenerative Biomaterials* 2 (3): 215-219. doi:10.1093/rb/rbv013.

[8] Seulki Lee, Jin Xie, Xiaoyuan Chen. 2010. "Peptide-Based Probes for Targeted Molecular Imaging." *Biochemistry* 49 (7): 1364-1376. doi:10.1021/bi901135x.

[9] Rachel M. Levine, Carolyn M. Scott, Efrosini Kokkoli. 2013. "Peptide functionalized nanoparticles for nonviral gene delivery." *Soft Matter* 9 (4): 985-1004. doi:10.1039/C2SM26633D.

[10] Yu Sakurai, Hiroto Hatakeyama, Yusuke Sato, Mamoru Hyodo, Hidetaka Akita, Noritaka Ohga, Kyoko Hida, Hideyoshi Harashima. 2014. "RNAi-mediated gene knockdown and anti-angiogenic therapy of RCCs using a cyclic RGD-modified liposomal-siRNA system." *Journal of Controlled Release* 173: 110-118. doi:10.1016/j.jconrel.2013.10.003.

[11] Ian Wheeldon, Arash Farhadi, Alexander G. Bick, Esmaiel Jabbari, Ali Khademhosseini. 2011. "Nanoscale tissue engineering: spatial control over cell-materials interactions." *Nanotechnology* 22 (21): p.212001.

[12] Pradeep Kumar, Viness Pillay, Girish Modi, Yahya E. Choonara, Lisa C. du Toit, Dinesh Naidoo. 2011. "Self-Assembling Peptides: Implications for Patenting in Drug Delivery and Tissue Engineering." *Recent Patents on Drug Delivery & Formulation* (Bentham Science Publishers) 5 (1): 24-51. doi:10.2174/187221111794109510.

[13] Anna Pratima Nikalje. 2015. "Nanotechnology and its Applications in Medicine." *Medicinal chemistry* 5 (2): 81-89. doi:10.4172/2161-0444.1000247.

[14] Yonggang Xiang, Nwe Nwe Linn Oo, Jin Ping Lee, Zibiao Li, Xian Jun Loh. 2017. "Recent development of synthetic nonviral systems for sustained gene delivery." *Drug Discovery Today* 22 (9): 1318-1335. doi:10.1016/j.drudis.2017.04.001.

[15] Michael K. Riley II, Wilfred Vermerris. 2017. "Recent Advances in Nanomaterials for Gene Delivery - A Review." *Nanomaterials* 7 (5): 94. doi:10.3390/nano7050094.

[16] Cynthia E. Dunbar, Katherine A. High, J. Keith Joung, Donald B. Kohn, Keiya Ozawa, Michel Sadelain. 2018. "Gene therapy comes of age." *Science* 359 (6372): eaan4672. doi:10.1126/science.aan4672.

[17] Xiangwei Xiao, Ping Guo, Chiyo Shiota, Ting Zhang, Gina M. Coudriet, Shane Fischbach, Krishna Prasadan, Joseph Fusco, Sabarinathan Ramachandran, Piotr Witkowski, Jon D. Piganelli, George K. Gittes. 2018. "Endogenous Reprogramming of Alpha Cells into Beta Cells, Induced by Viral Gene Therapy, Reverses Autoimmune Diabetes." *Cell Stem Cell* 22 (1): 78-90.e4. doi:10.1016/j.stem.2017.11.020.

[18] Wolfgang Miesbach, Karina Meijer, Michiel Coppens, Peter Kampmann, Robert Klamroth, Roger Schutgens, Marco Tangelder, Giancarlo Castaman, Joachim Schwable, Halvard Bonig, Erhard Seifried, Federica Cattaneo, Christian Meyer, Frank W. G. Leebeek. 2018. "Gene therapy with adeno-associated virus vector 5-human factor IX in adults with hemophilia B." *Blood* 131: 1022-1031. doi:10.1182/blood-2017-09-804419.

[19] Andrea Annoni, Silvia Gregori, Luigi Naldini, Alessio Cantore. 2019. "Modulation of immune responses in lentiviral vector-mediated gene transfer." *Cellular Immunology* 342: 103802. doi:10.1016/j.cellimm.2018.04.012.

[20] Conchita Tros de Ilarduya, Yan Sun, Nejat Duzgunes. 2010. "Gene delivery by lipoplexes and polyplexes." *European Journal of Pharmaceutical Sciences* 40 (3): 159-170. doi:10.1016/j.ejps.2010.03.019.

[21] Nirav Khatri, Dipesh Baradia, Imran Vhora, Mohan Rathi, Ambikanandan Misra. 2014. "cRGD grafted liposomes containing inorganic nanoprecipitate complexed siRNA for intracellular delivery in cancer cells." *Journal of Controlled Release* 182: 45-57. doi:10.1016/j.jconrel.2014.03.003.

[22] Andrew B. Hill, Mingfu Chen, Chih-Kuang Chen, Blaine A. Pfeifer, Charles H. Jones. 2016. "Overcoming Gene-Delivery Hurdles: Physiological Considerations for Nonviral Vectors." *Trends in Biotechnology* 34 (2): 91-105. doi:10.1016/j.tibtech.2015.11.004.

[23] Jenny K W Lam, Michael Y T Chow, Yu Zhang, Susan W S Leung. 2015. “siRNA Versus miRNA as Therapeutics for Gene Silencing.” *Molecular Therapy - Nucleic Acids* (American Society of Gene & Cell Therapy) 4 (9): e252. doi:10.1038/mtna.2015.23.

[24] Xian Jun Loh, Tung-Chun Lee, Qingqing Dou, G. Roshan Deen. 2016. “Utilising inorganic nanocarriers for gene delivery.” *Biomaterials Science* 4: 70-86. doi:10.1039/C5BM00277J.

[25] Kathryn A. Whitehead, Robert Langer, Daniel G. Anderson. 2009. “Knocking down barriers: advances in siRNA delivery.” *Nature Reviews Drug Discovery* 8: 129-138.

[26] Vladimir P. Torchilin, Tatyana S. Levchenko, Ram Rammohan, Natalia Volodina, Brigitte Papahadjopoulos-Sternberg, Gerard G. M. D'Souza. 2003. "Cell transfection in vitro and in vivo with nontoxic TAT peptide-liposome-DNA complexes." *PNAS* 100 (4): 1972-1977. doi:10.1073/pnas.0435906100.

[27] J. Soutschek, A. Akinc, B. Bramlage, K. Charisse, R. Constien, M. Donoghue, S. Elbashir, A. Geick, P. Hadwiger, J. Harborth, M. John, V. Kesavan, G. Lavine, R.K. Pandey, T. Racie, K.G. Rajeev, I. Rohl, I. Toudjarska, G. Wang, S. Wuschko, D. Bumcrot,. 2004. "Therapeutic silencng of an endogenous gene by systemic administration of modified siRNAs." *Nature* 432 (7014): 173-178. doi:10.1038/nature03121.

[28] Dwaine A. Braasch, Zain Paroo, Anca Constantinescu, Gang Ren, Orhan K. Oz, Ralph P. Mason, David R. Corey. 2004. "Biodistribution of phosphodiester and phosphorothioate siRNA." *Bioorganic & Medicinal Chemistry Letters* 14 (5): 1139-1143. doi:10.1016/j.bmcl.2003.12.074.

[29] Roosmarijn E. Vandenbroucke, Bruno G. De Geest, Stefan Bonne, Mathieu Vinken, Tamara Van Haecke, Harry Heimberg, Ernst Wagner, Vera Rogiers, Stefaan C. De Smedt, Joseph Demeester, Niek N. Sanders. 2008. "Prolonged gene silencing in hepatoma cells and primary hepatocytes after small interfering RNA delivery with biodegradable poly(beta-amino esters)." *The Journal of Gene Medicine* 10 (7): 783-794. doi:10.1002/jgm.1202.

[30] Dorota Napierska, Leen CJ Thomassen, Dominique Lison, Johan A. Martens, Peter H. Hoet. 2010. "The nanosilica hazard: another variable entity." *Particle and Fibre Toxicology* 7 (39). doi:10.1186/1743-8977-7-39.

[31] Elke AF Van Doren, Pieter-Jan RH De Temmerman, Michel Abi, Daoud Francisco, Jan Mast. 2011. "Determination of the volume-specific surface area by using transmission electron tomography for characterization and definition of nanomaterials." *Journal of Nanobiotechnology* 9: 17.

[32] Fedena Fanord, Korie Fairbairn, Harry Kim, Amanda Garces, Venkat Bhethanabotla, Vinay K Gupta. 2010. "Bisphosphonate-modified gold nanoparticles: a useful vehicle to study the treatment of osteonecrosis of the femoral head." *Nanotechnology* 22 (3): 035102. doi:10.1088/0957-4484/22/3/035102.

[33] Ken Donaldson, Paul JA Borm, Vincent Castranova, Mary Gulumian. 2009. "The limits of testing particle-mediated oxidative stress in vitro in predicting diverse pathologies; relevance for testing of nanoparticles." *Particle and Fibre Toxicology* 6 (13). doi:10.1186/1743-8977-6-13.

[34] MacLachlan, I. 2007. Chap. 9 in *Antisense Drug Technology: Principles, Strategies and Applications*, edited by S. T. Crooke, 237-270. CRC.

[35] David V. Morrissey, Jennifer A. Lockridge, Lucinda Shaw, Karin Blanchard, Kristi Jensen, Wendy Breen, Kimberly Hartsough, Lynn Machemer, Susan Radka, Vasant Jadhav, Narendra Vaish, Shawn Zinnen, Chandra Vargeese, Keith Bowman, Chris S. Shaffer. 2005. "Potent and persistent in vivo anti-HBV activity of chemically modified siRNAs." *Nature Biotechnology* 23: 1002-1007. doi:10.1038/nbt1122.

[36] Jr., Alexei A. Bogdanov. 2008. "Merging molecular imaging and RNA interference: Early experience in live animals." *Journal of Cellular Biochemistry* 104 (4): 1113-1123. doi:10.1002/jcb.21689.

[37] Wanyi Tai, Xiaohu Gao. 2017. “Functional peptides for siRNA delivery.” *Advanced Drug Delivery Reviews* 110-111: 157-168. doi:10.1016/j.addr.2016.08.004.

[38] Margaret A. Phillips, Martin L. Gran, Nicholas A. Peppas. 2010. "Targeted nanodelivery of drugs and disgnostics." *nanotoday* 5 (2): 143-159. doi:10.1016/j.nantod.2010.03.003.

[39] Raffaella Rossin, Dipanjan Pan, Kai Qi, Jeffrey L. Turner, Xiankai Sun, Karen L. Wooley, Michael J. Welch. 2005. "64Cu-Labeled Folate-Connjugated Shell Cross-Linked Nanoparticles for Tumor Imaging and Radiotherapy: Synthesis, Radiolabeling, and Biologic Evaluation." *The Journal of Nuclear Medicine* 46 (7): 1210-1218.

[40] Enrica De Rosa, Ciro Chiappini, Dongmei Fan, Xuewu Liu, Mauro Ferrari, Ennio Tasciotti. 2011. "Agarose Surface Coating Influences Intracellular Accumulation and Enhances Payload Stability of a Nano-delivery System." *Pharmaceutical Research* 28 (7): 1520-1530. doi:10.1007/s11095-011-0453-2.

[41] Prakash Ramalingam, Sang Woo Yoo, Young Tag Ko. 2016. "Nanodelivery systems based on mucoadhesive polymer coated solid lipid nanoparticles to improve the oral intake of food curcumin." *Food Research International* 84: 113-119. doi:10.1016/j.foodres.2016.03.031.

[42] Mariarenata Sessa, Alessandro A. Casazza, Patrizia Perego, Rong Tsao, Giovanna Ferrari, Francesco Donsi. 2013. "Exploitation of Polyphenolic Extracts from Grape Marc as Natural Antioxidants by Encapsulation in Lipid-Based Nanodelivery Systems." *Food and Bioprocess Technology* 6 (10): 2609-2620. doi:10.1007/s11947-012-0911-9.

[43] Handan Acar, Samanvaya Srivastava, Eun Ji Chung, Mathew R. Schnorenberg, John C. Barrett, James L. LaBelle, Matthew Tirrell. 2017. “Self-assembling peptide-based building blocks in medical applications.” *Advanced Drug Delivery Reviews* 110-111: 65-79. doi:10.1016/j.addr.2016.08.006.

[44] Helerin Margus, Piret Arukuusk, Ulo Langel, Margus Pooga. 2015. “Characteristics of Cell-Penetrating Peptide/Nucleic Acid Nanoparticles.” *Molecular Pharmaceutics* 13: 172-179. doi:10.1021/acs.molpharmaceut.5b00598.

[45] Taavi Lehto, Kariem Ezzat, Matthew J.A. Wood, Samir EL Andaloussi. 2016. “Peptides for nucleic acid delivery.” *Advanced Drug Delivery Reviews* 106 (A): 172-182. doi:10.1016/j.addr.2016.06.008.

[46] Zi Long, Meiying Liu, Ruming Jiang, Qing Wan, Liucheng Mao, Yiqun Wan, Fengjie Deng, Xiaoyong Zhang, Yen Wei. 2017. "Preparation of water soluble and biocompatible AIE-active fluorescent organic nanoparticles via multicomponent reaction and their biological imaging capability." *Chemical Engineering Journal* 308: 527-534. doi:10.1016/j.cej.2016.09.053.

[47] Klaus Kummerer, Jakob Menz, Thomas Schubert, Wim Thielemans. 2011. "Biodegradability of organic nanoparticles in the aqueous environment." *Chemosphere* 82 (10): 1387-1392. doi:10.1016/j.chemosphere.2010.11.069.

[48] Linlin Sun, Chunli Zheng, Thomas J. Webster. 2017. “Self-assembled peptide nanomaterials for biomedical applications: promises and pitfalls.” *International Journal of Nanomedicine* 12: 73-86. doi:10.2147/IJN.S117501.

[49] B. Mishra, Bhavesh B. Patel, Sanjay Tiwari. 2010. “Colloidal nanocarriers: a review on formulation technology, types and applications toward targeted drug delivery.” *Nanomedicine: Nanotechnology, Biology and Medicine* 6 (1): 9-24. doi:10.1016/j.nano.2009.04.008.

[50] Jeffrey D. Kingsley, Huanyu Dou, Justin Morehead, Barrett Rabinow, Howard E. Gendelman, Christopher J. Destache. 2006. "Nanotechnology: A Focus on Nanoparticles as a Drug Delivery System." *Journal of Neuroimmune Pharmacology* 1 (3): 340-350. doi:10.1007/s11481-006-9032-4.

[51] M. Luck, B.R. Paulke, W. Schroder, T. Blunk, R.H. Muller. 1998. "Analysis of plasma protein adsorption on polymeric nanoparticles with different surface characteristics." *Journal of Biomedical Materials Research* 39 (3): 478-485.

[52] Shiladitya Sengupta, David Eavarone, Ishan Capila, Ganlin Zhao, Nicki Watson, Tanyel Kiziltepe, Ram Sasisekharan. 2005. "Temporal targeting of tumour cells and neovasculature with a nanoscale delivery system." *Nature* 436: 568-572. doi:10.1038/nature03794.

[53] Jayanth Panyam, Vinod Labhasetwar. 2003. "Biodegradable nanoparticles for drug and gene delivery to cells and tissue." *Advanced Drug Delivery Reviews* 55 (3): 329-347. doi:10.1016/S0169-409X(02)00228-4.

[54] Alan Aderem, David M. Underhill. 1999. "Mechanisms of phagocytosis in macrophages." *Annual Review of Immunology* 17: 593-623. doi:10.1146/annurev.immunol.17.1.593.

[55] Hirsch, James G. 1962. "Cinemicrophotographic observations on granule lysis in polymorphonuclear leucocytes during phagocytosis." *The Journal of Experimental Medicine* 827-847.

[56] Aaron C. Anselmo, Samir Mitragotri. 2015. “A Review of Clinical Translation of Inorganic Nanoparticles.” *The AAPS Journal* 17 (5): 1041-1054. doi:10.1208/s12248-015-9780-2.

[57] David A. Giljohann, Dwight S. Seferos, Weston L. Daniel, Matthew D. Massich, Pinal C. Patel, Chad A. Mirkin. 2010. "Gold Nanoparticles for Biology and Medicine." *Angewandte Chemie International Edition English* 49 (19): 3280-3294. doi:10.1002/anie.200904359.

[58] Susie Eustis, Mostafa A. El-Sayed. 2006. "Why gold nanoparticles are more precious than pretty gold: Noble metal surface plasmon resonance and its enhancement of the radiative and nonradiative properties of nanocrystals of different shapes." *Chemical Society Reviews* 35: 209-217. doi:10.1039/B514191E.

[59] R. A. Sperling, W. J. Park. 2010. "Surface modification, functionalization and bioconjugation of colloidal inorganic nanoparticles." *Philosophical Transactions of the Royal Society A* (The Royal Society Publishing) 368: 1333-1383. doi:10.1098/rsta.2009.0273.

[60] Ivan H. El-Sayed, Xiaohua Huang, Mostafa A. El-Sayed. 2006. "Selective laser photo-thermal therapy of epithelial carcinoma using anti-EGFR antibody conjugated gold nanoparticles." *Cancer Letters* 239 (1): 129-135. doi:10.1016/j.canlet.2005.07.035.

[61] Juan J. Giner-Casares, Malou Henriksen-Lacey, Marc Coronado-Puchau, Luis M. Liz-Marzan. 2016. “Inorganic nanoparticles for biomedicine: where materials scientists meet medical research.” *Materials Today* 19 (1): 19-28. doi:10.1016/j.mattod.2015.07.004.

[62] Enyi Ye, Michelle D. Regulacio, Shuang-Yuan Zhang, Xian Jun Loh, Ming-Yong Han. 2015. "Anisotropically branched metal nanostructures." *Chemical Society Reviews* 44: 6001-6017. doi:10.1039/C5CS00213C.

[63] Enyi Ye, Xian Juh Loh. 2013. "Polymeric Hydrogels and Nanoparticles: A Merging and Emerging Field." *Australian Journal of Chemistry* 66 (9): 997-1007. doi:10.1071/CH13168.

[64] Wolfe T, Chatterjee D, Lee J. 2015. "Targeted gold nanoparticles enhance sensitization of prostate tumors to megavoltage radiation therapy in vivo." *Nanomedicine: Nanotechnology, Biology, and Medicine* 11 (5): 1277-1283.

[65] Stern JM, Kibanov Solomonov VV, Sazykina E, Schwartz JA, Gad SC, Goodrich GP. 2016. "Initial Evaluation of the Safety of Nanoshell-Directed Photothermal Therapy in the Treatment of Prostate Disease." *International Journal of Toxicology* 35 (1): 38-46.

[66] Rastinehad RA, Anastos H, Wajswol E, Winoker JS, Sfakianos JP, Doppalapudi SK, Carrick MR, Knauer CJ, Taouli B, Lewis SC, Tewari AK, Schwartz JA, Canfield SE, George AK, West JL, Naomi J. Hala NJ. 2019. "Gold nanoshell-localized photothermal ablation of prostate tumors in a clinical pilot device study." *Proceedings of the National Academy of Science.*

[67] Hirsch LR, Stafford RJ, Bankson JA, Sershen SR, Rivera B, Price RE. 2003. "Nanoshell-mediated near-infrared thermal therapy of tumors under magnetic resonance guidance." *Proceedings of the National Academy of Science* 100 (23): 13549-13554.

[68] Schwartz JA, Shetty AM, Price RE, Stafford RJ, Wang JC, Uthamanthil RK. 2009. "Feasibility study of particle-assisted laser ablation of brain tumors in orthotopic canine model." *Cancer Research* 69 (4): 1659-1667.

[69] Stern JM, Stanfield J, Kabbani W, Hsieh JT, Cadeddu JA. 2008. "Selective prostate cancer thermal ablation with laser activated gold nanoshells." *Journal or Urology* 179 (2): 748-753.

[70] Paithankar D, Hwang BH, Munavalli G, Kauvar A, Lloyd J, Blomgren R. 2015. "Ultrasonic delivery of silica-gold nanoshells for photthermolysis of sebaceous glands in humans: nanotechnology from the bench to clinic." *Journal of Controlled Release* 206: 30-36.

[71] Bhupinder S. Sekhon, Seema R. Kamboj. 2010. “Inorganic nanomedicine - Part 1.” *Nanomedicine: NBM* 6: 516-522. doi:10.1016/j.nano.2010.04.004.

[72] Sang Jun Son, Xia Bai, Sang Bok Lee. 2007. “Inorganic hollow nanoparticles and nanotubes in nanomedicine: Part 1. Drug/gene delivery applications.” *Drug Discovery Today* 12 (15-16): 650-656. doi:10.1016/j.drudis.2007.06.002.

[73] Francisco Silva, Ajit Zambre, Maria Paula Cabral Campello, Lurdes Gano, Isabel Santos, Ana Maria Ferraria, Maria Joao Ferreira, Amolak Singh, Anandhi Upendran, Antonion Paulo, Raghuraman Kannan. 2016. "Interrogating the Role of Receptor-Mediated Mechanisms: Biological Fate of Peptide-Functionalized Radiolabeled Gold Nanoparticles in Tumor mice." *Bioconjugate Chemistry* 27 (4): 1153-1164. doi:10.1021/acs.bioconjchem.6b00102.

[74] S. D. Kemkar, Milind Vaidya, Dipak Pinjari, Sammit Karekar, Sanjana Kemkar, Siddhesh Nanaware, Sanjukta Kemkar. 2017. "Application of mixed colloidal magnetic fluid of single domain Fe3O4 and NiFe2O4 ferrite nanoparticles in audio speakers." *International Journal of Engineering Research and Application* 7 (1): 11-18. doi:10.9790/9622-0701031118.

[75] Xiangcheng Sun, Yunhe Huang, David E. Nikles. 2004. "FePt and CoPt magnetic nanoparticles film for future high density data storage media." *International Journal of Nanotechnology* 1 (3): 328-346.

[76] Maxi A. Abakumov, Natalia V. Nukolova, Marina Sokolsky-Papkov, Sergey A. Shein, Tatiana O. Sandalova, Hemant M. Vishwasrao, Nadezhda F. Grinenko, Iliya L. Gubsky,

Artem M. Abakumov, Alexander V. Kabanov, Vladimir P. Chekhonin. 2015. "VEGF-targeted magnetic nanoparticles for MRI visualization of brain tumor." *Nanomedicine: Nanotechnolgy, Biology, and Medicine* 11 (4): 825-833. doi:10.1016/j.nano.2014.12.011.

[77] Hira Fatima, Kyo-Seon Kim. 2017. "Magnetic nanoparticles for bioseparation." *Korean Journal of Chemical Engineering* 34 (3): 589-599. doi:10.1007/s11814-016-0349-2.

[78] M C Bautisa, O Bomati-Miguel, X Zhao, M P Morales, T Gonzales-Carreno, R Perez de Alejo, J Ruiz-Cabello, S Veintemilla-Verdaguer. 2004. "Comparative study of ferrofluids based on dextran-coated iron oxide and metal nanoparticles for contrast agents in magnetic resonance imaging." *Nanotechnology* 15 (4): S154. doi:10.1088/0957-4484/15/4/008.

[79] Hongsub Bae, Tanveer Ahmad, Ilsu Rhee, Yongmin Chang, Seong-Uk Jin, Sungwook Hong. 2012. "Carbon-coated iron oxide nanoparicles as contrast agents in magnetic resonance imaging." *Nanoscale Research Letters* 7 (44). doi:10.1186/1556-276X-7-44.

[80] Frank Ludwig, Erik Heim, Meinhard Schilling. 2009. "Characterization of magnetic core-shell nanoparticles by fluxgate magnetorelaxometry, ac susceptibility, transmission electron microscopy and photo correlation spectroscopy - A comparative study." *Journal of Magnetism and Magnetic Materials* 321 (10): 1644-1647. doi:10.1016/j.jmmm.2009.02.105.

[81] Norio Morishita, Hironori Nakagami, Ryuichi Morishita, Shin-ichi Takeda, Fumihito Mishima, Bungo Terazono, Shigehiro Nishijima, Yasufumi Kaneda, Noriaki Tanaka. 2005. "Magnetic nanoparticles with surface modification enhanced gene delivery of HVJ-E vector." *Biochemical and Biophysical Research Communications* 334 (4): 1121-1126. doi:10.1016/j.bbrc.2005.06.204.

[82] David Hetzel, William Strauss, Kristine Bernard, Zhu Li, Audrone Urboniene, Lee F. Allen. 2014. "A Phase III, randomized, open-label trial of ferumoxytol compared with iron sucrose for the treatment of iron deficiency anemia in patients with a history of unsatisfactory oral iron therapy." *American Journal of Hemotology* 89 (6). doi:10.1002/ajh.23712.

[83] Akira Ito, Hiroyuki Honda. 2007. "Magnetic Nanoparticles for Tissue Engineering." *Nanotechnologies for the Life Scienes: Online.* doi:10.1002/9783527610419.ntls0102.

[84] Beata Chertok, Bradford A. Moffat, Allan E. David, Faquan Yu, Christian Bergemann, Brian D. Ross, Victor C. Yang. 2008. "Iron oxide nanoparticles as a drug delivery vehicle for MRI monitored magnetic targeting of brain tumors." *Biomaterials* 29 (4): 487-496. doi:10.1016/j.biomaterials.2007.08.050.

[85] H. Richter, M. Kettering, F. Wiekhorst, U Steinhoff, I Hilger, L Trahms. 2010. "Magnetorelaxometry for localization and quantification of magnetic nanoparticles for thermal ablation studies." *Physics in Medicine and Biology* 55 (3). doi:10.1088/0031-9155/55/3/005.

[86] Bruce S. Spinowitz, Annamaria T. Kausz, Jovanna Baptista, Sylvia D. Nobel, Renuka Sothinathan, Marializa V. Bernardo, Louis Brenner, Brian J. G. Pereira. 2008. "Ferumoxytol for Treating Iron Deficiency Anemia in CKD." *Journal of the American Society of Nephrology* 19 (8): 1599-1605. doi:10.1681/ASN.2007101156.

[87] Min Lu, Martin H Cohen, Dwaine Rieves, Richard Pazdur. 2010. "FDA report: Ferumoxytol for intravenous iron therapy in adult patients with chronic kidney disease." *American Journal of Hematology* 85 (5). doi:10.1002/ajh.21656.

[88] Burns DL, Pomposelli JJ. 1999. "Toxicity of parenteral iron dextran therapy." *Kidney International Supplements* 69: S119-124.

[89] Vychytil A, Haag-Weber M. 1999. "Iron status and iron supplementation in peritoneal dialysis patients." *Kidney International Supplements* 69: S71-78.

[90] Fishbane S, Ungureanu VD, Maesaka JK, Kaupke CJ, Lim V, Wish J. 1996. "The safety of intravenous iron dextran in hemodialysis patients." *American Journal of Kidney Disease* 28 (4): 529-534.

[91] Paul J. Kempen, Sarah Greasley, Kelly A. Parker, Jos L. Campbell, Huan-Yu Chang, Julian R. Jones, Robert Sinclair, Sanjiv S. Gambhir, Jesse V. Jokerst. 2015. "Theranostic Mesoporous Silica Nanoparticles Biodegrade after Pro-Survival Drug Delivery and Ultrasound/Magnetic Resonance Imaging of Stem Cells." *Theranostics* 5 (6): 631-642. doi:10.7150/thno.11389.

[92] Daniela Drescher, Guillermo Orts-Gil, Gregor Laube, Kishore Natte, Rudiger W. Veh, Werner Osterle, Janina Kneipp. 2011. "Toxicity of amorphous silica nanoparticles on eukaryotic cell model is determined by particle agglomeration and serum protein adsorption effects." *Analytical and Bioanalytical Chemistry* 400: 1367. doi:10.1007/s00216-011-4893-7.

[93] Slowing II, Trewyn BG, Giri S, Lin VY. 2007. "Mesoporous silica nanoparticles for drug delivery and biosensing applications." *Advanced Functional Materials* 17 (8): 1225-1236.

[94] Qhobosheane M, Santra S, Zhang P, Tan W. 2001. "Biochemically functionalized silica nanoparticles." *Analyst* 126 (8): 1274-1278.

[95] Albanese A, Tang PS, Chan WC. 2012. "The effect of nanoparticle size, shape, and surface chemistry on biological systems." *Annual Review of Biomedical Engineering* 14: 1-16.

[96] Gref R, Minamitake Y, Peracchia MT, Trubetskoy V, Torchilin V, Langer R. 1994. "Biodegradeable long-circulating polymeric nanospheres." *Science* 263 (5153): 1600-1603.

[97] Kolhar P, Anselmo AC, Gupta V, Pant K, Prabhakarpandian B, Ruoslhti E. 2013. "Using shape effects to target antibody-coated nanoparticles to lung and brain endothelium." *PNAS* 110 (26): 10753-10758.

[98] Klose D, Siepmann F, Elkharraz K, Krenzlin S, Siepmann J. 2006. "How porosity and size affect the drug release mechanisms from PLGA-based microparticles." *International Journal of Pharmaceutics* 314 (2): 198-206.

[99] Chithrani BD, Ghazani AA, Chan WC. 2006. "Determining the size and shape dependence of gold nanoparticle uptake into mammalian cells." *Nano Letters* 6 (4): 662-668.

[100] Champion JA, Mitragotri S. 2006. "Role of target geometry in phagocytosis." *PNAS* 103 (13): 4930-4934.

[101] Benezra M, Penate-Medina O, Zanzonico PB, Schaer D, Ow H, Burns A. 2011. "Multimodal silica nanoparticles are effective cancer-targeted probes in a model of human melanoma." *Journal of Clinical Investigation* 121 (7): 2768-2780.

[102] Bradbury MS, Phillips E, Montero PH, Cheal SM, Stambuk H, Durack JC. 2013. "Clinically-translated silica nanoparticles dual-modality cancer-targeted probes for image-guided surgery and interventions." *Integrative Biology* 5 (1): 74-86.

[103] Michalet X, Pinaud FF, Bentolila LA, Tsay JM, Doose S, Li JJ. 2005. "Quantum dots for live cells, in vivo imaging, and diagnostics." *Science* 307 (5709): 538-544.

[104] Sumistha Das, Nitai Debnath, Yingjun Cui, Jason Unrine, Subba Reddy Palli. 2015. "Chitosan, Carbon Quantum Dot, and Silica Nanoparticle Mediated dsRNA Delivery for Gene Silencing in Aedes aegypti: A Comparative Analysis." *ACS Applied Materials and Interfaces* 7 (35): 19530-19535. doi:10.1021/acsami.5b05232.

[105] X. Michalet, F.F. Pinaud, L.A. Bentolila, J.M. Tsay, S. Doose, J.J. Li. 2005. "Quantum dots for live cells, *in vivo* imaging, and diagnostics." *Science* 307 (5709): 538-544. doi:10.1126/science.1104274.

[106] Sumio Iijima. 1991. "Helical mictrotubules of graphitic carbon." *Nature* 354: 56-58. doi:10.1038/354056a0.

[107] Marya Ahmed, Xiaoze Jiang, Zhicheng Deng, Ravin Narain. 2009. "Cationic Glyco-Functionalized Single-Walled Carbon Nanotubes as Efficient Gene Delivery Vehicles." *Bioconjugate Chemistry* 20 (11): 2017-2022. doi:10.1021/bc900229v.

[108] Davide Pantarotto, Ravi Singh, David McCarthy, Mathieu Erhardt, Jean-Paul Briand, Maurizio Parto. 2004. "Functionalized Carbon Nanotubes for Plasmid DNA Gene Delivery." *Angewandte Chemie International Edition* 43 (39). doi:10.1002/anie.200460437.

[109] Zhuang Liu, Xiaoming Sun, Nozomi Nakayama-Ratchford, Hongjie Dai. 2007. "Supramolecular Chemistry on Water-Soluble Carbon Nanotubes for Drug Loading and Delivery." *ACS Nano* 1 (1): 50-56. doi:10.1021/nn700040t.

[110] Zhuang Liu, Joshua T. Robinson, Xiaoming Sun, Hongjie Dai. 2008. "PEGylated Nanographene Oxide for Delivery of Water-Insoluble Cancer Drugs." *JACS* 130 (33): 10876-10877. doi:10.1021/ja803688x.

[111] Nadine Wong Shi Kam, Zhuang Liu, Hongjie Dai. 2005. "Functionalization of Carbon Nanotubes via Cleavable Disulfide Bonds for Efficient Intracellular Delivery of siRNA and Potent Gene Silencing." *JACS* 127 (36): 12492-12493. doi:10.1021/ja053962k.

[112] Dong Cai, Jennifer M Mataraza, Zheng-Hong Qin, Zhongping Huang, Jianyu Huang, Thomas C Chiles, David Carnahan, Kris Kempa, Zhifeng Ren. 2005. "Highly efficient molecular delivery into mammalian cells using carbon nanotube spearing." *Nature Methods* 2: 449-454.

[113] Brahma N. Singh, Prateeksha, Vijai K. Gupta, Jieyin Chen, Atanas G. Atanasov. 2017. "Organic Nanoparticle-Based Combinatory Appraoches for Gene Therapy." *Trends in Biotechnology* 35 (12): 1121-1124. doi:10.1016/j.tibtech.2017.07.010.

[114] David W. Deamer. 2010. "From "Banghasomes" to liposomes: A memoir of Alec Bangham, 1921-2010." *The FASEB Journal - Milestone* 24: 1308-1310. doi:10.1096/fj.10-0503.

[115] A. D. Bangham, R. W. Horne. 1964. "Negative staining of phospholipids and their structural modification by surface-active agents as observed in the electron microscope." *Journal of Molecular Biology* 8 (5): 660-668.

[116] Melis Cagdas, Ali Demir Sezer, Seyda Bucak. 2014. "Liposomes as Potential Drug Carrier Systems for Drug Delivery." In *Application of Nanotechnology in Drug Delivery*, edited by Ali Demir Sezer. IntechOpen. doi:10.5772/58459.

[117] Peter C. Soema, Geert-Jan Willems, Wim Jiskoot, Jean-Pierre Amorij, Gideon F. Kersten. 2015. "Predicting the influence of liposomal lipid composition on liposome size, zeta potential and liposome-induced dendritic cell maturation using a design of experiments approach." *European Journal of Pharmaceutics and Biopharmaceutics* 94: 427-435. doi:10.1016/j.ejpb.2015.06.026.

[118] Yolanda Diebold, Miguel Jarrin, Victoria Saez, Edison LS Carvalho, Maria Orea, Margarita Calonge, Begona seijo, Maria J. Alonso. 2007. "Ocular drug delivery by liposome-chitosan nanoparticle complexes (LCS-NP)." *Biomaterials* 28 (8): 1553-1564. doi:10.1016/j.biomaterials.2006.11.028.

[119] Liangzhu Feng, Min Gao, Danlei Tao, Qian Chen, Hairong Wang, Ziliang Dong, Meiwan Chen, Zhuang Liu. 2016. "Cisplatin-Prodrug-Constructed Liposomes as a Versitile Theranostic Nanoplatform for Bimodal Imaging Guided Combination Cancer Therapy." *Advanced Functional Materials* 26 (13). doi:10.1002/adfm.201504899.

[120] Benvegnu T, Lemiegre L, Cammas-Marion S. 2009. "New generation of liposomes called archaeosomes based on natural or synthetic archaeal lipids as innovative formulations for drug delivery." *Recent Patents on Drug Delivery & Formulation* 3 (3): 206-220.

[121] Dinesh Mishra, Pradyumma Kumar Mishra, Sunil Dabadghao, Vaibhav Dubey, Manoj Nahar, Narendra K. Jain. 2010. "Comparative evaluation of hepatitis B surface antigen-loaded slastic liposomes and ethosomes for human dendritic cell uptake and immune response." *Nanomedicine: Nanotechnology, Biology and Medicine* 6 (1): 110-118. doi:10.1016/j.nano.2009.04.003.

[122] Clague P. Hodgson, Fauzia Solaiman. 1996. "Virosomes: Cationic Liposomes Enhance Retroviral Transduction." *Nature Biotechnology* 14: 339-342. doi:10.1038/nbt0396-339.

[123] Cevc, Gblume G. 1992. "Drug-Carrier and Stability Properties of the Long-Lived Lipid Vesicles. Cryptosomes, in vitro and in vivo." *Journal of Liposome Research* 2 (3): 355-368.

[124] Ijeoma F. Uchegbu, Suresh P. Vyas. 1998. "Non-ionic surfactant based vesicles (niosomes) in drug delivery." *International Journal of Pharmaceutics* 172 (1-2): 33-70. doi:10.1016/S0378-5173(98)00169-0.

[125] Benson, Heather AE. 2006. "Transfersomes for transdermal drug delivery." *Expert Opinion on drug delivery* 3 (6): 727-737.

[126] Rajesh K. Gupta, Carole L. Varanelli, Paul Griffin, Donald F.H. Wallach, George R. Siber. 1996. "Adjuvant properties of non-phospholipid liposomes (Novasomes) in experimental animals for human vaccine antigens." *Vaccine* 14 (3): 219-225. doi:10.1016/0264-410X(95)00182-Z.

[127] S. P. Vyas, Rasika Subhedar, Sanyog Jain. 2010. "Development and characterization of emulsomes for sustained and targeted delivery of an antiviral agent to liver." *Journal of Pharmacy and Pharmacology* 58 (3). doi:10.1211/jpp,58.3.0005.

[128] Lasic, D.D. 1997. "Recent developments in medical applications of liposomes: sterically stabilized liposomes in cancer therapy and gene delivery in vivo." *Journal of Controlled Release* 48 (2-3): 203-222. doi:10.1016/S0168-3659(97)00045-X.

[129] Yuhong Xu, Sek-Wen Hui, Peter Frederik, Francis C. Szoka Jr. 1999. "Physiochemical Characterization and Purification of Cationic Lipoplexes." *Biophysical Journal* 77 (1): 341-353. doi:10.1016/S0006-3495(99)76894-3.

[130] Yi-You Huang, Ching-Hua Wang. 2006. "Pulmonary delivery of insulin by liposomal carriers." *Journal of Controlled Release* 113 (1): 9-14. doi:10.1016/j.jconrel.2006.03.014.

[131] Thomas W. Geisbert, Amy CH Lee, Marjorie Robbins, Joan B. Geisbert, Anna N Honko, Vandana Sood, Joshua C. Johnson, Susan de Jong, Iran Tavakoli, Adam Judge, Lisa E. Hensley, Ian MacLachlan. 2010. "Postexposure protection of non-human primates against a lethal Ebola virus challenge with RNA interference: a proof-of-concept study." *The Lancet* 375 (9729): 1896-1905. doi:10.1016/S0140-6736(10)60357-1.

[132] Laura A. Smith, Xiaohua Liu, Peter X. Ma. 2008. "Tissue Engineering with nano-fibrous scaffolds." *Soft Matter* 4 (11): 2144-2149.

[133] Mario C. Filion, Nigel C. Phillips. 1997. "Toxicity and immunomodulatory activity of liposomal vectors formulated with cationic lipids toward immune effector cells." *Biochimica et Biophysica Acta (BBA) - Biomembranes* 1329 (2): 345-356.

[134] Hongtao Lv, Shubiao Zhang, Bing Wang, Shaohui Cui, Jie Yan. 2006. "Toxicity of cationic lipids and cationic polymers in gene delivery." *Journal of Controlled Release* 114 (1): 100-109. doi:10.1016/j.jconrel.2006.04.014.

[135] Gubernator, Jerzy. 2011. "Active methods of drug loading into iposomes: recent strategies for stable drug entrapment and increased in vivo activity." *Expert Opinion on Drug Delivery* 8 (5): 565-580.

[136] Daneil Bobo, Kye J. Robinson, Jiaul Islam, Kristofer J. Thurecht, Simon R. Corrie. 2016. "Nanoparticle-Based Medicines: A Review of FDA-Approved Materials and Clinical Trials to Date." *Pharmaceutical Research* 33 (10): 2373-2387. doi:10.1007/s11095-016-1958-5.

[137] Apurva Badkas, Evan Frank, Zilan Zhou, Mina Jafari, Harish Chandra, Vishnu Sriram, Joo-Youp Lee Jagjit S. Yadav. 2018. "Modulation of in vitro phagocytic uptake and immunogenicity potential of modified Herceptin - conjugated PLGA-PEG nanoparticles for drug delivery." *Colloids and Surfaces B: Biointerfaces* 162: 271-278. doi:10.1016/j.colsurfb.2017.12.001.

[138] James I. Andorko, Krystina L. Hess, Kevin G. Pineault, Christopher M. Jewell. 2016. "Intrinsic immunogenicity of rapidly-degradable polymers evolves during degradation." *Acta Biomaterialia* 32 (1): 24-34. doi:10.1016/j.actbio.2015.12.026.

[139] Rachel K. O'Reilly, Craig J. Hawker, Karen L. Wooley. 2006. "Cross-linked block copolymer micelles: functional nanostructures of great potential and versatility." *Chemical Society Reviews* 35: 1068-1083.

[140] Farha Masood. 2016. "Polymeric nanoparticles for targeted drug delivery system for cancer therapy." *Materials Science and Engineering* 60: 569-578. doi:10.1016/j.msec.2015.11.067.

[141] Jung Seok Lee, Jan Feijen. 2012. "Polymersomes for drug delivery: Design, formation and characterization." *Journal of Controlled Release* 161 (2): 473-483. doi:10.1016/j.jconrel.2011.10.005.

[142] Dalia Hope Levine, P. Peter Ghoroghchian, Jaclyn Freudenberg, Geng Zhang, Michael J. Therien, Mark I. Greene, Daniel A. Hammer, Ramachandran Murali. 2008. "Polymersomes: A new multi-functional tool for cancer diagnosis and therapy." *Methods* 46 (1): 25-32. doi:10.1016/j.ymeth.2008.05.006.

[143] Jing Xu, Qinghe Zhao, Yangmin Jin, Liyan Qiu. 2014. "High loading of hydrophilic/hydrphobic doxorubicin into polyphosphazene polymersome for breast cancer therapy." *Nanomedicine: Nanotechnology, Biology and Medicine* 10 (2): 349-358. doi:10.1016/j.nano.2013.08.004.

[144] Behr, Jean-Paul. 1997. "The Proton Sponge: A Trick to Enter Cells the Viruses Did Not Exploit." *CHIMIA International Journal for Chemistry* 51 (1-2): 34-36.

[145] Maryam Dabbaghi, Reza Kazemi Oskuee, Khadijeh Hashemi, Amir Afkhami Goli. 2018. "Evaluating polyethyleneimine/DNA nanoparticles-mediated damage to cellular organelles using endoplasmic reticulum stress profile." *Artificial Cells, Nanomedicine, and Biotechnology* 46 (1): 192-199. doi:10.1080/21691401.2017.1304406.

[146] Jaya Raju Lakkakula, Rui Werner Macedo Krause. 2014. "A vision for cyclodextrin nanoparticles in drug delivery systems and pharmaceutical applications." *Future Medicine* 9 (6).

[147] Jung Soo Suk, Qingguo Xu, Namho Kim, Justin Hanes, Laura M. Ensign. 2015. "PEGylation as a strategy for improving nanoparticle-based drug and gene delivery." *Advanced Drug Delivery Reviews* 99 (Pt A): 28-51. doi:10.1016/j.addr.2015.09.012.

[148] Siwen Hu-Lieskovan, Jeremy D. Heidel, Derek W. Bartlett, Mark E. Davis, Timothy J. Triche. 2005. "Sequence-Specific Knockdown of EWS-FL1 by targeted, nonviral delivery of small interfering RNA inhibits tumor growth in a murin model of metastatic ewig's sarcoma." *Cancer Research* 65 (19): 8984-8992.

[149] Jing Sun, Yubin Huang, Quan Shi, Xuesi Chen, Xiabin Jing. 2009. "Oxygen Carrier Based on Hemoglobin/Poly(L-lysine)-block-poly(L-phenylalanine) Vesicles." *Langmuir* 25 (24): 13726-13729. doi:10.1021/la901194k.

[150] Rafael Ischakov, Lihi Adler-Abramovich, Ludmila Buzhansky, Talia Shekhter, Ehud Gazit. 2013. "Peptide-based hydrogel nanoparticles as effective drug delivery agents." *Bioorganic & Medicinal Chemistry* 21 (12): 3517-3522. doi:10.1016/j.bmc.2013.03.012.

[151] Chaitali D. Dekiwadia, Ann C. Lawrie, John V. Fecondo. 2012. "Peptide-mediated cell penetration and targete delivery of gold nanoparticles into lysosomes." *Journal of Peptide Science* 18 (8). doi:10.1002/psc.2430.

[152] Julia Suhorutsenko, Nikita Oskolkov, Piret Arukuusk, Kaido Kurrikoff, Elo Eriste, Dana-Maria Copolovici, Ulo Langel. 2011. "Cell-Penetrating Peptides, PepFects, Show No Evidence of Toxicity and Immunogenicity In vitro and in vivo." *Bioconjugate Chemistry* 22 (1): 2255-2262. doi:10.1021/bc200293d.

[153] Nirmalya K Chaki, K Vijayamohanan. 2002. "Self-assembled monolayers as a tunable platform for biosensor applications." *Biosensors and Bioelectronics* 17 (1-2): 1-12. doi:10.1016/S0956-563(01)00277-9.

[154] Robert Chapman, Maarten Danial, Ming Liang Koh, Katrina A. Jolliffe, Sebastien Perrier. 2012. "Design and properties of functional nanotubes from the self-assembly of cyclic peptide templates." *Chemical Society Reviews* 41 (18): 6023-6041.

[155] Toral Patel, Jiangbing Zhou, Joseph M. Piepmeier, W. Mark Saltzman. 2012. "Polymeric nanoparticles for drug delivery to the central nervous system." *Advanced Drug Delivery Reviews* 64 (7): 701-705. doi:10.1016/j.addr.2011.12.006.

[156] Carlota Recio, Francesco Maione, Asif J. Iqbal, Nicola Mascolo, Vincenzo De Feo. 2017. "The potential therapeutic application of peptides and peptidomimetics in cardiovascular disease." *Frontiers in pharmacology* 526.

[157] Aimee Vasconcelos, Estefania Vega, Yolanda Perez, Maria J Gomara, Maria Luisa Garcia, Isabel Haro. 2015. "Conjugation of cell-penetrating peptides with poly (lactic-co-glycolic acid)-polyethylene glycol nanoparticles improves ocular drug delivery." *International Journal of Nanomedicine* 10: 609.

[158] Haitao Pan, Qixin Zheng, Xiaodong Guo, Yongchao Wu, Bin Wu. 2016. "Polydopamine-assised BMP2-derived peptides immobilization on biometric copolymer scaffold for enhanced bone induction in vitro and in vivo." *Colloids and surfaces B: Biointerfaces* 142: 1-9.

[159] Neda Habibi, Nazila Kamaly, Adnan Memic, Hadi Shafiee. 2016. "Self-assembled peptide-based nanostructures: Smart nanomaterials toward targeted drug delivery." *Nano today* 11 (1): 41-60.

[160] Sushanth Gudlur, Pinakin Sukthankar, Jian Gao, L. Adriana Avila, Yasuaki Hiromasa, Jianhan Chen, Takeo Iwamoto, John M. Tomich. 2012. “Peptide Nanovesicles Formed by the Self-Assembly of Branched Amphiphilic Peptides.” *PLOS ONE* 7 (9): e45374. doi:10.1371/journal.pone.0045374.

[161] Pinakin Sukthankar, Sushanth Gudlur, L. Adriana Avila, Susan K. Whitaker, Benjamin B. Katz, Yasuaki Hiromasa, Jian Gao, Prem Thapa, David Moore, Takeo Iwamoto, Jianhan Chen, John M. Tomich. 2013. “Branched oligopeptides form nano-capsules with lipid vesicle characteristics.” *Langmuir* (American Chemical Society) 29 (47): 14648-14654.

[162] Pinakin Sukthankar, L. Adriana Avila, Susan K. Whitaker, Takeo Iwamoto, Alfred Morgenstern, Christos Apostolidis, Ke Liu, Robert P. Hanzlik, Ekaterin Dadachova, John M. Tomich. 2014. “Branched amphiphilic peptide capsules: Cellular uptake and retention of encapsulated solutes.” *Biochimica et Biophysica Acta (BBA) - Biomembranes* 1838 (9): 2296-2305. doi:10.1016/j.bbamem.2014.02.005.

[163] L. Adriana Avila, Luana R. M. M. Aps, Pinakin Sukthankar, Nicoleta Ploscariu, Sushanth Gudlur, Ladislav Simo, Robert Szoszkiewicz, Yoonseong Park, Stella Y. Lee, Takeo Iwamoto, Luis C. S. Gerreira, John M. Tomich. 2015. “Branched Amphiphilics Cationic Oligopeptides Form Peptiplexes with DNA: A Study of Their Biophysical Properties and Transfection Efficiency.” *Molecular Pharmaceutics* 12 (3): 706-715. doi:10.1021/mp500524s.

[164] L. A. Avila, L.R.M.M. Aps, N. Ploscariu, P. Shukthankar, R. Guo, K.E. Wilkinson, P. Games, R. Szoszkiewicz. 2016. “Gene delivery and immunomodulatory effects of

plasmid DNA associated with Branched Amphiphilic Peptide Capsules.” *Journal of Controlled Release* 241: 15-24.

[165] A. Fire, D. Albertson, S.W. Harrison, D.G. Moerman. 1991. “Production of antisense RNA leads to effective and specific inhibition of gene expression in C. elegans muscle.” *Development* 113 (2): 503-514.

[166] Andrew Fire, SiQun Xu, Mary K. Montgomery, Steven A. Kostas, Samuel E. Driver, Craig C. Mello. 1998. “Potent and specific genetic interference by double-stranded RNA in Caenorhabditis elegans.” *Nature* 391 (6669): 806-811. doi:10.1038/35888.

[167] Xu Li, Yijie Chen, Mingqi Wang, Yongjie Ma, Weiliang Xia, Hongchen Gu. 2013. "A mesoporous silica nanoparticle-PEI-Fusogenic peptide system for siRNA delivery in cancer therapy." *Biomaterials* 34 (4): 1391-1401. doi:10.1016/j.biomaterials.2012.10.072.

[168] John DeVincenzo, Jeffrey E. Cehelsky, Rene Alvarez, Sayda Elbashir, Jens Harborth, Iva Toudjarska, Lubomir Nechev, Veeravagu Murugaiah, Andre Van Vliet, Akshay K. Vaishnaw, Rachel Meyers. 2008. "Evaluation of the safety, tolerability and pharmacokinetics of ALN-RSV01, a novel RNAi antiviral therapeutic directed against respiratory syncytical virus (RSV)." *Antiviral Research* 77 (3): 225-231. doi:10.1016/j.antiviral.2007.11.009.

[169] John DeVincenzo, Robert Lambkin-Williams, Tom Wilkinson, Jeffrey Cehelsky, Sara Nochur, Edward Walsh, Rachel Meyers, Jared Gollob, Akshay Vaishnaw. 2010. "A randomized, double-blind, placebo-controlled study of an RNAi-based therapy directed against respiratory syncytical virus." *PNAS* 107 (19): 8800-8805. doi:10.1073/pnas.0912186107.

[170] Hanneke Huvenne, Guy Smagghe. 2010. “Mechanisms of dsRNA uptake in insects and potential of RNAi for pest control: A review.” *Journal of Insect Physiology* 56 (3): 227-235. doi:10.1016/j.jinsphys.2009.10.004.

[171] Borovsky, D. 2005. "Insect peptide hormones and RNA-mediated interference (RNAi): promising technologies for future plan protection." *Phytoparasitica* 33 (2): 109-112.

[172] Karl H. J. Gordon, Peter M. Waterhouse. 2007. "RNAi for insect-proof plants." *Nature Biotechnology* 25: 1231-1232. doi:10.1038/nbt1107-1231.

[173] Ying-Bo Mao, Wen-Juan Cai, Jia-Wei Wang, Gao-Jie Hong, Xiao-Yuan Tao, Ling-Jian Wang, Yong-Ping Huang, Xiao-Ya Chen. 2007. "Silencing a cotton bollworm P450 monooxygenase gene by plant-mediated RNAi impairs larval tolerance of gossypol." *Nature Biotechnology* 25: 1307-1313. doi:10.1038/nbt1352.

[174] James A Baum, Thierry Bogaert, William Clinton, Gregory R Heck, Pasale Feldmann, Oliver Ilagan, Scott Johnson, Geert Plaetinck, Tichafa Munyikwa, Michael Pleau, Ty Vaughn, James Roberts. 2007. "Control of coleopteran insect pests through RNA interference." *Nature Biotechnology* 25: 1322-1326. doi:10.1038/nbt1359.

[175] Liuqi Gu, Douglas C. Knipple. 2013. “Recent Advances in RNA interference research in insects: Implications for future insect pest management strategies.” *Crop Protection* 45: 36-40. doi:10.1016/j.cropro.2012.10.004.

[176] Jennifer S. Whangbo, Craig P. Hunter. 2008. “Environmental RNA interference.” *Trends in Genetics* 24 (6): 297-305. doi:10.1016/j.tig.2008.03.007.

[177] Mallikarjuna R. Joga, Moises J. Zotti, Guy Smagghe, Olivier Christiaens. 2016. “RNAi Efficiency, Systemic Properties, and Novel Delivery Methods for Pest Insect Control: What We Know So Far.” *Frontiers in Physiology*. doi:10.3389/fphys.2016.00553.

[178] Kangxu Wang, Yingchuan Peng, Jian Pu, Wenxi Fu, Jiale Wang, Zhaojun Han. 2016. "Variation in RNAi efficacy among insect species is attributable to dsRNA degradation in vivo." *Insect Biochemistry and Molecular Biology* 77: 1-9. doi:10.1016/j.ibmb.2016.07.007.

[179] G. X. Quan, T. Kanda, T. Tamura. 2002. "Induction of the white egg 3 mutant phenotype by injection of the double-stranded RNA of the silkworm white gene." *Insect Molecular Biology* 11 (3). doi:10.1046/j.1365-2583.2002.00328.x.

[180] Mika Masumoto, Toshinobu Yanginuma, Teruyuki Niimi. 2009. "Functional analysis of Ultrabithorax in the silkworm, Bombyx mori, using RNAi." *Development Genes and Evolution* 219 (9-10): 437-444. doi:10.1007/s00427-009-0305-9.

[181] Olle Terenius, Alexie Papanicolaou, Jennie S. Garbutt, Ioannis Eleftherianos, Hanneke Huvenne, Sriamana Kanginakudru, Merete Albrechtsen, Chunju An, Jean-Luc Aymeric, Andrea Barthel, Piotr Bebas, Kavita Bitra, ..., Guy Smagghe. 2011. "RNA interference in Lepidoptera: An overview of successful and unsuccessful studies and implications for experimental design." *Journal of Insect Physiology* 57 (2): 231-245. doi:10.1016/j.jinsphys.2010.11.006.

[182] H-J. Xu, T. Chen, X-F. Ma, J. Xue, P-L. Pan, X-C. Zhang, J-A. Cheng, C-X. Zhang. 2013. “Genome-wide screening for components of small interfering RNA (siRNA) and micro-RNA (miRNA) pathways in the brown planthopper, Nilaparvata lugens (Hemiptera: Delphacidae).” *Insect Molecular Biology* 22 (6): 635-647. doi:10.1111/imb.12051.

[183] K. Cappelle, C.F.R. de Oliveira, B. Van Eynde, O. Christiaens, G. Smagghe. 2016. “The involvement of clathrin-mediated endocytosis and two Si-1-like transmembrane proteins in double-stranded RNA uptake in the Colorado potato beetle midgut.” *Insect Molecular Biology* 25 (3): 315-323. doi:10.1111/imb.12222.

[184] Yoshinori Tomoyasu, Sherry C. Miller, Shuichiro Tomita, Michael Schoppmeier, Daniela Grossmann, Gregor Bucher. 2008. “Exploring systemic RNA interference in insects: a genome-wide survey for RNAi genes in Tribolium.” *Genome Biology* 9 (1): R10. doi:10.1186/gb-2008-9-1-r10.

[185] Hao Zhang, Hai-Chao Li, Xue-Xia Miao. 2012. “Feasibility, limitation and possible solutions of RNAi-based technology for insect pest control.” *Insect Science* 20 (1): 15-30. doi:10.1111/j.1744-7917.2012.01513.x.

[186] L.A. Avila, R. Chandrasekar, K.E. Wilkinson, J. Balthazor, M. Heerman, J. Bechard, S. Brown, Y. Park, S. Dhar, G.R. Reeck, J.M. Tomich. 2018. “Delivery of lethal dsRNAs in insect diets by branched amphiphilic peptide capsules.” *Journal of Controlled Release* 273: 139-146.

[187] Tribolium Genome Sequencing Consortium. 2008. “The genome of the model beetle and pest Tribolium castaneum.” *Nature* 452: 949-955. doi:10.1038/nature06784.

[188] Kou-Wha Kuo, Shu-Hui Hsu, Yun-Ping Li, Wei-Ling Lin, Li-Feng Liu, Li-Ching Chang, Chih-Chao Lin, Chun-Nan Lin, Hamm-Ming Sheu. 2000. "Anticancer activity evaluation of the Solanum glycoalkaloid solamargine: Triggering apoptosis in human hepatoma cells." *Biochemical Pharmacology* 60 (12): 1865-1873. doi:10.1016/S0006-2952(00)00506-2.

[189] Anjiang Tan, Subba Reddy Palli. 2008. "Identification and characterization of nuclear receptors from the red flour beetle, Tribolium castaneum." *Insect Biochemistry and Molecular Biology* 38 (4): 430-439. doi:10.1016/j.ibmb.2007.09.012.

[190] Andria Apostolou, Yuxian Shen, Yan Liang, Jun Luo, Shengyun Fang. 2008. "Armet, a UPR-upregulated protein, inhibits cell proliferation and ER stress-induced cell death." *Experimental Cell Research* 314 (13): 2454-2467. doi:10.1016/j.yexcr.2008.05.001.

[191] Alexander G. Martynov, Elena N. Elpidina, Lindsey Perkin, Brenda Oppert. 2015. "Functional analysis of C1 family cysteine peptidases in the larval gut of Tenebrio molitor and Tribolium castaneum." *BMC Genomics* 16: 75. doi:10.1186/s12864-015-1306-x.

[192] Peter Walter, David Ron. 2011. “The Unfolded Protein Response: From Stress Pathway to Homeostatic Regulation.” *Science* 334 (6059): 1081-1086. doi:10.1126/science.1209038.

[193] Andria Apostolou, Yuxian Shen, Yan Liang, Jun Luo, Shengyun Fang. 2008. “Armet, a UPR-upregulated protein, inhibits cell proliferation and ER stress-induced cell death.” *Experimental Cell Research* 314 (13): 2454-2467. doi:10.1016/j.yexcr.2008.05.001.

[194] Miao Wang, Shiuan Wey, Yi Zhang, Risheng Ye, Amy S. Lee. 2009. “Role of the Unfolded Protein Response Regulator GRP78/BiP in Development, Cancer, and Neurological Disorders.” *Antioxidants and Redox Signaling* 11 (9): 2307-2316. doi:10.1089/ars.2009.2485.

[195] I. G Haas. 1994. “BiP (GRP78), an essential hsp70 resident protein in the endoplasmic reticulum.” *Experientia* 50 (11-12): 1012-1020. doi:10.1007/BF01923455.

[196] Ignacio Lopez, Anne-Sophie Tournillon, Rodrigo Prado Martins, Konstantinos Karakostis, Laurence Malbert-Colas, Karin Nylander, Robin Fahraeus. 2017. “p53-mediated

suppression of BiP triggers BIK-induced apoptosis during prolonged endoplasmic reticulum stress." *Cell Death & Differentiation* 24 (10): 1717-1729. doi:10.1038/cdd.2017.96.

[197] Archana Tadimalla, Peter J. Belmont, Donna J. Thuerauf, Matthew S. Glassy, Joshua J. Martindale, Natalie Gude, Mark A. Sussman, Christopher C. Glembotski. 2008. "Mesencephalic Astrocyte-Derived Neurotrophic Factor Is an Ischemia-Inucible Secreted Endoplasmic Reticulum Stress Response Protein in the Heart." *Circulation Research* 103 (11): 1249-1258. doi:10.1161/CIRCRESAHA.108.180679.

[198] n.d. DNA, RNA and oligo molecular weight (MW), mole, mass and molarity calculator. http://www.sciencelauncher.com/mwcalc.html.

[199] Richard W. Beeman, Jeffrey J. Stuart. 1990. "A Gene for Lindane + Cyclodiene Resistance in the Red Flour Beetle (Coleoptera: Tenebrionidae)." *Journal of Economic Entomology* 83 (5): 1745-1751. doi:10.1093/jee/83.5.1745.

[200] Yoshinori Tomoyasu, Robin E. Denell. 2004. "Larval RNAi in Tribolium (Coleoptera) for analyzing adult development." *Development Genes and Evolution* 214 (11): 575-578. doi:10.1007/s00427-004-0434-0.

[201] Estela L. Arrese, Jose L. Soulages. 2010. "Insect Fat Body: energy, metabolism, and regulation." *Annual Review of Entomology* 55: 207-225. doi:10.1146/annurev-ento-112408-085356.

[202] Claudia Aparecida Pacheco, Kaio Cesar Chaboli Alevi, Amanda Revazi, Maria Tercilia Vilela de Azeredo Oliverira. 2014. "Review: Malpighian Tubule, an Essential Organ for Insects." *Entomology, Ornithology & Herpetology: Current Research* 3 (2): 122. doi:10.4172/2161-0983.1000122.

[203] Sherry C. Miller, Keita Miyata, Susan J. Brown, Yoshinori Tomoyasu. 2012. "Dissecting Systemic RNA Interference in the Red Flour Beetle Tribolium castaneum: Parameters Affecting the Efficiency of RNAi." *PLoS ONE* 7 (10): e47431. doi:10.1371/journal.pone.0047431.

[204] Okoro Uchechi, John D. N. Ogbonna, Anthony A. Attama. 2014. "Nanoparticles for Dermal and Transdermal Drug Delivery." In *Application of Nanotechnology in Drug Delivery*, edited by Ali Demir Sezer. IntechOpen. doi:10.5772/58672.

[205] Prerana Carter, Balaji Narasimhan, Qun Wang. 2019. "Biocompatible nanoparticles and vesicular systems in transdermal drug delivery for various skin diseases." *International Journal of Pharmaceutics* 555: 49-62. doi:10.1016/j.ijpharm.2018.11.032.

[206] Xianfeng Chen. 2018. "Current and future technological advances in transdermal gene delivery." *Advanced Drug Delivery Reviews* 127: 85-105. doi:10.1016/j.addr.2017.12.014.

[207] Mohammad Hedayati, Bedri Abubaker-Sharif, Mohamed Khattab, Allen Razavi, Isa Mohammed, Arsalan Nejad, Michele Wabler, Haoming Zhou, Jana Mihalic, Cordula Gruettner, Theodore DeWeese, Robert Ivkov. 2018. "An optimised spectrophotometric assay for convenient and accurate quantitation of intracellular iron from iron oxide nanoparticles." *International Journal of Hyperthermia* 34 (4): 373-381. doi:10.1080/02656736.2017.1354403.

[208] Nazanin Hoshyar, Samantha Gray, Hongbin Han, Gang Bao. 2016. "The effect of nanoparticle size on *in vivo* pharmacokinetics and cellular interaction." *Nanomedicine* 11 (6): 673-692. doi:10.2217/nnm.16.5.

[209] Shyh-Dar Li, Leaf Huang. 2008. "Pharmacokinetics and Biodistribution of Nanoparticles." *Molecular Pharmaceutics* 5 (4): 496-504. doi:10.1021/mp800049w.

[210] Zhoumeng Lin, Nancy A. Monteiro-Riviere, Jim E. Riviere. 2014. "Pharmacokinetics of metallic nanoparticles." *WIREs: Nanomedicine and Nanobiotechnology* 7 (2): 189-217. doi:10.1002/wnan.1304.

[211] B.N. Swanson. 1985. "Medical use of dimethyl sulfoxide (DMSO)." *Reviews in Clinical & Basic Pharmacology* 5 (1-2):1-33.

[212] Rebecca Notman, Wouter K. den Otter, Masimo G. Noro, W.J. Briels, Jamshed Anwar. 2007. "The Permeability Enhancing Mechanism of DMSO in Ceramide Bilayers Simulated by Molecular Dynamics." *Biophysical Journal* 93 (6): 2056-2068. doi:10.1529/biophysj.107.104703

[213] Mark R. Prausnitz, Robert Langer. 2009. "Transdermal drug delivery." *Nature Biotechnology* 26 (11): 1261-1268. doi:10.1038/nbt.1504

[214] Jennifer Le. 2019. "Drug Administration." *MSD Manual Consumer Version.* Merck and Co., Inc. (MSD). https://www.msdmanuals.com/en-in/home/drugs/administration-and-kinetics-of-drugs/drug-administration.

[215] Ryan F. Donnelly. 2017. "Vaccine delivery systems." *Human Vaccines and Immunotherapeutics* 13 (1): 17-18. doi:10.1080/21645515.2016.1259043.

[216] Carlos Gamazo, Yadira Pastor, Eneko Larraneta, Melibea Berzosa, Juan M Irache, Ryan F. Donnelly. 2018. "Understanding the basis of transcutaneous vaccine delivery." *Therapeutic Delivery* 10 (1): 63-80. doi:10.4155/tde-2018-0054.

[217] Christine Case-Lo. 2017. "What is a subcutaneous injection?" Edited by Carissa Stephens, RN, CCRN, CPN. https://www.healthline.com/health/subcutaneous-injection.

[218] Carol Taylor. 2008. *Fundamentals of Nursing: The Art and Science of Nursng Care.* Philadelphia: Lippincott Williams & Wilkins.

[219] Jacquelyn Cafasso. 2017. “What are intramuscular injections?” Edited by Deborah Weatherspoon, PhD, RN, CRNA. https://www.healthline.com/health/intramuscular-injection.

[220] Christine Case-Lo. 2016. “Intravenous Medication Administration: What to Know.” Edited by Aleah Rodriguez, PharmD. https://www.healthline.com/health/intravenous-medication-administration-what-to-know.

[221] E. Criscuolo, V. Caputo, R. A. Diotti, G. A. Sautto, G. A. Kirchenbaum, N. Clementi. 2019. “Alternative Methods of Vaccine Delivery: An Overview of Edible and Intradermal Vaccines.” *Journal of Immunology Research* 2019. doi:10.1155/2019/8303648.

[222] Glynda Reese Doyle, Jodie Anita McCutcheon. 2019. “Parenteral Medical Administration.” Chapter 7 in *Clinical Procedures for Safer Patient Care*. B.C. Open Textbook project. https://opentextbc.ca/clinicalskills/chapter/7-1-introduction/.

[223] Chia-Lang Fang, Ibrahim A. Aljuffali, Yi-Ching Li, Jia-You Fang. 2014. “Delivery and targeting of nanoparticles into hair follicles.” *Therapeutic Delivery* 5 (9): 991-1006. doi:10.4155/tde.14.61.

[224] Alexa Patzelt, Heike Richter, Fanny Knorr, Ulrich Schafer, Claus-Michael Lehr, Lars Dahne, Wolfram Sterry, Juergen Lademann. 2011. “Selective follicular targeting by modification of the particle sizes.” *Journal of Controlled Release* 150 (1): 45-48. doi:10.1016/j.jconrel.2010.11.015

[225] 2019. *Biologicals: DNA vaccines.* https://www.who.int/biologicals/areas/vaccines/dna/en/.

[226] Terence R. Flotte, Shan Lu. 2018. "DNA Vaccination in 2018: An Update." *Huan Gene Therapy* 29 (9): 963-965. doi:10.1089/hum.2018.29073.trf.

[227] Karuppiah Muthumani, Peter Block, Seleeke Flingai, Nagarajan Muruganantham, Itta Krishna Chaaithanya, Colleen Tingey, Megan Wise, Emma L. Reuschel, Christopher Chung, Abirami Muthumani. 2016. "Rapid and Long-Term Immunity Elicited by DNA-Encoded Antibody Prophylaxis and DNA Vaccination Against Chikungunya Virus." *The Journal of Infectious Diseases* 214 (3): 369-378. doi:10.1093/infdis/jiw111.

[228] Bryan D. Griffin, Kar Muthumani, Gary P. Kobinger. 2017. "DNA vaccination protects mice against Zika virus-induced damage to the testes." *Nature Communications* 8: 15743. doi:10.1038/ncomms15743.

[229] Spela Kos, Kevin Vanvarenberg, Tanja Dolinsek, Maja Cemazar, Jure Jelenc, Veronique Preat, Gregor Sersa, Gaelle Vandermeulen. 2017. "Gene electrotransfer into skin using noninvasive multi-electrode array for vaccination and wound healing." *Bioelectrochemistry* 114: 33-41. doi:10.1016/j.bioelechem.2016.12.002.

[230] Xiaoyi Sun, Linghui Zeng, Yongzhuo Huang. 2019. "Transcutaneous delivery of DNA/mRNA for cancer therapeutic vaccination." *The Journal of Gene Medicine* 21 (7). doi:10.1002/jgm.3089.

[231] Michael Zakrewsky, Sunny Kumar, Samir Mitragotri. 2015. "Nucleic acid delivery into skin for the treatment of skin disease: Proofs-of-concept, potential impact, and remaining challenges." *Journal of Controlled Release* 219: 445-456. doi:10.1016/j.jconrel.2015.09.017.

[232] Pinaki R. Desai, Srujan Marepally, Apurva R. Patel, Chandrashekhar Voshavar, Arabinda Chaudhuri, Mandip Singh. 2013. "Topical Delivery of anti- TNFalpha siRNA and capsicin via novel lipid-polymer hybrid nanoparticles efficiently inhibits skin inflammation in vivo." *Journal of Controlled Release* 170 (1): 51-63.

[233] Suman Labala, Anup Jose, Venkata Vamsi Krishna Venuganti. 2016. "Transcutaneous iontophoretic delivery of STAT3 siRNA using layer-by layer chitosan coated gold nanoparticles to treat melanoma." *Colloids and Surfaces B: Biointerfaces* 146: 188-197.

[234] Jiong Li, Xia Li, Yan Zhang, Xi K. Zhou, Han S. Yang, Xian C. Chen, Yong S. Wang, Yu Q. Wei, Li J. Chen, Huo Z. Hu, Chang Y. Liu. 2010. "Gene therapy for psoriasis in the K14-VEGF transgenic mouse model by topical transdermal delivery of interleukin-4 using ultradeformable cationic liposome." *The Journal of Gene Medicine* 12 (6). doi:10.1002/jgm.1459.

[235] Tamae Uchida, Takanori Kanazawa, Yuuki Takashima, Hiroaki Okada. 2011. "Development of an efficient transdermal delivery system of small interfering RNA using functional peptides, Tat and AT-1002." *Chemical and Pharmaceutical Bulletin* 59 (2): 196-201.

[236] Anna U. Bielinkska, Ann Yen, Huai Liang Wu, Kathleen M Zahos, Rong Sun, Norman D. Weiner, James R. Baker Jr, Blake J. Roessler. 2000. "Application of membrane-based dendrimer/DNA complexes for solid phase transfection in vitro and in vivo." *Biomaterials* 21 (9): 877-887.

[237] Inayat Bashir Pathan, C. Mallikarjuna Setty. 2009. "Chemical penetration enhancers for transdermal drug delivery systems." *Tropical Journal of Pharmaceutical Research* 8 (2).

[238] Brayton, C. Flagg. 1986. "Dimethyl sulfoxide (DMSO): a review." *The Cornell Veterinarian* 76 (1): 61-90.

[239] Joana Galvao, Benjamin Davis, Mark Tilley, Eduardo Normando, Michael R. Duchen, M. Francesca Cordeiro. 2014. "Unexpected low-dose toxicity of the universal solvent DMSO." *The FASEB Journal* 28 (3): 1317-1330.

[240] Marie Gaumet, Angelica Vargas, Robert Gurney, Florence Delie. 2008. "Nanoparticles for drug delivery: The need for preision in reporting particle size parameters." *European Journal of Pharmaceutics and Biopharmaceutics* 69 (1): 1-9. doi:10.1016/j.ejpb.2007.08.001.

[241] R. Nakaoka, Y. Tabata, T. Yamaoka, Y. Ikada. 1997. "Prolongation of the serum half-life period of superoxide dismutase by poly(ethylene glycol) modification." *Journal of Controlled Release* 46: 253-261.

[242] S.M. Moghimi, A.C. Hunter, J.C. Murray. 2001. "Long-crculating and target-specific nanoparticles: theory to practice." *Pharmacological Reviews* 53: 283-318.

[243] Susumu Nagayama, Ken-ichi Ogawara, Yoshiko Fukuoka, Kazutaka Higaki, Toshikiro Kimura. 2007. "Time-dependent changes in opsonin amount associated on nanoparticles alter their hepatic uptake characteristics." *International Journal of Pharmaceutics* 342 (1-2): 215-221.

[244] Moghimi, S.M. 1995. "Mechanisms of splenic clearance of blood cells and particles: towards development of new splenotropic agents." *Advanced Drug Delivery Reviews* 17: 103-115.

[245] Moghimi, S.M. 1995. "Exploiting bone marrow microvascular structure for drug delivery and future therapies." *Advanced Drug Delivery Reviews* 17: 61-73.

[246] T. Banerjee, S. Mitra, S.A. Kumar, S.R. Kumar, A. Maitra. 2002. "Preparation, characterization and biodistribution of ultrafine chitosan nanoparticles." *International Journal of Pharmaceutics* 243: 93-105.

[247] Blanca del Rosal, Irene Villa, Daniel Jaque, Francisco Sanz-Rodriguez. 2015. "In vivo autofluorescence in the biological windows: the role of pigmentation." *Journal of Biophotonics* 9 (10). doi:10.1002/jbio.201500271.

[248] Pavithra Natarajan, Pinakin Sukthankar, Jessica Changstrom, Christopher S. Holland, Shannon Barry, Wayne B. Hunter, Christopher M. Sorensen, John M. Tomich. 2018. "Synthesis and Characterization of Multifunctional Branched Amphiphilic Peptide Bilayer Conjugated Gold Nanoparticles." *ACS Omega* 3 (9): 11071-11083. doi:10.1021/acsomega.8b01633.

[249] Po-Wei Lee, Sheng-Hsiang Hsu, Jin-Sheng Tsai, Fu-Rong Chen, Pei-Jai Huang, Cherng-Jyh Ke, Zi-Xian Liao, Chun-Wen Hsiao, Hao-Jan Lin, Hsing-Wen Sung. 2010. "Multifunctional core-shell polymeric nanoparticles for transdermal DNA delivery and epidermal Langerhans cells tracking." *Biomaterials* 31 (8): 2425-2434. doi:10.1016/j.biomaterials.2009.11.100.

[250] J.A. Mikszta, J.B. Alarcon, J.M. Brittingham, D.E. Sutter, R.J. Pettis, N.G. Harvey. 2002. "Improved genetic immunization via micromechanical disruption of skin-barrier function and targeted epidermal delivery." *Nature Medicine* 8: 415-419.

[251] U. Masaki, N. Hideshi, K. Tohru, S. Toshinobu, O. Masahiko, J. Kazuhiko. 2006. "Immunization by particle bombardment of antigen-loaded poly-(DL-lactide-co-glycolide) microspheres in mice." *Vaccine* 24: 2120-2130.

[252] Z. Cui, R.J. Mumper. 2001. "Chitosan-based nanoparticles for topical genetic immunization." *Journal of Controlled Release* 75: 409-419.

[253] S.T. Reddy, M.A. Swartz, J.A. Hubbell. 206. "Targeting dendritic cells with biomaterials: developing the next generation of vaccines." *Trends in Immunology* 27: 573-579.

[254] S. Garg, A. Oran, J. Wajchman, S. Sasaki, C.H. Maris, J.A. Kapp. 2003. "Genetic tagging shows increased frequency and longevity of antigen-presenting, skin-derived dendritic cells in vivo." *Nature Immunology* 4: 907-912.

[255] Z. Davoudi, N. Peroutka-Bigus, B. Bellaire, M. Wannemuehler, T.A. Barrett, B. Narasimhan. 2018. "Intestinal organoids containing poly (lactic-co-glycolic acid) nanoparticles for the treatment of inflammatory bowl diseases." *Journal of Biomedical Materials Research Part A* 106 (4): 876-886.

[256] H. Zheng, L. Yin, X. Zhang, R. Hu, Y. Yin. 2016. "Redox sensitive shell and core crosslinked hyaluronic acid nanocarriers for tumor-targeted drug delivery." *Journal of Biomedical Nanotechnology* 12 (8): 1641-1653.

[257] R. Hu, H. Zheng, J. Cao, Z. Davoudi, Q. Wang. 2017. "Self-assembled hyaluronic acid nanoparticles for pH-sensitive release of doxorubicin: synthesis and in vitro characterization." *Journal of Biomedical Nanotechnology* 13 (9): 1058-1068.

[258] T.X. Nguyen, L. Huang, M. Gauthier, G. Yang, Q. Wang. 2016. "Recent advances in liposomes surface modification for oral drug delivery." *Nanomedicine* 11 (9): 1169-1185.

[259] C.O. Silva, P. Rijo, J. Molpeceres, I.V. Figueiredo, L. Ascensao, A.S. Fernandes. 2015. "Polymeric nanoparticles modified with fatty acids encapsulating betamethasone for anti-inflammatory treatment." *International Journal of Pharmaceutics* 493 (1-2): 271-284.

[260] C.L. Fang, I.A. Aljuffali, Y.C. Li, J.Y. Fang. 2014. "Delivery and targeting of nanoparticles into hair follicles." *Therapeutic Delivery* 5 (9): 991-1006.

[261] Dean L. 2005. Blood Groups and Red Cell Antigens [Internet]. Bethesda (MD): National Center for Biotechnology Information (US). Chapter 1, Blood and the cells it contains. Available from: https://www.ncbi.nlm.nih.gov/books/NBK2263/

[262] Saljoughian, M. 2007. “Iron Deficiency Anemia: A Closer Look.” *U.S. Pharmacist* 32 (8): HS26-HS37.

[263] L.G. Barron, L. Gagne, F.C. Szoka Jr. 1999. “Lipoplex-mediated gene delivery to the lung occurs within 60 minutes of intravenous administration.” *Human Gene Therapy* 10: 1683-1694.

[264] M.B. Bally, P. Harvie, F.M. Wong. 2000. “Use of poly(ethylene glycol)lipid conjugates to regulate the surface attributes and transfection ativity of lipid-dna particles.” *Journal of Pharmaceutical Sciences* 89: 652-663

[265] Adrian Chrastina, Kerri A. Massey, Jan E. Schnitzer. 2011. “Overcoming in vivo barriers to targeted nanodelivery.” *Wiley Interdisciplinary Reviews: Nanomedicine and Nanobiotechnology* 3 (4).

[266] S.M. Elbashir, W. Lendeckel, T. Tuschl. 2001. “RNA interference is mediated by 21- and 22-nucleotide RNAs.” *Genes & Development* 15 (2): 188-200.

[267] S.M. Hammond, S. Boettcher, A.A. Caudy, R. Kobayashi, G.J. Hannon. 2001. “Argonaute2, a link between genetic and biochemical analyses of RNAi.” *Science* 293 (5532): 1146-1150.

[268] G. Meister, T. Tuschl. 2004. “Mechanisms of gene silencing by double-stranded RNA.” *Nature* 431 (7006): 343-349.

[269] Y. Tomari, P.D. Zamore. 2005. “Perspective: machines for RNAi.” *Genes & Development* 19 (5): 517-529.

[270] Yifan Wu, Wuxu Zhang, Yuxia Wang, Qian Li, Guo Gao, Na Dong, Hengyao Hu, Kan Wang, Junhua Wu, Zhongcai Gao, Daxiang Cui. 2012. “Establishment of a method to determine the magnetic particles in mouse tissues.” *Nanoscale Research Letters* 7 (1): 665. doi:10.1186/1556-276X-7-665

# Appendix A - Chapter 2 Supplemental Data

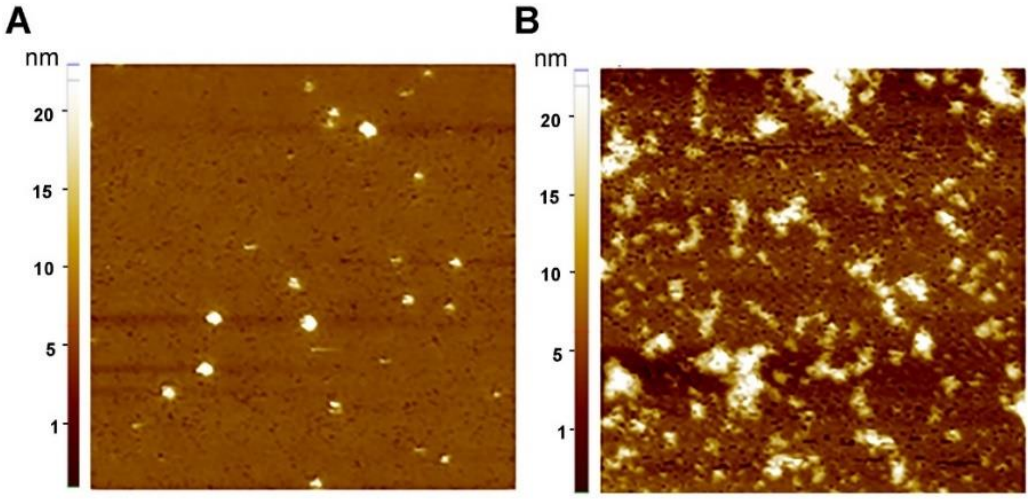


**Figure A.1 - AFM of BAPC Complexes**

**(A)** Atomic Force Microscopy (AFM) image analysis of the BAPC nanoparticles (40 μM). **(B)** AFM image analysis of dsRNA-BAPC complexes (1 μg and 40 μM respectively). Data and images collected by another lab member. Reprinted with permission from Avila, L. Adriana et al. 2018. Delivery of lethal dsRNAs in insect diets by branched amphiphilic peptide capsules. Journal of Controlled Release 273: 139-146. Copyright 2018 Elsevier B.V.

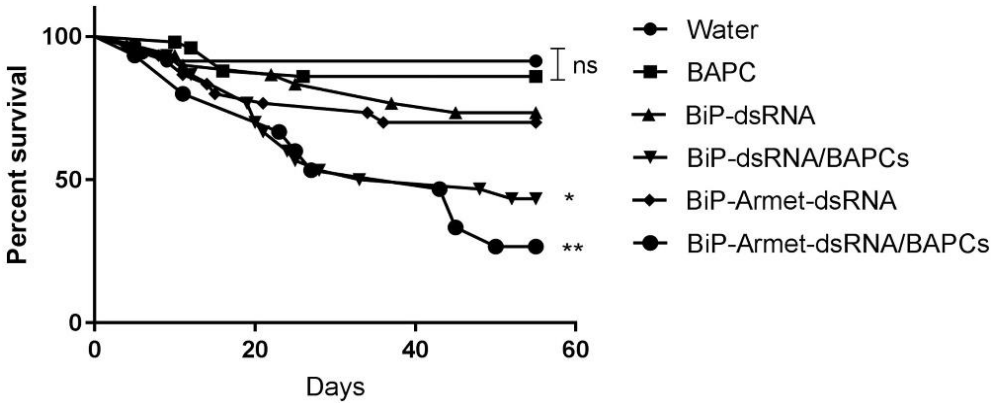


**Figure A.2 - Survival Curves Showing Effect of dsRNA-BAPC Complexes in *T. castaneum***

Early-instar larvae were fed wheat-flour/yeast extract diet supplemented with Armet- and BiP-dsRNA alone or together (1µg; 500 ng of each when fed together) with or without BAPCs. Day 1 represents the first day of feeding. After 6 days, the insects were transferred to the standard diet, lacking dsRNA or BAPC additions. Diseased Tribolium were counted on a daily basis. The number of insects on day 1 were 35 (diet alone); 30 (water plus CaCl2); 50 (BAPCs only control); 30 (Armet-dsRNA alone); 30 (BiP-dsRNA alone); 30 (BiP-dsRNA/BAPC complexes); 30(BiP-Armet-dsRNA/BAPC complexes). Pupation started over a range of days, averaging about day 30, with eclosion (emergence of adults from pupae) over a range starting about day 40. No deaths occurred in the adult stage. Statistical significance: (*) $p < 0.05$, (**) $p < 0.01$, versus control groups treated with naked BiP-dsRNA or BiP-Armet-dsRNA. Non-statistical significance (ns) was considered when $p > 0.05$. Differences between values were compared by Log-rank (Mentel-Cox) test. Some diet was prepared by Kayla Nutsch, other data collection and *T. castaneum* monitoring was carried out by other lab members. Reprinted with permission from Avila, L. Adriana et al. 2018. Delivery of lethal dsRNAs in insect diets by branched amphiphilic peptide capsules. Journal of Controlled Release 273: 139-146. Copyright 2018 Elsevier B.V.

# Appendix B - Chapter 3 Supplemental Data

| Incubation Time / Trial | Exposure Time (min) | Kidney (g) | Spleen (g) | Lungs (g) | Liver (g) | Feces (g) |
|---|---|---|---|---|---|---|
| 1 h - Trail 1 | 30m | 0.194 | 0.069 | 0.13 | 0.467 | 0.043 |
| | 15m | 0.219 | 0.087 | 0.082 | 0.272 | 0.061 |
| | 5m | 0.205 | 0.086 | 0.053 | 0.487 | 0.067 |
| | 1m | 0.221 | 0.067 | 0.146 | 0.506 | 0.151 |
| | No30m | 0.241 | 0.072 | 0.143 | 0.461 | 0.165 |
| 1 h - Trial 2 | 30m | 0.205 | 0.017 | 0.123 | 0.476 | 0.153 |
| | 15m | 0.184 | 0.087 | 0.184 | 0.595 | 0.101 |
| | 5m | 0.257 | 0.027 | 0.12 | 0.552 | 0.023 |
| | 1m | 0.174 | 0.091 | 0.14 | 0.6 | 0.126 |
| | No30m | 0.221 | 0.075 | 0.128 | 0.593 | 0.041 |
| 1 h - Trial 3 | 30m | 0.154 | 0.075 | 0.122 | 0.481 | 0.087 |
| | 15m | 0.212 | 0.066 | 0.175 | 0.418 | 0.121 |
| | 5m | 0.227 | 0.102 | 0.075 | 0.549 | 0.082 |
| | No30m | 0.146 | 0.087 | 0.139 | 0.472 | 0.046 |
| 8 h - Trial 1 | 30m | 0.23 | 0.047 | 0.126 | 0.396 | 0.123 |
| | 15m | 0.236 | 0.074 | 0.075 | 0.345 | 0.08 |
| | 5m | 0.23 | 0.08 | 0.131 | 0.457 | 0.053 |
| | 1m | 0.181 | 0.096 | 0.145 | 0.25 | 0.057 |
| | No30m | 0.188 | 0.035 | 0.047 | 0.346 | 0.108 |
| 8 h - Trial 2 | 30m | 0.219 | 0.08 | 0.118 | 0.217 | 0.119 |
| | 15m | 0.161 | 0.061 | 0.144 | 0.373 | 0.064 |
| | 5m | 0.233 | 0.061 | 0.079 | 0.414 | 0.102 |
| | 1m | 0.218 | 0.062 | 0.148 | 0.307 | 0.055 |
| | No30m | 0.226 | 0.075 | 0.122 | 0.355 | 0.138 |
| 8 h - Trial 3 | 30m | 0.198 | 0.048 | 0.064 | 0.41 | 0.108 |
| | 15m | 0.162 | 0.049 | 0.044 | 0.3 | 0.123 |
| | 5m | 0.232 | 0.078 | 0.063 | 0.44 | 0.122 |
| | 1m | 0.201 | 0.086 | 0.168 | 0.384 | 0.064 |
| | No30m | 0.189 | 0.061 | 0.154 | 0.328 | 0.107 |
| 24 h - Trial 1 | 30m | 0.233 | 0.096 | 0.164 | 0.52 | 0.083 |
| | 15m | 0.261 | 0.067 | 0.117 | 0.343 | 0.143 |
| | 5m | 0.211 | 0.074 | 0.131 | 0.451 | 0.079 |
| | 1m | 0.223 | 0.075 | 0.06 | 0.558 | 0.133 |
| | No30m | 0.213 | 0.061 | 0.04 | 0.513 | 0.128 |
| 24 h - Trial 2 | 30m | 0.237 | 0.082 | 0.05 | 0.58 | 0.103 |
| | 15m | 0.201 | 0.082 | 0.109 | 0.497 | 0.118 |
| | 5m | 0.228 | 0.081 | 0.08 | 0.476 | 0.143 |
| | 1m | 0.23 | 0.091 | 0.154 | 0.467 | 0.074 |
| | No30m | 0.223 | 0.017 | 0.107 | 0.292 | 0.122 |
| 24 h - Trial 3 | 30m | 0.18 | 0.077 | 0.144 | 0.451 | 0.155 |
| | 15m | 0.202 | 0.01 | 0.122 | 0.439 | 0.217 |
| | 5m | 0.203 | 0.081 | 0.102 | 0.479 | 0.166 |
| | 1m | 0.214 | 0.052 | 0.155 | 0.449 | 0.109 |
| | No30m | 0.234 | 0.093 | 0.213 | 0.439 | 0.092 |

**Table B.1 - Weight of Tissues**

Weight of tissues collected. Incubation time refers to the time post exposure until euthanasia. Exposure time refers to the amount of time the tail was dipped into the solution containing BAP-MNBs with or without DMSO. 15m refers to 15 min exposure time with 0.1% DMSO. No30m refers to 30 min exposure time without DMSO.

| Incubation Time / Trial | Exposure Time (min) | Kidney (MNBs/g) | Spleen (MNBs/g) | Lungs (MNBs/g) | Liver (MNBs/g) | Feces (MNBs/g) |
|---|---|---|---|---|---|---|
| 1 h - Trail 1 | 30m | 2.53E+08 | 7.11E+08 | 4.16E+07 | 1.98E+08 | 2.35E+10 |
| | 15m | 6.22E+08 | 1.57E+09 | 1.13E+09 | 3.41E+08 | 2.23E+09 |
| | 5m | 4.52E+08 | 2.09E+09 | 9.25E+08 | 3.69E+08 | 4.64E+09 |
| | 1m | 2.22E+08 | 0.00E+00 | 1.53E+09 | 5.28E+08 | 1.48E+09 |
| | No30m | 5.65E+08 | 1.89E+09 | 9.53E+08 | 2.01E+08 | 8.26E+08 |
| 1 h - Trial 2 | 30m | 6.65E+08 | 5.45E+09 | 4.40E+07 | 1.95E+08 | 3.54E+07 |
| | 15m | 7.41E+08 | 1.07E+09 | 2.94E+07 | 1.56E+08 | 5.36E+07 |
| | 5m | 3.61E+08 | 3.43E+09 | 4.09E+08 | 1.12E+09 | 2.13E+09 |
| | 1m | 5.33E+08 | 1.02E+09 | 0.00E+00 | 9.02E+06 | 0.00E+00 |
| | No30m | 0.00E+00 | 0.00E+00 | 0.00E+00 | 0.00E+00 | 0.00E+00 |
| 1 h - Trial 3 | 30m | 3.52E+07 | 0.00E+00 | 8.63E+09 | 2.28E+09 | 0.00E+00 |
| | 15m | 6.43E+08 | 8.20E+07 | 2.80E+08 | 1.17E+08 | 4.47E+07 |
| | 5m | 2.38E+07 | 5.31E+07 | 6.54E+08 | 0.00E+00 | 4.85E+09 |
| | No30m | 1.23E+09 | 5.64E+08 | 0.00E+00 | 2.89E+08 | 0.00E+00 |
| 8 h - Trial 1 | 30m | 0.00E+00 | 0.00E+00 | 4.30E+07 | 0.00E+00 | 0.00E+00 |
| | 15m | 2.29E+07 | 2.07E+10 | 2.98E+09 | 5.21E+08 | 2.25E+09 |
| | 5m | 2.13E+08 | 2.79E+09 | 1.04E+09 | 2.98E+08 | 1.75E+09 |
| | 1m | 9.94E+08 | 5.64E+07 | 3.38E+08 | 2.17E+07 | 0.00E+00 |
| | No30m | 0.00E+00 | 1.55E+08 | 1.04E+09 | 5.20E+08 | 8.58E+08 |
| 8 h - Trial 2 | 30m | 2.47E+07 | 0.00E+00 | 4.59E+07 | 2.26E+08 | 4.12E+08 |
| | 15m | 2.74E+09 | 1.52E+09 | 9.46E+08 | 1.31E+08 | 8.46E+07 |
| | 5m | 2.32E+07 | 8.04E+08 | 6.21E+08 | 1.31E+07 | 1.34E+09 |
| | 1m | 0.00E+00 | 4.31E+09 | 0.00E+00 | 1.60E+08 | 3.27E+09 |
| | No30m | 9.89E+08 | 1.82E+09 | 4.02E+08 | 2.61E+08 | 3.55E+08 |
| 8 h - Trial 3 | 30m | 4.68E+08 | 1.02E+09 | 2.81E+09 | 2.26E+08 | 2.88E+09 |
| | 15m | 3.03E+08 | 1.70E+10 | 1.11E+09 | 3.09E+08 | 7.53E+08 |
| | 5m | 2.11E+08 | 3.42E+09 | 1.47E+09 | 3.18E+09 | 4.02E+08 |
| | 1m | 4.61E+08 | 8.69E+09 | 0.00E+00 | 0.00E+00 | 2.13E+09 |
| | No30m | 0.00E+00 | 0.00E+00 | 0.00E+00 | 9.47E+08 | 5.06E+07 |
| 24 h - Trial 1 | 30m | 0.00E+00 | 0.00E+00 | 3.30E+07 | 8.49E+08 | 2.17E+09 |
| | 15m | 2.07E+07 | 7.32E+08 | 0.00E+00 | 0.00E+00 | 0.00E+00 |
| | 5m | 0.00E+00 | 7.32E+07 | 0.00E+00 | 0.00E+00 | 0.00E+00 |
| | 1m | 2.76E+09 | 2.98E+09 | 9.02E+07 | 1.66E+08 | 1.35E+09 |
| | No30m | 0.00E+00 | 0.00E+00 | 0.00E+00 | 0.00E+00 | 0.00E+00 |
| 24 h - Trial 2 | 30m | 2.28E+07 | 0.00E+00 | 2.54E+10 | 3.85E+08 | 1.75E+09 |
| | 15m | 1.11E+09 | 5.98E+08 | 1.25E+09 | 1.86E+08 | 4.16E+08 |
| | 5m | 2.15E+08 | 1.14E+09 | 6.77E+07 | 1.14E+07 | 3.79E+07 |
| | 1m | 0.00E+00 | 0.00E+00 | 3.52E+07 | 1.16E+07 | 7.32E+07 |
| | No30m | 2.20E+08 | 0.00E+00 | 5.06E+07 | 1.68E+08 | 0.00E+00 |
| 24 h - Trial 3 | 30m | 2.72E+08 | 1.48E+10 | 3.41E+08 | 1.09E+08 | 2.85E+09 |
| | 15m | 2.43E+08 | 9.27E+09 | 1.47E+09 | 3.10E+08 | 1.03E+09 |
| | 5m | 4.56E+08 | 6.68E+07 | 4.81E+08 | 0.00E+00 | 1.08E+09 |
| | 1m | 8.41E+08 | 2.44E+10 | 5.98E+08 | 9.84E+08 | 3.65E+09 |
| | No30m | 2.07E+09 | 5.27E+08 | 4.35E+08 | 3.10E+08 | 1.96E+09 |

**Table B.2 - Number of MNBs per gram of Tissue for each Condition**

MNBs present in tissues were quantified as outlined in materials and methods and were divided by grams of tissue (Table A.2) to normalize values to MNBs per gram of tissue. Incubation time refers to the time post exposure until euthanasia. Exposure time refers to the amount of time the tail was dipped into the solution containing BAP-MNBs with or without DMSO. 15m refers to 15 min exposure time with 0.1% DMSO. No30m refers to 30 min exposure time without DMSO.

| Incubation Time | Exposure Time (min) | Kidney (MNBs/g) | Spleen (MNBs/g) | Lungs (MNBs/g) | Liver (MNBs/g) | Feces (MNBs/g) |
|---|---|---|---|---|---|---|
| 1 h | 30m | 3.18E+08 | 2.05E+09 | 2.90E+09 | 8.91E+08 | 7.83E+09 |
| | 15m | 6.69E+08 | 9.04E+08 | 4.80E+08 | 2.05E+08 | 7.77E+08 |
| | 5m | 2.79E+08 | 1.86E+09 | 6.63E+08 | 4.95E+08 | 3.87E+09 |
| | 1m | 3.77E+08 | 5.09E+08 | 7.65E+08 | 2.68E+08 | 7.40E+08 |
| | No30m | 5.99E+08 | 8.19E+08 | 3.18E+08 | 1.63E+08 | 2.75E+08 |
| 8 h | 30m | 1.64E+08 | 3.41E+08 | 9.67E+08 | 1.51E+08 | 1.10E+09 |
| | 15m | 1.02E+09 | 1.31E+10 | 1.68E+09 | 3.21E+08 | 1.03E+09 |
| | 5m | 1.49E+08 | 2.34E+09 | 1.04E+09 | 1.17E+09 | 1.16E+09 |
| | 1m | 4.85E+08 | 4.35E+09 | 1.13E+08 | 6.05E+07 | 1.80E+09 |
| | No30m | 3.30E+08 | 6.57E+08 | 4.82E+08 | 5.76E+08 | 4.21E+08 |
| 24 h | 30m | 9.84E+07 | 4.93E+09 | 8.59E+09 | 4.48E+08 | 2.25E+09 |
| | 15m | 4.59E+08 | 3.53E+09 | 9.08E+08 | 1.66E+08 | 4.82E+08 |
| | 5m | 2.24E+08 | 4.28E+08 | 1.83E+08 | 3.79E+06 | 3.74E+08 |
| | 1m | 1.20E+09 | 9.14E+09 | 2.41E+08 | 3.87E+08 | 1.69E+09 |
| | No30m | 7.65E+08 | 1.76E+08 | 1.62E+08 | 1.59E+08 | 6.52E+08 |

**Table B.3 - Average Number of MNBs per gram of Tissue between Trials**

MNBs/g values from Table A.3 were averaged between the 3 trials for each condition. Incubation time refers to the time post exposure until death. Exposure time refers to the amount of time the tail was dipped into the solution containing BAP-MNBs with or without DMSO. 15m refers to 15 min exposure time with 0.1% DMSO. No30m refers to 30 min exposure time without DMSO.

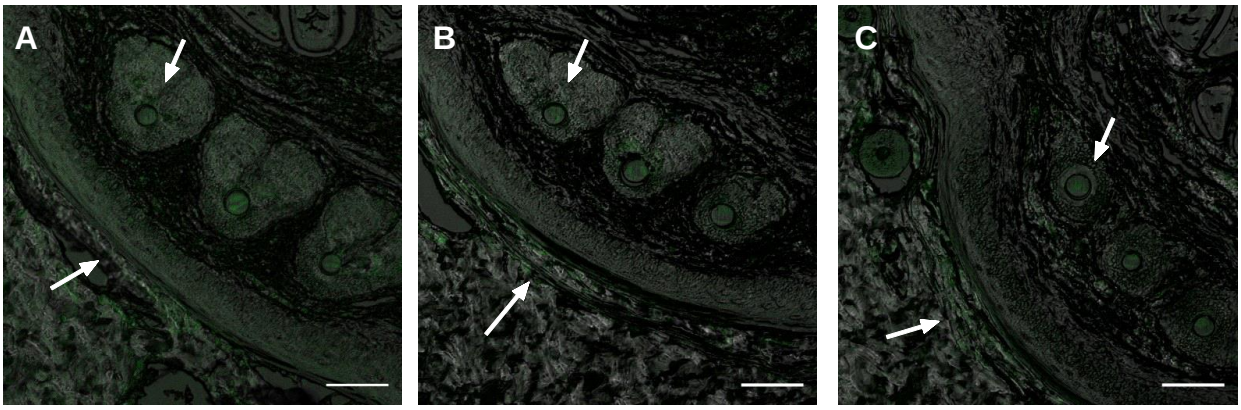


**Figure B.1 - Atto633 Encapsulated BAPCs Visualized in Mice Tails Post Transdermal Exposure**

Images taken 1, 8, or 24 h post 15 min exposure as indicated. The fluorescence is shown as green on the bright-field background. All pictures were captured in the same condition in a LSM700 confocal microscope. (A) 1 h incubation time post 15 min exposure; (B) 8 h incubation time post 15 min exposure; (C) 24 h incubation time post 15 min exposure. For each group N = 1. Bottom arrow indicates the edge of the epidermis, where the arrow's physical location is outside of the tail pointing in. The top arrow in each image is highlighting a hair follicle structure. Scale bar = 50 µm.

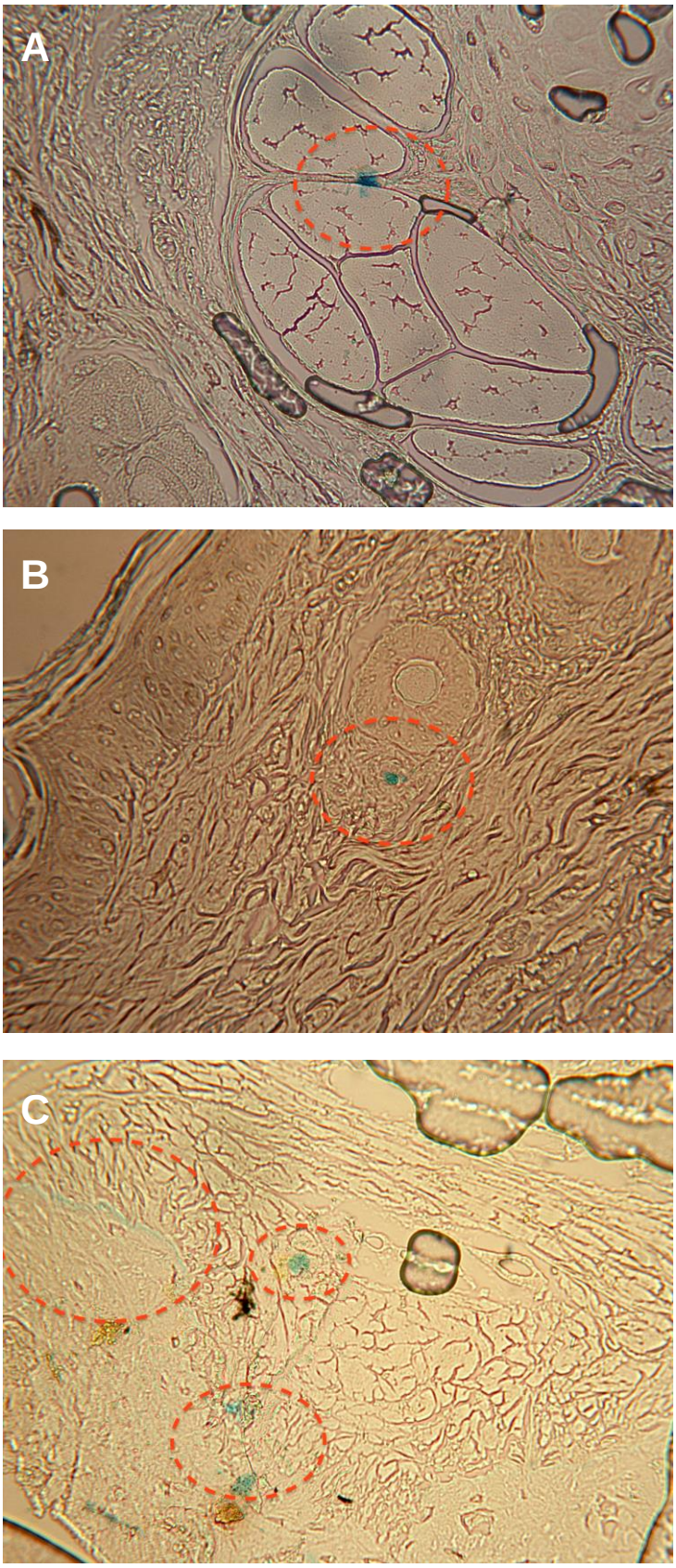


**Figure B.2 - Prussian Blue Staining of MNBs in Mice Tails**

MNBs were stained with Prussian blue. (A) 15 min exposure time, 1 h incubation time. (B) 15 min exposure time, 8 h incubation time. (C) 15 min exposure time, 24 h incubation time. For each group N = 1.

# Appendix C - Copyright Permissions

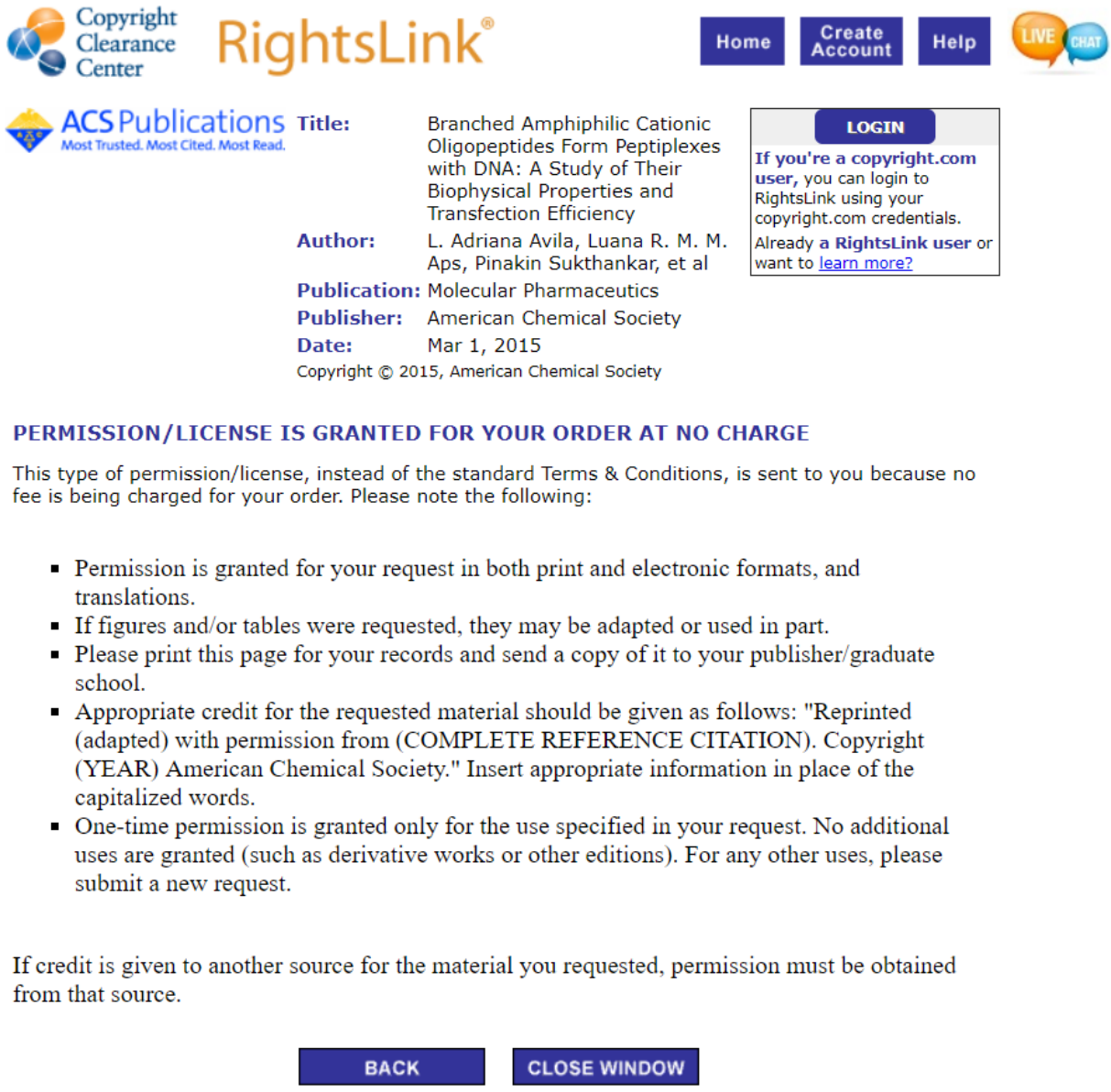

Copyright Clearance Center RightsLink®

Home | Create Account | Help | LIVE CHAT

ACS Publications
Most Trusted. Most Cited. Most Read.

**Title:** Branched Amphiphilic Cationic Oligopeptides Form Peptiplexes with DNA: A Study of Their Biophysical Properties and Transfection Efficiency

**Author:** L. Adriana Avila, Luana R. M. M. Aps, Pinakin Sukthankar, et al

**Publication:** Molecular Pharmaceutics

**Publisher:** American Chemical Society

**Date:** Mar 1, 2015

Copyright © 2015, American Chemical Society

LOGIN

**If you're a copyright.com user,** you can login to RightsLink using your copyright.com credentials.

Already **a RightsLink user** or want to learn more?

**PERMISSION/LICENSE IS GRANTED FOR YOUR ORDER AT NO CHARGE**

This type of permission/license, instead of the standard Terms & Conditions, is sent to you because no fee is being charged for your order. Please note the following:

- Permission is granted for your request in both print and electronic formats, and translations.
- If figures and/or tables were requested, they may be adapted or used in part.
- Please print this page for your records and send a copy of it to your publisher/graduate school.
- Appropriate credit for the requested material should be given as follows: "Reprinted (adapted) with permission from (COMPLETE REFERENCE CITATION). Copyright (YEAR) American Chemical Society." Insert appropriate information in place of the capitalized words.
- One-time permission is granted only for the use specified in your request. No additional uses are granted (such as derivative works or other editions). For any other uses, please submit a new request.

If credit is given to another source for the material you requested, permission must be obtained from that source.

BACK | CLOSE WINDOW

**Figure C.1 - Copyright Permission for Avila et al. 2015. *Molec. Pharm.* 12(3): 706-715**

Copyright permissions for Figure 1.2 and Figure 1.3.


**Figure C.2 - Copyright Permission for Avila et al. 2018. *J. Controlled Release* 273: 139-146.**

Copyright permissions for Figure 2.1 C, Figure 2.2, Figure 2.5, Figure A.1, and Figure A.2 as well as related content in Chapter 2.